Università degli Studi di Bergamo

Dipartimento di Ingegneria

Scuola di dottorato in Meccatronica, Informazione, Tecnologie Innovative e Metodi Matematici

XXV Ciclo

AN ELASTOPLASTIC FINITE ELEMENT FORMULATION FOR THE STRUCTURAL ANALYSIS OF TRUSS FRAMES WITH APPLICATION TO A HISTORICAL IRON ARCH BRIDGE

Doctoral dissertation of

Rosalba FERRARI

Advisor: Prof. **Egidio RIZZI**

Co-advisor: Prof. **Giuseppe COCCHETTI**

To my parents, Maria e Giovanni

"Che spettacolo strano e imponente!

Campato come in aria, sopra l'abisso,

mi sembra d'essere diventato leggero e di volare.

Giù in fondo, i vortici dell'Adda spumeggiano e s'incalzano,

fortemente rumoreggiando, ma non li temo.

Pare quasi che imprechino a chi con tanto lavoro ardito

ha saputo appianare e ricongiungere distanze scavate dai secoli".

L'Eco di Bergamo, 1889.

Summary

This doctoral thesis presents a comprehensive structural analysis of the Paderno d'Adda bridge, an impressive iron arch viaduct built in 1889 and located in the Lombardia region (Italy).

The thesis falls within the context of a research project started at the University of Bergamo since 2005, that keeps ongoing and aims at achieving a reliable evaluation of the present structural performance of the bridge.
Indeed, the bridge is still in service and its crucial position in the context of the local transportation network will soon requires queries about its future destinations, with particular attention to the evaluation of its residual structural capacity.

To this end, a comprehensive structural approach has been developed, including an inelastic structural analysis of the bridge, up to perfectly-elastoplastic collapse. This analysis has been carried-out through an implemented autonomous formulation for elastoplastic 3D truss frame structures, which has been developed within the classical frame of the Theory of Plasticity and Limit Analysis and runs within a MATLAB environment.

The main characteristic ingredients of the implemented elastoplastic FEM formulation are the following: beam finite elements; perfectly-plastic joints (as a generalization of classical plastic hinges); piecewise linear yield domains; "exact" time integration and resulting pure evolutive response up to plastic collapse; estimate of the collapse mode.

The code has been implemented in conjunction with the following original features: determination of the tangent stiffness matrix through Gaussian elimination; treatment of mutual connections by static condensation and Gaussian elimination.
These peculiar features are presented in detail in the thesis.

The procedure is applied to a structure with considerable complexity, as that of the Paderno d'Adda bridge, the FEM model of which involves roughly 5300 beam finite elements and 13300 degrees of freedom.
It demonstrated to be very much able to track the limit structural behaviour of the bridge, by reaching convergence with smooth runs up to the true limit load and effective determination of the corresponding collapse displacements.

About presentation of this work, the first part of the thesis presents the FEM modelling of the bridge (all implementations referring to design stage conditions) and includes various static analyses. Comparisons with available recorded data proved the consistency of the assembled FEM model.
In light of the reliable outcomes coming from the static analyses, further insight on the modal dynamic behaviour of the viaduct was investigated, in terms of the estimation of its natural frequencies and associated mode shapes.

The second part of the thesis presents the FEM elastoplastic formulation and the inelastic structural analysis of the bridge, as mentioned above.

Acknowledgements

I wish to express my deep gratitude to my advisor, Prof. Egidio Rizzi, for his continuous guidance and encouragement during my doctoral studies. Every conversation with him was precious to me.

Special thanks to Prof. Giuseppe Cocchetti, for his kind and precious scientific guidance in the finite element implementations presented in this thesis. It was my great honour to learn from him.

I would like to express my thanks to all the people who are close to me with their constant presence and love. Little I would have done without their support.

Rosalba

Index

Introduction

Since 2005, when it has been the subject of the research work attached to the writer's Graduation Theses (Ferrari, 2006, 2009), the Paderno d'Adda bridge inspires his studies in structural engineering and represents the reference research target, as a case study, of his further education within the present doctoral programme.

This doctoral dissertation collects the research studies that been have conducted on the bridge during the doctoral programme and the main achieved results, concerning specifically a comprehensive structural analysis of the bridge.

The Paderno d'Adda bridge is an impressive riveted iron viaduct with a doubly-built-in parabolic arch that crosses the Adda river near Milano, between Paderno d'Adda and Calusco d'Adda, in Lombardy, northern Italy. It was built in 1889 by the "Società nazionale delle Officine di Savigliano" (SNOS).
The bridge is one of the very first great iron constructions designed through the practical application of the so-called "Theory of the ellipse of elasticity", a graphical-analytical method of structural analysis that was developed in the 19th century (Belluzzi, 1942; Culmann, 1880; Timoshenko, 1953; Benvenuto, 1981).

The writer approached the study on the bridge initially in order to inspect the original architectural and engineering conception at design stage and the outcomes of the graphical-analytical method towards the true calculation of the structure. This opened-up the way for a research project that currently keeps on at the University of Bergamo.

These first studies were conducted before the beginning of the doctoral programme, and therefore they will not be reinterpreted here. Despite this, they are considered as integral part of the whole research work that the writer has been dedicating to the bridge. A specific account on these earlier aspects is provided in compact English form in Ferrari and Rizzi (2008). In this paper, a short presentation on the theory of the ellipse of elasticity, as applied to the design of the bridge, is reported. In light of the definition of the so-called elastic weight of the structure and through some basic concepts of projective geometry, it has been shown that it is possible to bring back the problem of the determination of the flexural elastic deformation of a beam to a problem of pure geometry of masses. Moreover, a description of the practical application of the theory to the structural analysis of the bridge is presented and an independent validation of the original design results with analytical-numerical methods is provided.

Nowadays, after 124 years of continuous duty, the viaduct is still in service with trains crossing at slow speed and alternated one-way road traffic restricted to no heavy-weight vehicles.
Despite this duty, the bridge seems to have suffered from limited maintenance, especially in the last thirty years or so.
Today it appears rusted and most-likely set in a state of diffused and localized corrosion damage. Thus, serious queries on the structural efficiency of the bridge arise at present.

The bridge still plays a crucial role in the current local transportation network. Thus, this may soon require studies on possible conservation and restoration interventions.

The goal of assessing the present structural health conditions of the Paderno d'Adda bridge called for attempting a research activity concerning its structural performance, according to both static and dynamic behaviours.

Initially, a complete FEM model of the bridge was created, taking into account the conceived geometry of the structure at design stage, as it appeared from the original technical drawings.
The FEM model was implemented within a commercial FEM code (ABAQUS).
Some of the original static loading configurations used for the design of the viaduct were analysed, as well as the loading conditions that were implemented in the first try-outs in 1889.
A comparison to the results of the original Technical Report by the SNOS (SNOS, 1889) displayed full consistency among recorded data and FEM predictions, namely the trustworthiness of the implemented FEM model of the bridge (Ferrari et al., 2010b).

In light of the reliable outcomes coming from these preliminary static analyses, further output on the dynamic behaviour of the viaduct was sought, specifically concerning the scopes of possible modal dynamic identification of the structural properties of the bridge.
In particular, the main natural frequencies and associated mode shapes of the structure were determined through the same FEM implementation in ABAQUS.
The main dynamical results on the modal characteristics of the bridge were then elaborated and discussed (Ferrari and Rizzi, 2011b).
A first qualitative comparison to the available results coming from preliminary field investigations and attached dynamic identification on the bridge was also performed, based on ambient vibration tests carried-out by colleagues at Politecnico di Milano (Gentile and Saisi, 2010a, b; Gentile et al., 2010, 2011).

Afterwards, the research on the bridge was extended to the modelling of its global non-linear elastoplastic behaviour.

In this context, an autonomous elastoplastic formulation and implementation in a computer code apt to model general 3D truss frame structures was developed within the classical framework of the Theory of Plasticity and Limit Analysis.

The code, named *Beam3DStp*, runs in a MATLAB environment. At present, the implemented FEM model of the bridge still refers to the characteristics at design stage, whereby the morphological and geometrical features of the structure have been exported from the previous FEM model assembled in ABAQUS.

The main characteristics of the elastoplastic FEM formulation and relevant coding are the following: 3D beam finite elements, perfectly-plastic joints, piecewise linear yield domains and “exact” time integration apt to trace the evolutive piecewise linear response up to true structural collapse.

The code allows for the determination of the collapse load multiplier and relevant collapse mechanism of the structure. Simulations were made by referring to the static try-out railway loading conditions performed on the bridge. The characteristic load/displacement curves were traced by incremental analyses until failure. The critical members in the various parts of the structure were also identified.

The present doctoral dissertation is organized in two main parts.

In Part I the Paderno d’Adda bridge is briefly presented and the results of static and modal dynamic analysis are reported. The FEM model of the bridge is introduced through an explanation of its main characteristics and the considerations that have been taken into account for its assembly.

In Part II the elastoplastic finite element formulation is presented: the general framing of the solving algorithm is outlined and its characteristic computational features are presented.
The following technical aspects and topics shall be specifically considered to have been developed with original formulations: piecewise linear representation of the interaction domain of the section internal actions adopted in the beam finite

elements; treatment of mutual member connections by static condensation and Gaussian elimination; tangent stiffness formulation and sub-step incrementation in the driving algorithm.
In this part the salient results obtained by the elastoplastic analyses performed through the assembled code are also presented and discussed.

Brief Abstracts introduce both Part I and Part II.

The thesis ends with Conclusions, which report as well the research perspectives of the present study.

Three Appendices report the core routine of the code *Beam3DStp*, some illustrations of the Paderno d'Adda bridge and some of the original design drawings produced by the SNOS.

PART I

STATIC AND DYNAMIC LINEAR ANALYSES

Abstract of Part I

In Part I the Paderno d'Adda bridge is presented, together with the numerical static and dynamic analyses conducted on it.

In Chapter 1 a brief description of the main technical features of the bridge is reported, as well as the characterization of the complete FEM model of the structure.

In Chapter 2 the static elastic response of the bridge is presented, by considering the loading conditions that were implemented in the first try-outs in 1889.
These analyses have pursued two principal objectives: to appreciate the structural response of the bridge as a whole and to demonstrate the consistency of the assembled FEM model.
In particular, the vertical deflections of the arch as obtained through the FEM model of the bridge have been compared to the observed and calculated displacements for the four try-out tests by the SNOS. Also, the axial forces in the bars and relevant normal stresses have been calculated at different locations of the FEM model, with good correspondence to the SNOS values. Furthermore, a brief check about the implemented counterslope of the upper continuous beam has been conducted.

In Chapter 3 the first results obtained on the modal dynamic response of the structure through the FEM model of the bridge are presented, in terms of the estimated main natural frequencies and associated mode shapes of the structure. Some considerations about the assembly of the FEM model of the viaduct, in view of quering its dynamic behaviour are presented. Then, main dynamic results on the modal characteristics are

discussed, with a first qualitative comparison to available data on the experimental dynamic identification of the natural modes of the structure.

Chapter 1

The Paderno d'Adda bridge

The Paderno d'Adda bridge, also known as San Michele bridge, is a metallic viaduct that crosses the Adda river between Paderno d'Adda and Calusco d'Adda at a height of approximately 85 m from water. It allows connecting the provinces of Lecco and Bergamo, near Milano, in Lombardia, northern Italy. At that location the river flows-down from Lecco's branch of Como's lake to the Po river, through an impressive natural scenery.

The viaduct was quickly constructed between 1887 and 1889 (thus practically at the same time of the most celebrated Tour Eiffel), to comply with the needs of the growing industrial activities in Lombardy. It was built by the Società Nazionale delle Officine di Savigliano (SNOS), Cuneo, Italy, under the technical direction of Swiss Engineer Jules Röthlisberger (1851-1911), the man to whom the design of the bridge is normally attributed to. He was educated at the Polytechnic of Zürich, where he graduated in 1872 and got later in charge of the Technical Office of the SNOS for 25 years, since 1885.

The Paderno d'Adda bridge is one of the very first large structures designed through a scrupulous application of the so-called *Theory of the Ellipse of Elasticity*, an elegant graphical-analytical method for the analysis of the flexural elastic response of a

structure (Belluzzi, 1942), originally conceived by Karl Culmann (1821-1881) and then systematically developed and applied by his pupil Wilhelm Ritter (1847-1906).
At that time the so-called Graphic Statics was probably showing its best effectiveness in many practical design problems (Culmann, 1880; Timoshenko, 1953; Benvenuto, 1981).
In light of this, the bridge represents today not only a true industrial monument but also a living testimony of the scientific and technological developments of that time.

The bridge is made with a wrought iron material and structural elements connected by riveted joints. According to the original SNOS Report (SNOS, 1889), about 2600 tons of metals were employed in the construction of the viaduct.
It is composed of: an elegant doubly-built-in parabolic arch of about 150 m of horizontal span and 37.5 m of vertical rise; vertical bearing piers with a height up to 31.5 m; an upper continuous beam of 266 m of length. The main upper continuous beam, 5 m wide, is formed by a metallic truss supported by nine bearings, four of which are supported by the arch.
The bridge shares its architectural style with similar arch bridges built in Europe at the time (Timoshenko, 1953; Benvenuto, 1981; Nascè et al., 1984), like e.g. that of Garabit (1884, France, Eiffel and Boyer) and Maria Pia (1887, Oporto, Eiffel and Seyrig), both doubly hinged at the shoulders, and the Dom Luiz I (1886, Oporto, Seyrig), doubly built-in as that of Paderno.

Fig. 1: Bottom view of the Paderno d'Adda bridge (1889), from downstream.

During its history the Paderno d'Adda bridge has undergone a few modifications and repairs. A restoration was carried out to repair damage caused by bombing during World War II. The whole roadway deck was replaced in 1972 by a steel orthotropic deck, connected by rivets to the original structure. Furthermore, in the early nineties, other interventions were held: the replacement of some damaged structural members, the stiffening of the upper metallic box girder, a sand-blasting treatment and partial repainting.

Today, after about 124 years of duty, the viaduct is still in service, as a combined railway and road bridge, with trains crossing at slow speed and alternated one-way automotive traffic restricted to no heavy-weight vehicles.

1.1 Structural description of the bridge

The main technical features of the bridge are reported in detail in Nascè et al. (1984), which is, to the knowledge of the author, the most comprehensive publication on the bridge, among the very few existing. Reference is made much on this valuable contribution and on the Technical Report (SNOS, 1889) that was originally issued by the SNOS at the time of the first try-outs.

The 266 m long upper flyover is made by a continuous box girder with nine equally-distributed supports, at 33.25 m distance from each other.
Four of the supports are sustained by a big parabolic metallic arch; two bear directly on the same masonry arch abutments (made with Moltrasio masonry, with Baveno granite coverings); a seventh, on the Calusco bank, rests on a smaller masonry foundation placed between the arch shoulder and the higher bridge supports; the last two, in masonry work as well, are the two direct beam bearings at its two ends, on top of the two river banks.

The four piers resting on the arch are placed symmetrically with respect to the keystone.

The inner side of the beam girder, on which the railway is located, runs at about 255.00 m on the sea level (osl); the rails are placed at 255.45 m osl, the upper road at 261.75 m osl.

The main vertical longitudinal trussed beams of the upper continuous girder are 6.25 m high and placed at a respective transverse distance of 5.00 m, leaving a free passage of 4.60 m for the trains. They are composed of two main T-ribs connected by a metallic truss.

The upper-level road is 5.00 m wide and includes two additional cantilever sidewalks, each 1 m wide, with iron parapets of 1.50 m high.

The big arch is composed by two couples of secondary inclined arches. Each couple is formed by two arches posed at a respective distance of 1 m and laying symmetrically with respect to a mean plane inclined of about $\pm 8.63°$ to the vertical. The parabolic axis of the arch has a span of 150.00 m and a rise of 37.50 m in the inclined plane. The transverse arch's cross section is 4.00 m high at the keystone and 8.00 m high at the abutments (i.e. in the same 1:2 ratio between rise and half span). The two mean inclined planes of the arches are located at a mutual distance of 5.096 m at the keystone and 16.346 m at the shoulders.

The wall of each composing arch is also constituted by a truss structure with two main T-ribs connected by vertical and inclined bars. The two couples of twin arches are gathered together by two transverse brace systems located at the extrados and at the intrados of the arch body.

In essence, the resulting cross section of the main parabolic arch supporting the horizontal beam is trapezoidal, with variable, increasing cross section from the crown to the shoulders.

This, and specifically the inclination of the twin arches, is a beautiful key feature of Röthlisberger's conception of the bridge, in view of counteracting effectively wind and transverse horizontal actions, in spite of the considerable slenderness of the structure.

The arch cross section at the impost is inclined of 45° to the horizontal, so as the local tangent to the parabolic axis of the arch to the vertical.
The vertical bridge piers that sustain the upper continuous beam are made by eight T-section columns, linked to each other by a bracing system with horizontal bars and St. Andrew's crosses and, on top, by transverse beams that directly serve as supports for the bearing devices of the upper beam.
A 1 m large boardwalk is provided into the body of the arch for inspection and maintenance purposes. Inside the bridge piers, a system of ladders along their height is also provided for the same reasons.
Some illustrations of the bridge are shown in Appendix B.

The bridge is a riveted wrought iron structure of about 2600 t of metals, with near 100000 rivets just in the arch.

The executive drawings, including the various cross sections of the structural elements, the details of the riveted joints and part of the graphical/analytical calculations are reported in 147 amazing drawing tables, which are guarded at the Archivio Storico Nazionale di Torino. They are still in excellent conditions and show the meticulous design of the complex structure of the bridge and how the structural calculus has been integrated in the drawing itself, which testifies the beautiful, intimate link between conception, structural analysis and executive design of the bridge.
Some of the original design drawings are reported in Appendix C.

Through a scrupulous screening of the original drawings it was possible to analyze in detail all the cross sections of the members of the bridge. The sections have been reproduced in digital form. This made it easier to determine the geometrical characteristics of each section. The collected data are reported in Ferrari and Rizzi (2011a). By this work it has been possible to put in place a FEM model of the bridge, which will be described next.

1.2 FEM modelling of the bridge

The FEM model of the bridge has been implemented first within a commercial code (ABAQUS), by assembling a true 3D truss frame with beam elements, mutually built-in at the nodes.

The morphology of the bridge appears to be quite intricate. It is represented by an impressive level of detail in the original technical drawings. For instance, the longitudinal structural members are often assembled by a variable number of riveted plates. Moreover, as a further example, additional reinforcing plates, conceived for local stiffening often appear at sub-structure junctions.

Some simplifications have been necessarily considered in the model: it has been outlined by assigning always bars with constant average cross section between the truss nodes, endowed with equivalent geometrical characteristics (area, principal moments and torsional inertias). Also, the additional reinforcing plates have not been explicitly represented, whereas the cross sections of the limiting bars that contour such stiffening plates have been assumed with higher geometrical characteristics, i.e. one thousand times the values that should be directly assigned to them. This way to proceed was mentioned by Nascè et al. (1984), which have already presented a first, much stylised, FEM model of the bridge.

Indeed, the driving idea in the FEM assembly has been that of developing a true 3D truss structure that would resemble the real 3D design geometry of the viaduct.

The FEM model has been created in four main steps:

1) modelling of the parabolic arch (a partial account on this has been given in Ferrari and Rizzi (2008))
2) outline of the vertical piers
3) realisation of the upper continuous box beam
4) assembly of the whole model by tying together the three structural parts

In the first three phases, the different parts have been tested first as stand-alone structural elements. Later, numerical simulations have been developed for the

entire structure, in order to appreciate the structural response of the bridge as a whole and to prove the consistency of the FEM model through a comparison between the results obtained therein and the original SNOS data.

The different parts and the total assembly are shortly described below, with reference to the technical descriptions of the real structural members that has been advanced in details in Nascè et al. (1984) and briefly reported in Ferrari and Rizzi (2008).

1.2.1 Arch

The 3D truss frame of the arch consists of two planar parabolic trusses laying into two inclined planes (of an angle $\alpha \cong \pm 8.63°$ to the vertical, with $sin\alpha = 0.15$), symmetrically located with respect to the vertical longitudinal plane of the viaduct.

The inclined planes are placed at a relative distance of 5.096 m at the keystone.

A single arch profile is considered in each inclined plane, with an arch body that accounts for the true presence of two secondary twin inclined arches, on the two sides of such inclined plane.

The truss nodes are linked to each other through a reticular system that corresponds to the true bracing system of the arch.

As said above, the additional reinforcing plates between the vertical bars in each of the secondary twin inclined arches, placed at the locations of the arch/bearings connections have not been explicitly represented, whereas the cross sections of the limiting vertical bars contouring the stiffening plates have been endowed with larger geometrical characteristics.

The model of the arch is comprised of 1051 beam elements and 342 nodes.

1.2.2 Vertical piers

Five of the nine bearings of the upper box beam are constituted by truss piers with appreciable vertical body (the two inner bearings on the arch symmetrically located by the crown lay directly on the arch extrados). Four of these piers are placed symmetrically, in couples, to the keystone: one couple of piers, about 14 m high, rests on the haunches (*piers on the arch*); the other, 31.5 m high (*big piers*), lies directly on built-in stone supports on the river banks, which host as well the arch shoulders. The other single pier, 11.1 m high (*intermediate pier*), is located on the Calusco bank and constitutes an additional support, since the upper beam is not placed symmetrically to the crown (see Fig. 2).

The morphological analysis of the piers and the corresponding FEM modelling has therefore focused on *three pier typologies*.

They appear to have been derived from a unique generating pyramid, sectioned first at the same height on top and then at different heights on bottom, depending on the relative distance between the upper truss beam and the piers/ground or piers/arch connections.

The upper rectangular closing frame on top, which hosts as well the bearing devices, appears to be the same for all the piers, with longitudinal (in a front view of the longitudinal plane of the bridge) 1.6 m and transverse (in planes orthogonal to the longitudinal plane) 6.3 m widths.

Of the four faces of the box profile of the piers, the front ones lay in the same α -inclined planes of the arch profile (thus, in a sense, the piers protrude from the arch towards the top, where $\alpha \cong 8.63°$); the lateral ones lay in β-inclined planes of a smaller inclination angle β of around $\beta \cong 2.8°$.

The piers are made by a pair of front box trusses, each formed by four T-section columns linked longitudinally by short horizontal bars and St. Andrew's crosses, and transversally by even shorter horizontal and inclined bars.

The two box trusses are further connected transversally by a windbracing system with slender horizontal bars and St. Andrew's crosses.

In the FEM model, each box truss has been described by a single planar frame laying in the α -inclined plane of the front face, with transverse mutual connections between the two box trusses that resemble the true transverse windbracing system.
Finally, concerning the stiffened connections beam/pier (and pier/arch, in the piers on the arch) the corner columns have been prolonged on top to the upper height of the reinforcing plates (and on bottom to the height of the arch extrados, in the piers on the arch) and their local sections have been treated with higher inertia, as above.
The digits (elements, nodes) of the piers' model are as follows: big pier (224, 92), pier on the arch (120, 52), intermediate pier (110, 50), for a total of 798 elements and 338 nodes.

1.2.3 Upper continuous beam

The 266 m long upper continuous box beam is composed of eight spans, each 33.25 m long. The spans have similar morphologies but some of the cross sections of their structural elements slightly differ. Despite this, the structure of the upper beam is symmetric with respect to Bearing III at half length (which is on the side of the arch crown towards the Calusco bank, Fig. 2). Also, the first two spans, around half length, of the four spans of each symmetric part are identical (Spans 3−4 and 5−6, Fig. 2).
Thus, only *three span typologies* of the upper continuous beam have been modelled.
The FEM model of the beam has been obtained by assembling the models of the separate spans, which have been bound by tie constrains.
The assembly of the model has been set-up also by taking into account a pre-imposed vertical counterslope of the upper beam, which is appearing in the drawings.
In fact, the beam supports are located to a height that increases of 3 cm per span length, from the extremities towards the centre of the bridge. The counterslope profile is symmetric with respect to the crown of the arch: Span 4, located just above the crown, and Span 8, on the Calusco bank, have no counterslope (see Fig. 2).

The FEM model of the beam structure presents two vertical longitudinal truss girders that are 6.25 m high, placed at a respective transverse distance of 5 m. These girders

are made by main longitudinal members on top and on bottom, connected by a series of front cross bars, inclined of about 45°.

Between the two wall beams, transverse beam connections are provided every 3.325 m, both on top, which constitutes the support system of the road, and on bottom, for the support of the railway deck.

These transverse systems are further connected longitudinally by four beams placed every 1 m, on the upper level and by two beams right underneath the above rails, on the lower level.

The digits (elements, nodes) of the beam model are: (436, 192) per span, for 8 spans, for a total of 3488 elements and 1536 tied nodes.

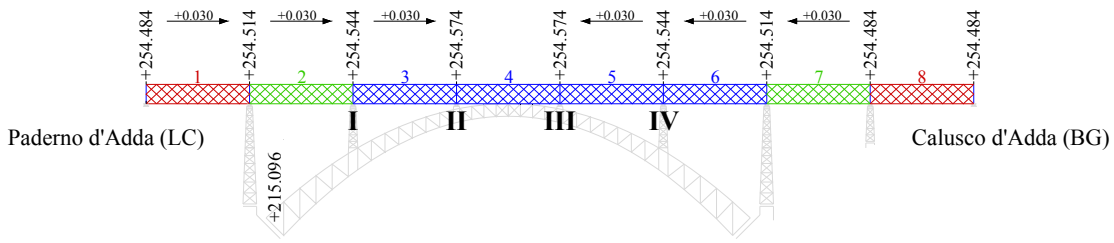

Fig. 2: Scheme with indication of the four beam bearings resting symmetrically on the arch (view from downstream). Bearing III on the side of the left bank is at half length of the upper continuous beam.

1.2.4 FEM assembly

The complete FEM model of the bridge has been made by assembling the parts by coupling (mutual) constraints, with boundary conditions corresponding to what was designed by the SNOS:

- absolute built-in constraints are imposed at the nodes of the arch shoulders and at the bases of the piers bearing on the ground
- absolute rollers with single free translation along the longitudinal plane of the bridge are imposed at the bottom nodes of the main longitudinal elements of the wall beams, at the extremities of the beam on the river banks

- similar relative rollers are imposed between the upper truss beam and the piers or bearings, except for Bearing III at half length (Fig. 2), which is imposed as a relative hinge (these connections look immaterial in Fig. 3)
- mutual built-in constrains are imposed at the pier/arch interfaces.

The FEM model of the bridge is endowed with the following material properties, characteristic of a wrought iron material (Nascè et al., 1984; SNOS, 1889):

- Young's modulus $E = 17 \cdot 10^6$ t /m^2
- Poisson's ratio $\upsilon = 0.3$ (corresponding shear modulus $G = 6.54 \cdot 10^6$ t/m^2)
- mass density $\rho = 7.7$ t/m^3.

The final assembly of the complete 3D truss beam FEM model of the Paderno d'Adda bridge is represented in Fig. 3; it is overall comprised of 5337 beam elements and 2216 tied nodes, by displaying 13296 degrees of freedom (among displacements and rotations of the nodes). It is fully symmetric with respect to the vertical longitudinal plane of the viaduct.

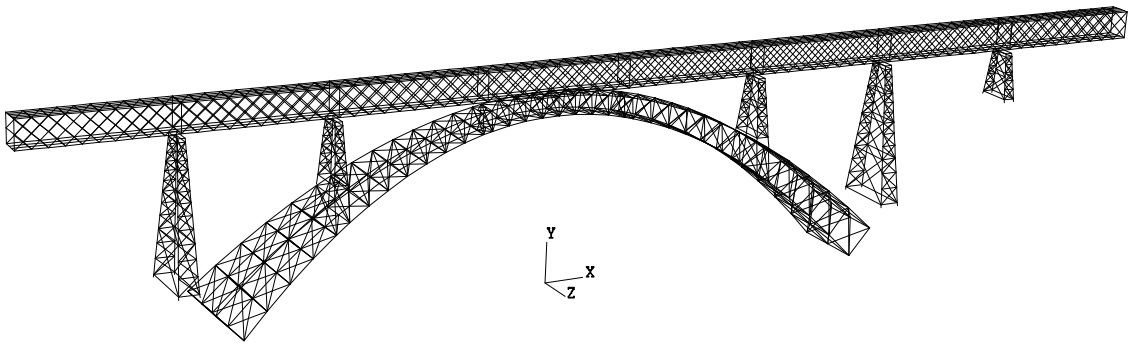

Fig. 3: Assembled FEM model of the Paderno d'Adda bridge (1889).

Chapter 2

Static analysis of the bridge

In order to prove the consistency of the FEM model of the bridge, a study on its response has been attempted in the linear elastic range and a comparison between the obtained results and the data (theoretical and experimental) of the original SNOS Report has been produced.

The SNOS Report (SNOS, 1889) collects two sets of loading configurations.
The first one refers to different design loadings acting on the arch and analyzed independently by the SNOS, one by one, for subsequent superposition of effects:

- permanent weight of the arch, of the upper beam and of the bridge piers
- vertical actions induced by the wind acting on the girder beam
- accidental vertical load on the upper beam, according to different distributions
- temperature effects and compression on the arch due to the horizontal thrust
- direct horizontal wind action on the arch

For each item, the SNOS reports the calculation of the axial forces in the various arch elements, as well as the final values that arise by superposition of effects. The corresponding deflections at the arch/bearings connections are reported as well.
Most of the loading configurations referred to the above mentioned first set have been considered to act on the FEM model of the bridge.
The obtained results have shown good correspondence with the original values reported by the SNOS.

The second set of loading configurations refers to the viaduct tests which took place from 12th to 19th May 1889 (Fig. 4).

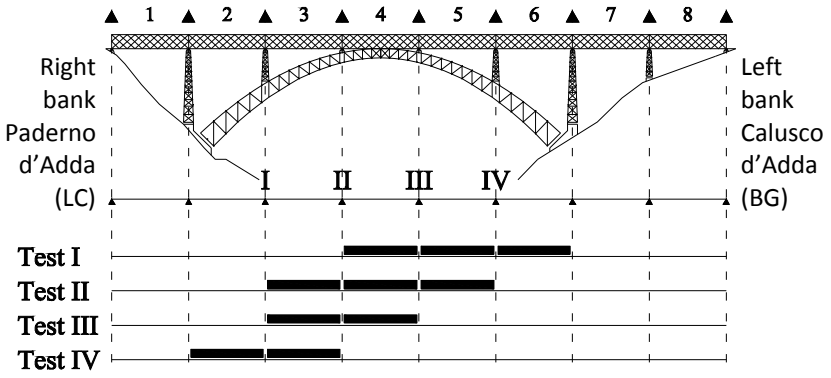

Fig. 4: Scheme with four try-out configurations, with indication of the four beam bearings resting symmetrically on the arch (view from down-stream; Paderno left side, Calusco right side). Bearing III on the side of the left bank is at half length of the upper continuous beam.

The tests were carried-out in two moments: first, the different road loads were obtained by deposition of gravel on the upper deck; second, with a uniformly distributed gravel load of 3.9 t/m all over the road, 6 locomotives with tender, each of 83 t of weight, corresponding to a distributed load of 5.1 t/m, were displaced on the railway track according to four loading configurations (Fig. 4).
The results reported in the SNOS Report seem to have regarded only the vertical displacements caused by the locomotives. Thus, the same loading configurations have

been considered in the FEM model, with distributed loads of 5.1 t/m as reported in Fig. 4 and consequent output on the vertical deflections.

Table 1 below lists the comparison on the observed and calculated vertical deflections of the arch at Bearings I-IV.

Table 1: Arch vertical deflections [mm] observed and calculated for the four try-out tests in Fig. 3 (SNOS 1889, p. 71) vs. FEM results. Negative values indicate downward displacements.

Arch deflections [mm]	**Bearing I**			**Bearing II**			**Bearing III**			**Bearing IV**		
	SNOS		**FEM**	**SNOS**		**FEM**	**SNOS**		**FEM**	**SNOS**		**FEM**
	Obs.	*Calc.*		*Obs.*	*Calc.*		*Obs.*	*Calc.*		*Obs.*	*Calc.*	
Test I	+3.8	+3.3	+4.2	+0.1	−1.0	−0.9	−10.6	−10.8	−11.3	−5.6	−6.6	−6.6
Test II	+0.0	−1.6	−1.0	−7.9	−8.0	−8.6	−10.2	−8.0	−8.4	−1.2	−1.6	−0.9
Test III	−1.6	−4.0	−3.6	−10.2	−10.1	−11.1	−1.4	−2.2	−2.2	+2.5	+2.7	+3.5
Test IV	−6.3	−6.8	−7.6	−5.8	−6.4	−6.6	+4.2	+3.5	+4.0	+2.6	+3.1	+3.6

The FEM outcomes confirm, to quite a good degree of accuracy, the values supplied in the original Report. In Figs. 5−8, the corresponding magnified deformed configurations of the bridge are reported.

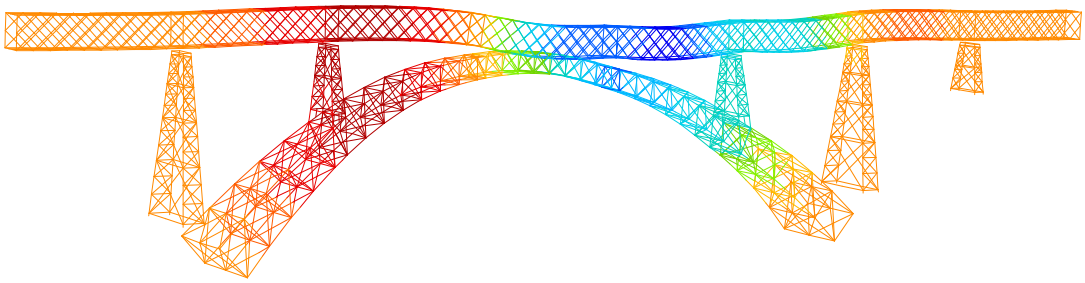

Fig. 5: FEM deformed configuration of try-out Test I in Fig. 4 (amplification factor = 250).

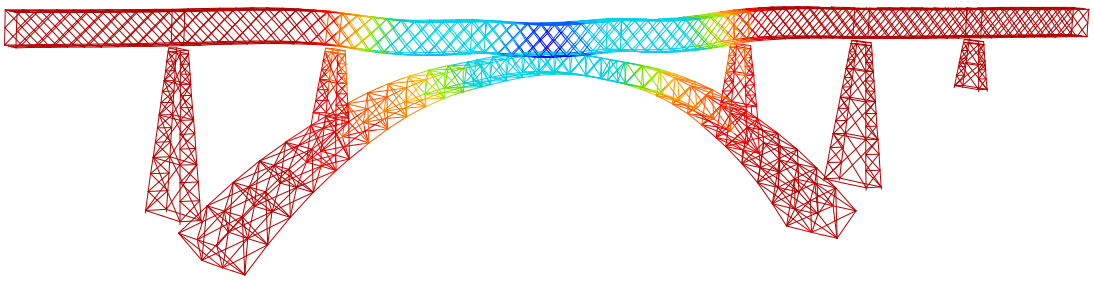

Fig. 6: FEM deformed configuration of try-out Test II in Fig. 4 (amplification factor = 250).

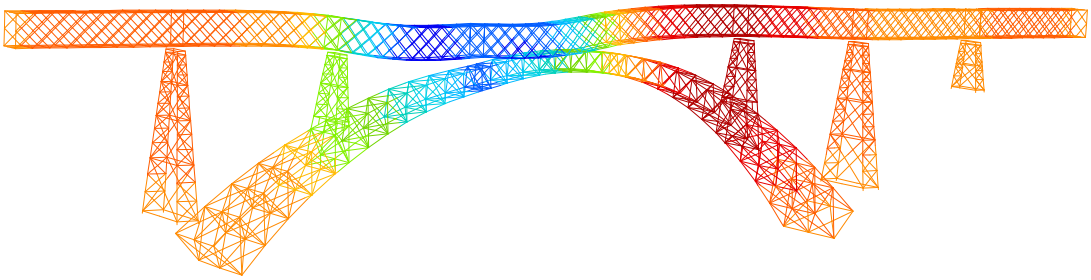

Fig. 7: FEM deformed configuration of try-out Test III in Fig. 4 (amplification factor = 250).

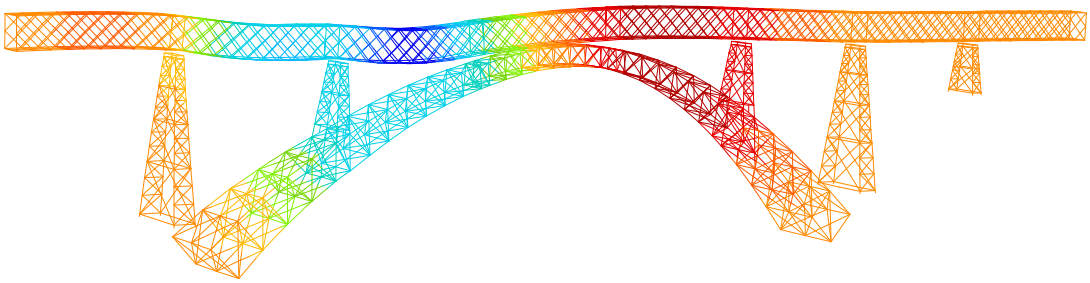

Fig. 8: FEM deformed configuration of try-out Test IV in Fig. 4 (amplification factor = 250).

For the same try-out loading configurations shown in Fig. 4, further FEM results have been inquired.

In particular, the vertical displacements of the upper truss beam of the bridge have been read, at half length of each span and at the bearings in between them. These results could be compared to the nominal target value of $l/1500 = 22.17$ mm, that could be taken as a limit reference indication for bridges with railway traffic.

The corresponding results are reported in Table 2, showing that the deflections are always less than such limit.

Notice also that, due to the counterslope implemented at design stage, despite the negative inflections, the inner bearings in deformed configuration turn-out located always above the ground elevation of the bearings at the extremities of the continuous beam. Thus, the implemented counterslope appears to be effective in this sense.

Table 2: Beam FEM vertical deflections [mm] at half length of each numbered span (1−8) and inner bearings, for the four tests in Fig. 4. Negative values indicate downward displacements.

Beam defl. [mm]	**1**	▲	**2**	▲	**3**	▲	**4**	▲	**5**	▲	**6**	▲	**7**	▲	**8**
Test I	−0.4	+0.1	+2.2	+4.2	+4.0	−0.9	−11.0	−11.3	−13.6	−7.7	−8.1	−1.1	+0.9	+0.1	−0.2
Test II	−0.1	+0.1	+1.0	−1.5	−9.2	−8.6	−12.4	−8.4	−9.0	−1.5	+0.9	+0.1	−0.1	−0.0	+0.0
Test III	+0.1	+0.1	−0.2	−4.1	−12.6	−11.1	−11.7	−2.3	+2.8	+3.5	+1.9	+0.1	−0.3	−0.0	+0.1
Test IV	+1.1	−1.1	−8.7	−8.5	−13.1	−6.6	−0.1	+4.0	+4.7	+3.4	+1.5	+0.1	−0.2	−0.0	+0.1

In addition, axial forces in the bars and relevant normal stresses have been inquired at different locations of the members of the FEM model of the bridge. The admissible stresses in the structural members are indicated as σ_a = 6.0 kg /mm^2, with reduction to σ_a = 4.2 kg /mm^2 for the slender bars of the transverse windbracing systems.

Table 3 reports the values of such actions at the extrados and intrados of the arch shoulders, together with the minimum and maximum values in the various bridge elements (appearing in the arch). The stresses are all below the target admissible values.

Table 3: Bridge FEM axial forces N [t] and stresses σ [kg /mm²] at the arch shoulders and min/max values, for the test distributions shown in Fig. 4. Negative values indicate compression.

N [t] σ [kg/mm²]	**Right-bank shoulder**		**Left-bank shoulder**		**Bridge elements (arch)**			
	Extrados A_e = 159844 mm²	Intrados A_i	Intrados A_i = 243844 mm²	Extrados A_e	Min	A [mm²]	Max	A [mm²]
Test I	−157.542 −0.99	−0.949 −0.00	−231.236 −0.95	+50.421 +0.32	−231.236 −0.95	243844	+51.916 +1.00	51688
Test II	−79.128 −0.50	−138.811 −0.57	−137.517 −0.56	−80.401 −0.50	−155.707 −0.97	159844	+48.690 +1.11	44048
Test III	+1.000 +0.01	−163.615 −0.67	−11.339 −0.05	−137.167 −0.86	−169.752 −1.06	159844	+51.664 +0.44	117844
Test IV	+108.101 +0.68	−196.050 −0.80	+36.078 +0.15	−101.594 −0.64	−196.050 −0.80	243844	+108.101 +0.68	159844

Some studies concerning only the response of the FEM model of the piers were also conducted. Specifically, the pier on the arch has been analysed separately, with absolute built-in constraints at the bottom nodes. These studies have been attempted in the elastic range, for different static loading configurations, based on those relating to the pier reported in the SNOS Report. A specific account on these analyses is reported in Ferrari et al. (2010a).

The outcomes of the analysis conducted through the complete FEM model of the viaduct appear to be consistent with what reported by SNOS (SNOS, 1889), showing that the model is able to provide a coherent account of the bridge structure at design stage.

In light of this, further studies have been carried-out by means of the FEM model. First of all, the modal dynamic characteristics of the bridge have been inquired, which are reported next.

PART II

ELASTOPLASTIC NON-LINEAR ANALYSES

Abstract of Part II

This part consists of two chapters, Chapter 4 and Chapter 5.

Chapter 4 presents the characteristic features of the elastoplastic FEM formulation implemented within MATLAB in the code *Beam3DStp*.
As formerly explained, the algorithm is able to allow a non-linear elastoplastic analysis of a 3D truss frame structure.

In Section 4.1 the hypotheses assumed for the modelling of such a truss frame structure are presented. Among these, the piecewise linear (PWL) model adopted for plastic joint behaviour is briefly discussed.

In the algorithm, the tangent stiffness formulation is adopted in the solving procedure. Section 4.2 treats the determination of such tangent stiffness matrix when PWL yield functions describe the behaviour of the critical sections of the structure.

Later, in Section 4.3, the determination of the tangent stiffness matrix is handled in a particular case, i.e. when the yield domain is represented by the uncoupled condition. In this case the tangent stiffness matrix is determined through a Gaussian elimination procedure. As mentioned in Introduction, this issue represents an original computational peculiarity of the code *Beam3DStp*, as well as the treatment of mutual connections by static condensation and Gaussian elimination, which is dealt with in Section 4.4.

For purposes of compactness, Sections 4.2–4.4 refer to a usual 2D interpretation of building frames. The validity of these considerations keeps holding even in the 3D case.

Section 4.5 presents the sub-step incrementation in the driving algorithm.

Chapter 5 illustrates the main results of the elastoplastic analyses of the Paderno d'Adda bridge that have been then performed through the code *Beam3DStp*.

Chapter 4

Formulation and implementation of an elastoplastic computational algorithm

In order to evaluate the global non-linear elastoplastic behaviour of the Paderno d'Adda bridge, an autonomous elastoplastic formulation and implementation in a computer code apt to model general 3D truss frame structures has been developed. The code, named *Beam3DStp*, allows for the determination of the collapse multiplier and relevant collapse mechanism of the structure. It runs in a MATLAB environment.

The elastoplastic formulation adopted in the code is based on the traditional idealization of "plastic hinges", namely possible plastic deformations (not necessarily only flexural) that are confined just to "critical sections" or "plastic joints", located between adjacent conventional finite elements which model 3D elastic beams. The behaviour of these critical sections is described by elastic perfectly-plastic models which are piecewise linear (PWL) (see e.g. Maier, 1970, 1976; Capurso, 1971; Hodge, 1977; Tin-Loi, 1990; Olsen, 1998).

In the following Section 4.1 a brief description of such elastoplastic FE formulation and PWL models for plastic joints behaviour is presented.

4.1 Elastoplastic FE formulation

According to traditional FEM modelling in structural engineering, frame structures are modelled herein by conventional finite elements, i.e. the structure is assumed to be the assembly of various elements connected at a discrete number of points (nodes). External forces and constraints are reduced to act on these points.

In particular, the FEM formulation is based on classical Euler-Bernoulli beam finite elements, according to the following peculiar hypotheses: straight elements, uniform cross section, homogeneous material properties, transverse displacements modelled by cubic shape functions (i.e. negligible shear strain effects are considered), axial displacements and rotations varying linearly along the beam element.
Moreover, possible deformations are manifested only at pre-selected sections (plastic joints). In particular it is assumed that the critical sections are located between adjacent conventional finite elements, where two plastic joints, as a generalization of the classical plastic hinge concept in the Limit Analysis of frames (see e.g. Cocchetti and Maier, 2003 and references quoted therein), are considered.

The behaviour of the critical sections is described by an elastoplastic (perfectly-plastic) model with piecewise linear (PWL) yield functions. This means that the relationships between static and kinematic generalized variables of the beam cross sections are piecewise linearized (see Maier, 1970, 1976; Capurso, 1971; Hodge, 1977; Tin-Loi, 1990; Olsen, 1998).

A general formulation of PWL elastoplastic models relates in time t the generalized strain history $\mathbf{q}$ to the generalized stress history $\mathbf{N}$ in a critical section. According to the idealizations above this may be expressed as:

$$\mathbf{q} = \mathbf{e} + \boldsymbol{\eta}, \qquad \mathbf{e} = \mathbf{K}^{-1}\mathbf{N}, \qquad \boldsymbol{\eta} = \mathbf{n}\boldsymbol{\lambda} \tag{1}$$

$$\boldsymbol{\varphi} = \mathbf{n}^{\mathrm{T}}\mathbf{N} - \mathbf{Y} \le \mathbf{0}, \qquad \dot{\boldsymbol{\lambda}} \ge \mathbf{0}, \qquad \boldsymbol{\varphi}^{\mathrm{T}}\dot{\boldsymbol{\lambda}} = 0 \tag{2}$$

Eq. (1) splits the strain variable vector $\mathbf{q}$ into an elastic addend $\mathbf{e}$ and a plastic contribution $\boldsymbol{\eta}$, and relates the former to the stress vector $\mathbf{N}$, through an elastic stiffness matrix $\mathbf{K}$, the latter to the vector of plastic multipliers $\boldsymbol{\lambda}$ through matrix $\mathbf{n}$, the columns of which can be interpreted as $\mathbf{N}$-gradients of linear (or linearized) yield functions (associativity is adopted herein). In Eq. (2) the yield functions are collected by vector $\boldsymbol{\varphi}$. Finally, the constant vector $\mathbf{Y}$ collects the "yield limits" (perfect plasticity), the ith component of which represents the distance of the ith yield plane $(i = 1,\ldots,y)$ to the origin in the space of generalized stresses $\mathbf{N}$.

The inverse formulation of the PWL model, governing the generalized stress response $\mathbf{N}(t)$ to an assigned strain path $\mathbf{q}(t)$, is represented by the following relations:

$$\mathbf{N} = \mathbf{K}\,\mathbf{q} - \mathbf{K}\,\mathbf{n}\,\boldsymbol{\lambda} \tag{3}$$

$$\boldsymbol{\varphi} = \mathbf{n}^{\mathrm{T}}\mathbf{K}\,\mathbf{q} - \mathbf{n}^{\mathrm{T}}\mathbf{K}\,\mathbf{n}\,\boldsymbol{\lambda} - \mathbf{Y} \le \mathbf{0}, \qquad \dot{\boldsymbol{\lambda}} \ge \mathbf{0}, \qquad \boldsymbol{\varphi}^{\mathrm{T}}\dot{\boldsymbol{\lambda}} = 0 \tag{4}$$

In the usual 2D interpretation of frames, the generalized stresses gathered in vector $\mathbf{N}$ are the bending moments at the extremities of the beam and the axial force; the generalized strains in vector $\mathbf{q}$ consist of relative rotations at the extremities of the beam (with respect to a principal centroidal axis of the section) and axial elongation (discontinuity of displacement along the centroidal axis of the beam).

In the discrete idealization of the structure, the deformation patterns of each element i are prescribed to depend on the generalized strains collected in vector $\mathbf{q}$, which are

defined, in turn, by the nodal displacements vector $\mathbf{u}$ of the beam element. If plastic deformations do not occur, the nodal displacements $\mathbf{u}$ imply, through the elastic stiffness matrix $\mathbf{K}$, the nodal force at the extremity of the beam element. Meanwhile, if plastic deformations occur, the static variables at the extremity of the beam element will be calculated through the superposition of effects, expressed by the following linear relationship:

$$\mathbf{H} = \mathbf{K}\mathbf{u} + \mathbf{D}\boldsymbol{\eta} \tag{5}$$

where matrix $\mathbf{H}$ represents the self-equilibrated nodal forces associated to the nodal displacements $\mathbf{u}$ of the beam element and $\mathbf{D}$ represents the plastic stiffness matrix. Fig. 11 reports the description of the static and kinematic variables of an illustrating 2D beam finite element.

Kinematic (external) variables

$$\mathbf{u}^T = [u_A \; v_A \; \varphi_A \; u_B \; v_B \; \varphi_B]$$

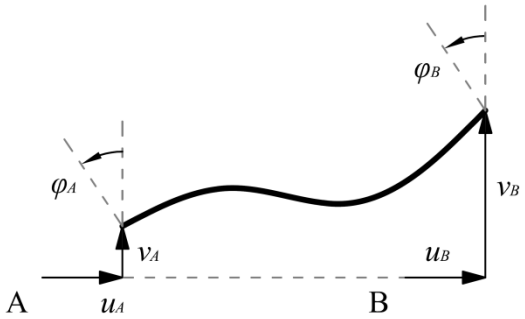

Static (external) variables

$$\mathbf{H}^T = [H_A \; V_A \; W_A \; H_B \; V_B \; W_B]$$

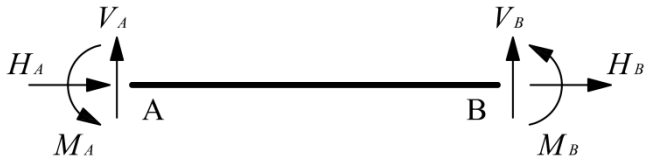

Kinematic internal variables

$$\boldsymbol{\eta}^T = [\mu \;\; \varphi_A \; \varphi_B]$$

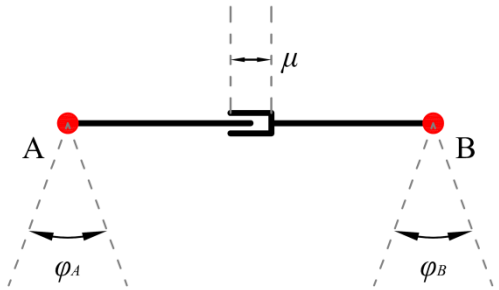

Static internal variables

$$\mathbf{N}^T = [N \;\; M_A \; M_B]$$

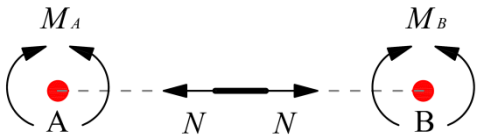

Fig. 11: Description of a 2D beam finite element with plastic joints.

The expression of the above mentioned matrix $\mathbf{D}$ can be obtained by the following treatment.

Consider an unconstrained beam finite element subjected to self-equilibrated nodal forces $\mathbf{H}$; when some kinematic internal variables $\boldsymbol{\eta}$ are applied, the resulting nodal displacements $\mathbf{u}$ (associated to the former) and the static internal variables $\mathbf{N}$ (associated to the latter) are related to each other through the Virtual Power Principle:

$$P_{\text{int}} = \mathbf{N}^T \dot{\boldsymbol{\eta}} = \mathbf{H}^T \dot{\mathbf{u}} = P_{ext} \quad \forall \mathbf{H} \;\; \textit{self-equilibrated} \tag{6}$$

Moreover, in light of the sign assumptions represented in Fig. 11, the generalized stress vector $\mathbf{N}$ is related to the vector of the static variables $\mathbf{H}$ as follows:

$$\mathbf{N} = \mathbf{Q}\,\mathbf{H}, \qquad \mathbf{Q} = \begin{bmatrix} 0 & 0 & 0 & 1 & 0 & 0 \\ 0 & 0 & -1 & 0 & 0 & 0 \\ 0 & 0 & 0 & 0 & 0 & 1 \end{bmatrix} \tag{7}$$

By substituting the first expression in Eq. (7) into Eq. (6), an incremental relationship between the kinematic internal variables $\boldsymbol{\eta}$ and the displacements $\mathbf{u}$ can be obtained for the generic finite element:

$$\dot{\mathbf{u}} = \mathbf{Q}^T \dot{\boldsymbol{\eta}} + \dot{\mathbf{u}}^* \qquad \textit{with} \;\; \mathbf{H}^T \dot{\mathbf{u}}^* \equiv 0 \;\; (\dot{\mathbf{u}}^* = \textit{rigid body motion}) \tag{8}$$

When no external actions are applied:

$$\mathbf{H} = \mathbf{0} \quad \Rightarrow \quad \mathbf{H} = \mathbf{K}\mathbf{u} + \mathbf{D}\boldsymbol{\eta} = \mathbf{0} \quad \Rightarrow \quad \mathbf{K}\mathbf{Q}^T\boldsymbol{\eta} + \mathbf{K}\mathbf{u}^* + \mathbf{D}\boldsymbol{\eta} = \mathbf{0} \quad \forall \boldsymbol{\eta}$$

$$\Rightarrow \quad \mathbf{D} = -\mathbf{K}\mathbf{Q}^T \tag{9}$$

Being the elastic stiffness matrix $\mathbf{K}$ of a 2D finite beam element equal to:

$$\mathbf{K} = \begin{bmatrix} EA/L & 0 & 0 & -EA/L & 0 & 0 \\ 0 & 12EJ/L^3 & 6EJ/L^2 & 0 & -12EJ/L^3 & 6EJ/L^2 \\ 0 & 6EJ/L^2 & 4EJ/L & 0 & -6EJ/L^2 & 2EJ/L \\ -EA/L & 0 & 0 & EA/L & 0 & 0 \\ 0 & -12EJ/L^3 & -6EJ/L^2 & 0 & 12EJ/L^3 & -6EJ/L^2 \\ 0 & 6EJ/L^2 & 2EJ/L & 0 & -6EJ/L^2 & 4EJ/L \end{bmatrix} = \mathbf{K}^T$$

the matrix $\mathbf{D}$ takes the following expression:

$$\mathbf{D} = -\mathbf{K}\mathbf{Q}^T = \begin{bmatrix} EA/L & 0 & 0 \\ 0 & 6EJ/L^2 & -6EJ/L^2 \\ 0 & 4EJ/L & -2EJ/L \\ -EA/L & 0 & 0 \\ 0 & -6EJ/L^2 & 6EJ/L^2 \\ 0 & 2EJ/L & -4EJ/L \end{bmatrix}$$

In light of the above relations, the general formulation of PWL elastoplastic models described in Eqs. (1) and (2) becomes:

$$\mathbf{q} = \mathbf{K}^{-1}\mathbf{N} + \mathbf{n}\boldsymbol{\lambda} \tag{10}$$

$$\boldsymbol{\varphi} = \mathbf{n}^{\mathrm{T}}\mathbf{Q}\,\mathbf{K}\,\mathbf{u} - \mathbf{n}^{\mathrm{T}}\mathbf{Q}\,\mathbf{K}\,\mathbf{Q}^{\mathrm{T}}\mathbf{n}\,\boldsymbol{\lambda} - \mathbf{Y} \le \mathbf{0}, \qquad \dot{\boldsymbol{\lambda}} \ge \mathbf{0}, \qquad \boldsymbol{\varphi}^{\mathrm{T}}\dot{\boldsymbol{\lambda}} = 0 \tag{11}$$

and Eq. (5) becomes:

$$\mathbf{H} = \mathbf{K}\mathbf{u} - \mathbf{K}\mathbf{Q}^T\boldsymbol{\eta} \tag{12}$$

In the resolutive procedure of the computer code *Beam3DStp* mentioned above, the static external variables $\mathbf{H}$ of a beam element are directly related to the nodal displacements $\mathbf{u}$ through the determination of the tangent stiffness matrix.

The following Section 4.2 discusses the tangent stiffness determination when piecewise linear (PWL) yield functions describe the behaviour of the plastic joints.
In particular, the determination of the tangent stiffness matrix will be presented in cases in which the stress point $\mathbf{N}$ belongs to one yield plane only or simultaneously to $n>1$ planes in the space of the static variables. In particular, the cases in which $n=2,\,3,\,4$ will be discussed. It will be underlined that when the intersection of 3 or more planes occurs, the tangent stiffness matrix vanishes.
The determination of the tangent stiffness matrix will be finally discussed in the case in which the stress point $\mathbf{N}$ belongs to a generic number "m" of yield planes.

4.2 Tangent stiffness determination

Consider, according to the above mentioned idealizations concerning the usual 2D interpretations of building frames, a yield surface schematically shown in Fig. 12.

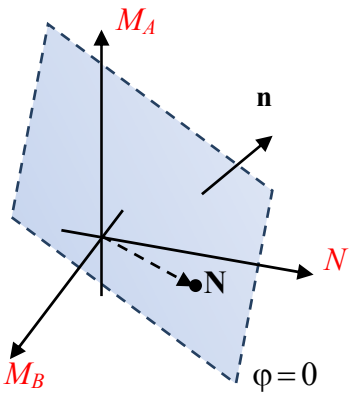

$$\varphi = \mathbf{n}^T \mathbf{N} - y \leq 0 \tag{13}$$

Fig. 12: Schematic representation of one hyper-plane in the $\mathbf{N}$-dimensional space of the static variables $\mathbf{N}$.

The coordinates of the point $\mathbf{N}$ represent the static internal variables of a critical section, in which the development of plastic strains requires that the yield condition has been activated, i.e. $\varphi = 0$.

From the mathematical point of view, the equality $\varphi = 0$ represents a constraint equation (between the internal static variables) to be added to the "constitutive" relationship of the finite element, namely the relationship between the vector $\mathbf{N}$ and the vector $\boldsymbol{\eta}$.

In view of the incremental form of the governing equations, the rate form of the first relation in Eq. (2) and Eq. (7) is adopted:

$$\dot{\varphi} = \mathbf{n}^T \dot{\mathbf{N}} = \mathbf{n}^T \mathbf{Q} \dot{\mathbf{H}} = 0 \tag{14}$$

Note that, being the distance y of the yield plane from the origin of the $\mathbf{N}$-space constant, it disappears in the rate expression of the yield function.

Using the general relationship between external actions and kinematic quantities stated by Eq. (5), one obtaines:

$$\dot{\varphi} = \mathbf{n}^T \mathbf{Q}\,\mathbf{K}\dot{\mathbf{u}} + \mathbf{n}^T \mathbf{Q}\,\mathbf{D}\dot{\boldsymbol{\eta}} = 0 \tag{15}$$

According to the normality flow-rule, the internal kinematic variables are expressed in terms of the plastic multiplier rate $\dot{\lambda}$:

$$\dot{\boldsymbol{\eta}} = \mathbf{n}\dot{\lambda} \tag{16}$$

for which the complementarity rule holds:

$$\dot{\lambda} \geq 0, \qquad \varphi \leq 0, \qquad \varphi\dot{\lambda} = 0 \tag{17}$$

Substituting in Eq. (15) the final relation of Eq. (9) and Eq. (16), the plastic multiplier rate can be computed as follows:

$$\dot{\varphi} = \mathbf{n}^T \mathbf{Q}\,\mathbf{K}\dot{\mathbf{u}} - \mathbf{n}^T \mathbf{Q}\,\mathbf{K}\mathbf{Q}^T \mathbf{n}\,\dot{\lambda} = 0 \qquad \Rightarrow \qquad \dot{\lambda} = \frac{\mathbf{n}^T \mathbf{Q}\,\mathbf{K}}{\mathbf{n}^T \mathbf{Q}\,\mathbf{K}\mathbf{Q}^T \mathbf{n}}\dot{\mathbf{u}} \tag{18}$$

Finally, a direct force/displacement incremental (linear) relationship governed by a symmetric elastic-plastic stiffness matrix $\mathbf{K}_{ep}$ can be obtained for the generic finite element:

$$\dot{\mathbf{H}} = \mathbf{K}\dot{\mathbf{u}} - \mathbf{K}\mathbf{Q}^T\dot{\boldsymbol{\eta}} = \mathbf{K}\dot{\mathbf{u}} - \mathbf{K}\mathbf{Q}^T\mathbf{n}\frac{\mathbf{n}^T\mathbf{Q}\,\mathbf{K}}{\mathbf{n}^T\mathbf{Q}\,\mathbf{K}\mathbf{Q}^T\mathbf{n}}\dot{\mathbf{u}} = \underbrace{\left[\mathbf{K} - \frac{\mathbf{K}\mathbf{Q}^T\mathbf{n}\,\mathbf{n}^T\mathbf{Q}\,\mathbf{K}}{\mathbf{n}^T\mathbf{Q}\,\mathbf{K}\mathbf{Q}^T\mathbf{n}}\right]}_{\mathbf{K}_{ep}}\dot{\mathbf{u}} = \mathbf{K}_{ep}\,\dot{\mathbf{u}} \tag{19}$$

Note that:

$$\mathbf{QKQ}^T = -\mathbf{QD} = \begin{bmatrix} EA/L & 0 & 0 \\ 0 & 4EJ/L & -2EJ/L \\ 0 & -2EJ/L & 4EJ/L \end{bmatrix} \tag{20}$$

and:

$$\mathrm{eig}\left(\mathbf{QKQ}^T\right) = \left\{ \frac{EA}{L},\ 2\frac{EJ}{L},\ 6\frac{EJ}{L} \right\} \tag{21}$$

So, matrix $\mathbf{QKQ}^T$ is positive definite and, being $\mathbf{n}$ a versor, the denominator of $\mathbf{K}_{ep}$ in previous Eqs. (18) and (19) is always strictly positive.

Matrix $\mathbf{K}_{ep}$ is called *tangent stiffness matrix* and represents a direct force/displacement incremental relationship of a generic finite element when plastic deformation occurs, namely when the stress point $\mathbf{N}$ in the space of the static variables keeps moving on a specific yield plane.

The above treatment refers to the case in which the stress point $\mathbf{N}$ belongs to one yield plane only. In general, the stress point $\mathbf{N}$ may belong also to more than one plane at the same time.

In the following, the generalization of the determination of the tangent stiffness matrix $\mathbf{K}_{ep}$ is presented for the cases in which the stress point $\mathbf{N}$ belongs simultaneously to $n > 1$ planes in the space of the static variables. In particular, the cases in which $n = 2,\ 3,\ 4$ will be handled. Finally, the determination of the tangent stiffness matrix will be discussed in the case in which the stress point $\mathbf{N}$ belongs to generic m yield planes.

The discussion is set up as a premise to Section 4.3, where the tangent stiffness matrix is determined for a particular case, i.e. when the yield domain is represented by uncoupled yield conditions.

Determination of matrix $\mathbf{K}_{ep}$ **with *2 intersecting yield planes*** $\left(\mathbf{n}_1 \neq \mathbf{n}_2\right)$

Consider now, according to the treatment above, the two yield surfaces schematically shown in following Fig. 13.

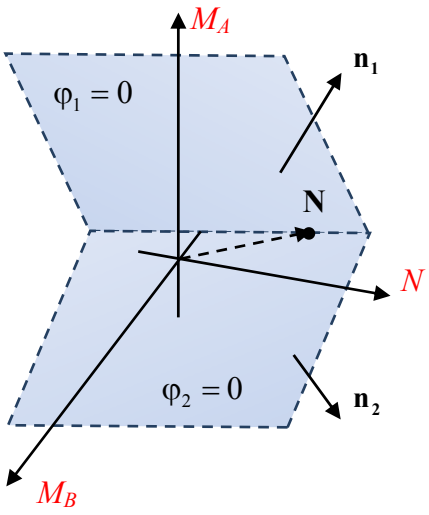

$$\varphi_1 = \mathbf{n}_1^T \mathbf{N} - y_1 \leq 0$$
$$\varphi_2 = \mathbf{n}_2^T \mathbf{N} - y_2 \leq 0 \qquad (22)$$

Fig. 13: Schematic representation of two hyper-planes in the $\mathbf{N}$-dimensional space of the static variables.

As obtained in Eq. (14), the incremental form of the constraint equations (between the internal static variables) gives:

$$\begin{bmatrix} \dot{\varphi}_1 \\ \dot{\varphi}_2 \end{bmatrix} = \begin{bmatrix} \mathbf{n}_1^T \\ \mathbf{n}_2^T \end{bmatrix} \dot{\mathbf{N}} = \begin{bmatrix} \mathbf{n}_1^T \\ \mathbf{n}_2^T \end{bmatrix} \mathbf{Q}\, \dot{\mathbf{H}} = \begin{bmatrix} 0 \\ 0 \end{bmatrix} \qquad (23)$$

By using the general relationship between external actions and kinematic quantities, one has:

$$\begin{bmatrix} \dot{\varphi}_1 \\ \dot{\varphi}_2 \end{bmatrix} = \begin{bmatrix} \mathbf{n}_1^T \\ \mathbf{n}_2^T \end{bmatrix} \mathbf{Q}\,\mathbf{K}\dot{\mathbf{u}} + \begin{bmatrix} \mathbf{n}_1^T \\ \mathbf{n}_2^T \end{bmatrix} \mathbf{Q}\,\mathbf{D}\dot{\boldsymbol{\eta}} = \begin{bmatrix} 0 \\ 0 \end{bmatrix} \tag{24}$$

When the stress point $\mathbf{N}$ lies at the intersection of some yield planes, the plastic strain rate vector $\dot{\boldsymbol{\eta}}$ belongs to the convex polyhedral cone defined by the outward normals $\mathbf{n}_i$ to the yield planes intersecting there, and amounts to the sum of the contributions of the strain rate vectors $\dot{\boldsymbol{\eta}}_i$ of the various yielding modes acting independently.

So, according to the normality flow-rule, the internal kinematic variables are expressed as follows:

$$\dot{\boldsymbol{\eta}} = \left[\mathbf{n}_1\,,\mathbf{n}_2\right] \begin{bmatrix} \dot{\lambda}_1 \\ \dot{\lambda}_2 \end{bmatrix} \tag{25}$$

for which the complementarity rule holds:

$$\begin{bmatrix} \dot{\lambda}_1 \\ \dot{\lambda}_2 \end{bmatrix} \geq \mathbf{0}, \quad \begin{bmatrix} \varphi_1 \\ \varphi_2 \end{bmatrix} \leq 0, \quad \varphi_1\dot{\lambda}_1 + \varphi_2\dot{\lambda}_2 = 0 \tag{26}$$

It should be noted that, due to the sign restriction of the first two relations in Eq. (26), the third linear equality of the same equation is satisfied also considering the equality $\varphi_i\,\dot{\lambda}_i = 0$ for each product independently.

Then, the plastic multiplier rates can be easily computed:

$$\begin{bmatrix} \dot{\varphi}_1 \\ \dot{\varphi}_2 \end{bmatrix} = \begin{bmatrix} \mathbf{n}_1^T \\ \mathbf{n}_2^T \end{bmatrix} \mathbf{Q}\,\mathbf{K}\dot{\mathbf{u}} - \begin{bmatrix} \mathbf{n}_1^T \\ \mathbf{n}_2^T \end{bmatrix} \mathbf{Q}\,\mathbf{K}\mathbf{Q}^T \left[\mathbf{n}_1\,,\mathbf{n}_2\right] \begin{bmatrix} \dot{\lambda}_1 \\ \dot{\lambda}_2 \end{bmatrix} = \begin{bmatrix} 0 \\ 0 \end{bmatrix}$$

$$\Rightarrow \quad \begin{bmatrix} \dot{\lambda}_1 \\ \dot{\lambda}_2 \end{bmatrix} = \left(\begin{bmatrix} \mathbf{n}_1^T \\ \mathbf{n}_2^T \end{bmatrix} \mathbf{Q}\,\mathbf{K}\mathbf{Q}^T \left[\mathbf{n}_1\,,\mathbf{n}_2\right] \right)^{-1} \begin{bmatrix} \mathbf{n}_1^T \\ \mathbf{n}_2^T \end{bmatrix} \mathbf{Q}\,\mathbf{K}\dot{\mathbf{u}} \tag{27}$$

Note that the determination of the plastic multipliers given by Eq. (27) can be achieved without problems of computational nature because versors $\mathbf{n_1}, \mathbf{n_2}$ are linearly independent and, in light of Eqs. (20)-(21), matrix $\mathbf{QKQ}^T$ is positive definite. Thus, nominal inversion of the matrix in Eq. (27) may always be performed.

Finally, the elastic-plastic stiffness matrix of the element is obtained in the case of two active yield planes in the time increment:

$$\begin{aligned} \dot{\mathbf{H}} &= \mathbf{K}\dot{\mathbf{u}} - \mathbf{K}\mathbf{Q}^T \left[\mathbf{n}_1\,,\mathbf{n}_2\right] \begin{bmatrix} \dot{\lambda}_1 \\ \dot{\lambda}_2 \end{bmatrix} = \\ &= \mathbf{K}\dot{\mathbf{u}} - \mathbf{K}\mathbf{Q}^T \left[\mathbf{n}_1\,,\mathbf{n}_2\right] \left(\begin{bmatrix} \mathbf{n}_1^T \\ \mathbf{n}_2^T \end{bmatrix} \mathbf{Q}\,\mathbf{K}\mathbf{Q}^T \left[\mathbf{n}_1\,,\mathbf{n}_2\right] \right)^{-1} \begin{bmatrix} \mathbf{n}_1^T \\ \mathbf{n}_2^T \end{bmatrix} \mathbf{Q}\,\mathbf{K}\dot{\mathbf{u}} = \\ &= \underbrace{\left[\mathbf{K} - \mathbf{K}\mathbf{Q}^T \left[\mathbf{n}_1\,,\mathbf{n}_2\right] \left(\begin{bmatrix} \mathbf{n}_1^T \\ \mathbf{n}_2^T \end{bmatrix} \mathbf{Q}\,\mathbf{K}\mathbf{Q}^T \left[\mathbf{n}_1\,,\mathbf{n}_2\right] \right)^{-1} \begin{bmatrix} \mathbf{n}_1^T \\ \mathbf{n}_2^T \end{bmatrix} \mathbf{Q}\,\mathbf{K} \right]}_{\mathbf{K}_{ep}} \dot{\mathbf{u}} \end{aligned} \tag{28}$$

Similarly, one may proceed for cases of more interacting yield planes, as outlined next.

Determination of matrix $\mathbf{K}_{ep}$ **with *3 intersecting yield planes*** $\left(\mathbf{n}_1 \neq \mathbf{n}_2 \neq \mathbf{n}_3\right)$

Consider the three yield surfaces schematically shown in following Fig. 14.

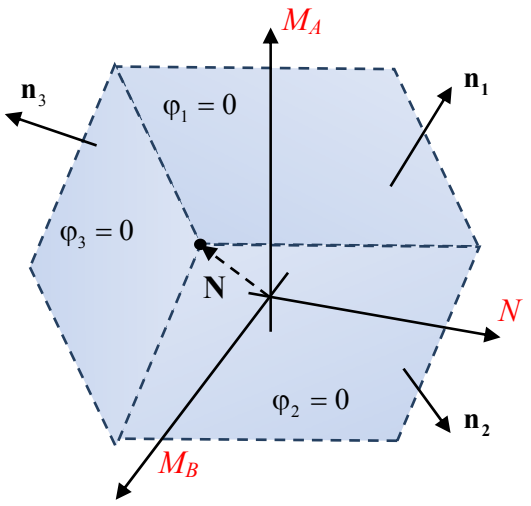

$$\begin{aligned}\varphi_1 &= \mathbf{n}_1^T\mathbf{N} - y_1 \leq 0\\ \varphi_2 &= \mathbf{n}_2^T\mathbf{N} - y_2 \leq 0\\ \varphi_3 &= \mathbf{n}_3^T\mathbf{N} - y_3 \leq 0\end{aligned} \tag{29}$$

Fig. 14: Schematic representation of three hyper-planes in the $\mathbf{N}$-dimensional space of the static variables.

As obtained in Eq. (24), the incremental form of the constraint equations (between the internal static variables) gives:

$$\begin{bmatrix}\dot{\varphi}_1\\ \dot{\varphi}_2\\ \dot{\varphi}_3\end{bmatrix} = \begin{bmatrix}\mathbf{n}_1^T\\ \mathbf{n}_2^T\\ \mathbf{n}_3^T\end{bmatrix}\dot{\mathbf{N}} = \begin{bmatrix}\mathbf{n}_1^T\\ \mathbf{n}_2^T\\ \mathbf{n}_3^T\end{bmatrix}\mathbf{Q}\,\dot{\mathbf{H}} = \begin{bmatrix}0\\ 0\\ 0\end{bmatrix} \tag{30}$$

By using the general relationship between external actions and kinematical quantities, one has:

$$\begin{bmatrix}\dot{\varphi}_1\\ \dot{\varphi}_2\\ \dot{\varphi}_3\end{bmatrix} = \begin{bmatrix}\mathbf{n}_1^T\\ \mathbf{n}_2^T\\ \mathbf{n}_3^T\end{bmatrix}\mathbf{Q}\,\mathbf{K}\dot{\mathbf{u}} + \begin{bmatrix}\mathbf{n}_1^T\\ \mathbf{n}_2^T\\ \mathbf{n}_3^T\end{bmatrix}\mathbf{Q}\,\mathbf{D}\dot{\boldsymbol{\eta}} = \begin{bmatrix}0\\ 0\\ 0\end{bmatrix} \tag{31}$$

According to the normality flow-rule, the internal kinematic variables are expressed as functions of the plastic multiplier rates:

$$\dot{\boldsymbol{\eta}} = \left[\mathbf{n}_1 , \mathbf{n}_2 , \mathbf{n}_3\right] \begin{bmatrix} \dot{\lambda}_1 \\ \dot{\lambda}_2 \\ \dot{\lambda}_3 \end{bmatrix} \tag{32}$$

for which the complementarity rule holds:

$$\begin{bmatrix} \dot{\lambda}_1 \\ \dot{\lambda}_2 \\ \dot{\lambda}_3 \end{bmatrix} \geq \mathbf{0}, \qquad \begin{bmatrix} \varphi_1 \\ \varphi_2 \\ \varphi_3 \end{bmatrix} \leq \mathbf{0}, \qquad \varphi_1 \dot{\lambda}_1 + \varphi_2 \dot{\lambda}_2 + \varphi_3 \dot{\lambda}_3 = 0 \tag{33}$$

Then, the plastic multipliers can be easily computed:

$$\begin{bmatrix} \dot{\varphi}_1 \\ \dot{\varphi}_2 \\ \dot{\varphi}_3 \end{bmatrix} = \begin{bmatrix} \mathbf{n}_1^T \\ \mathbf{n}_2^T \\ \mathbf{n}_3^T \end{bmatrix} \mathbf{Q}\,\mathbf{K}\dot{\mathbf{u}} - \begin{bmatrix} \mathbf{n}_1^T \\ \mathbf{n}_2^T \\ \mathbf{n}_3^T \end{bmatrix} \mathbf{Q}\,\mathbf{K}\mathbf{Q}^T \left[\mathbf{n}_1 , \mathbf{n}_2 , \mathbf{n}_3\right] \begin{bmatrix} \dot{\lambda}_1 \\ \dot{\lambda}_2 \\ \dot{\lambda}_3 \end{bmatrix} = \begin{bmatrix} 0 \\ 0 \\ 0 \end{bmatrix}$$

$$\Rightarrow \quad \begin{bmatrix} \dot{\lambda}_1 \\ \dot{\lambda}_2 \\ \dot{\lambda}_3 \end{bmatrix} = \left(\begin{bmatrix} \mathbf{n}_1^T \\ \mathbf{n}_2^T \\ \mathbf{n}_3^T \end{bmatrix} \mathbf{Q}\,\mathbf{K}\mathbf{Q}^T \left[\mathbf{n}_1 , \mathbf{n}_2 , \mathbf{n}_3\right] \right)^{-1} \begin{bmatrix} \mathbf{n}_1^T \\ \mathbf{n}_2^T \\ \mathbf{n}_3^T \end{bmatrix} \mathbf{Q}\,\mathbf{K}\dot{\mathbf{u}} = \left[\mathbf{n}_1 , \mathbf{n}_2 , \mathbf{n}_3\right]^{-1} \left(\mathbf{Q}\,\mathbf{K}\mathbf{Q}^T\right)^{-1} \mathbf{Q}\,\mathbf{K}\dot{\mathbf{u}} \tag{34}$$

Finally, the elastic-plastic stiffness matrix of the element, in the case in which three yield planes are active in the same time increment, is obtained as follows:

$$\dot{\mathbf{H}} = \mathbf{K}\dot{\mathbf{u}} - \mathbf{K}\mathbf{Q}^T\left[\mathbf{n}_1, \mathbf{n}_2, \mathbf{n}_3\right]\begin{bmatrix}\dot{\lambda}_1\\ \dot{\lambda}_2\\ \dot{\lambda}_3\end{bmatrix} = \mathbf{K}\dot{\mathbf{u}} - \mathbf{K}\mathbf{Q}^T\left(\mathbf{Q}\mathbf{K}\mathbf{Q}^T\right)^{-1}\mathbf{Q}\mathbf{K}\dot{\mathbf{u}} =$$

$$= \underbrace{\left[\mathbf{K} - \mathbf{K}\mathbf{Q}^T\left(\mathbf{Q}\mathbf{K}\mathbf{Q}^T\right)^{-1}\mathbf{Q}\mathbf{K}\right]}_{\mathbf{K}_{ep}}\dot{\mathbf{u}} \equiv \mathbf{0} \tag{35}$$

Through numerical implementations conducted separately, it was observed that matrix $\mathbf{K}_{ep}$ given by Eq. (35) becomes null.

From the mechanical point of view, the writing off of the tangent stiffness matrix can be interpreted as the impossibility of the beam finite element of increasing its static variables in the current step. In fact, for the case in which three perfectly-plastic yield planes keeps active at the same time, the stress point $\mathbf{N}$ is locked at the intersection of these planes, namely in a specific vertex: during the step the motion of the stress point $\mathbf{N}$ is blocked on that corner and the stress rate vector $\dot{\mathbf{N}}$ vanishes.

Determination of matrix $\mathbf{K}_{ep}$ **with** ***4 intersecting yield planes (with, for instance, three*** $(\mathbf{n}_1, \mathbf{n}_2, \mathbf{n}_3)$ ***linearly independent versors)***

It should be underlined that the intersection of more than 3 planes introduces a loss of uniqueness in the analytical description. If, as an example, four planes are considered, according to the previous developments, the plastic multiplier rates are solution of the following linear system:

$$\begin{bmatrix} \dot{\varphi}_1 \\ \dot{\varphi}_2 \\ \dot{\varphi}_3 \\ \dot{\varphi}_4 \end{bmatrix} = \begin{bmatrix} \mathbf{n}_1^T \\ \mathbf{n}_2^T \\ \mathbf{n}_3^T \\ \mathbf{n}_4^T \end{bmatrix} \mathbf{Q}\mathbf{K}\dot{\mathbf{u}} - \begin{bmatrix} \mathbf{n}_1^T \\ \mathbf{n}_2^T \\ \mathbf{n}_3^T \\ \mathbf{n}_4^T \end{bmatrix} \mathbf{Q}\mathbf{K}\mathbf{Q}^T \left[\mathbf{n}_1, \mathbf{n}_2, \mathbf{n}_3, \mathbf{n}_4\right] \begin{bmatrix} \dot{\lambda}_1 \\ \dot{\lambda}_2 \\ \dot{\lambda}_3 \\ \dot{\lambda}_4 \end{bmatrix} = \begin{bmatrix} 0 \\ 0 \\ 0 \\ 0 \end{bmatrix} \tag{36}$$

in which the four normal versors are linearly dependent:

$$\left[\mathbf{n}_1, \mathbf{n}_2, \mathbf{n}_3, \mathbf{n}_4\right] \begin{bmatrix} \zeta_1 \\ \zeta_2 \\ \zeta_3 \\ \zeta_4 \end{bmatrix} = 0 \tag{37}$$

Thus the coefficient matrix of the system in Eq. (36) becomes singular:

$$\det\left(\begin{bmatrix} \mathbf{n}_1^T \\ \mathbf{n}_2^T \\ \mathbf{n}_3^T \\ \mathbf{n}_4^T \end{bmatrix} \mathbf{Q}\mathbf{K}\mathbf{Q}^T \left[\mathbf{n}_1, \mathbf{n}_2, \mathbf{n}_3, \mathbf{n}_4\right] \right) = 0 \tag{38}$$

making it impossible the computation of the plastic multiplier rates.

According to the assumption that the first three versors $(\mathbf{n}_1, \mathbf{n}_2, \mathbf{n}_3)$ are linearly independent (ζ_4 assuming necessarily a non-zero value in this case), one may write:

$$\mathbf{n}_4 = -\left[\mathbf{n}_1, \mathbf{n}_2, \mathbf{n}_3\right] \begin{bmatrix} \zeta_1 \\ \zeta_2 \\ \zeta_3 \end{bmatrix} \frac{1}{\zeta_4} \tag{39}$$

Then, the system admits a solution, given by the following expression:

$$\begin{cases} \begin{bmatrix} \dot{\lambda}_1 \\ \dot{\lambda}_2 \\ \dot{\lambda}_3 \end{bmatrix} = \left[\mathbf{n}_1, \mathbf{n}_2, \mathbf{n}_3\right]^{-1} \left(\mathbf{Q}\,\mathbf{K}\mathbf{Q}^T\right)^{-1} \mathbf{Q}\,\mathbf{K}\dot{\mathbf{u}} + \begin{bmatrix} \zeta_1 \\ \zeta_2 \\ \zeta_3 \end{bmatrix} \rho \\ \dot{\lambda}_4 = \zeta_4\, \rho \end{cases} \tag{40}$$

in which ρ is an arbitrary scalar variable. Therefore, the stress increment becomes:

$$\dot{\mathbf{H}} = \mathbf{K}\dot{\mathbf{u}} - \mathbf{K}\mathbf{Q}^T \left[\mathbf{n}_1, \mathbf{n}_2, \mathbf{n}_3, \mathbf{n}_4\right] \begin{bmatrix} \dot{\lambda}_1 \\ \dot{\lambda}_2 \\ \dot{\lambda}_3 \\ \dot{\lambda}_4 \end{bmatrix} = \underbrace{\left[\mathbf{K} - \mathbf{K}\mathbf{Q}^T \left(\mathbf{Q}\,\mathbf{K}\mathbf{Q}^T\right)^{-1} \mathbf{Q}\,\mathbf{K}\right]}_{\mathbf{K}_{ep}} \dot{\mathbf{u}} \equiv \mathbf{0} \tag{41}$$

As expected, being the stress vector stuck to a vertex of simultaneously-active multiple perfectly-plastic yield planes, the same solution $\dot{\mathbf{H}} = 0$ of the previous three-plane case is obtained.

Determination of matrix $\mathbf{K}_{ep}$ with a generic number "m" of intersecting planes

The discussion outlined in the previous points shows that when the case of "m" intersecting planes is considered, the solution to be used depends on the maximum number i of linearly independent versors and it has to be chosen as the $i-th$ between the previous three solutions, with $n = 1, 2, 3$ planes in the space of the static variables.

4.3 Tangent stiffness determination: a special case

As a simplifying assumption, a piecewise linear uncoupled behaviour can be adopted for the internal static variables, namely a Rankine-type boxed-form yield domain can be assumed in the space of static variables (i.e. a set of couples of planes each orthogonal to the axes of the stress space).

In the following treatment it is shown that, in such a case, the determination of the tangent stiffness matrix presented in previous Section 4.2 can be performed through a Gaussian elimination procedure.

In Fig. 15 a Rankine-type boxed-form yield domain is represented according to the usual 2D interpretation of frames, in which the generalized stresses gathered in vector $\mathbf{N}$ are the bending moments at the extremities of the beam and the axial force (see Section 4.1, Fig. 11).

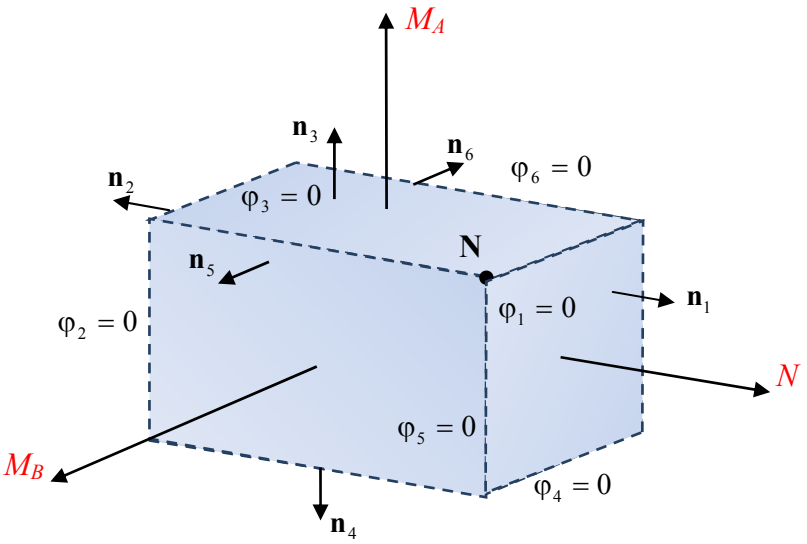

Fig. 15: Rankine-type boxed-form yield domain in the 3-dimensional space of the static variables.

In Section 4.2 it has been demonstrated that, in cases in which the stress point $\mathbf{N}$ belongs simultaneously to 3 or more planes in the space of the static variables, the tangent stiffness matrix becomes null. In the following, the determination of the tangent stiffness matrix through Gaussian elimination is therefore handled in the cases in which only 1 or simultaneously 2 planes are active.

A quite specific case is represented by trusses: being the bending moments identically null, the stress vector is directed along the "N" (*axial*) axis and the same holds for the plastic strain rate vector.

Activation planes:

$$\varphi_1 = \mathbf{n}_1^T \mathbf{N} - y_1 = N - y_1 \le 0$$
$$\varphi_2 = \mathbf{n}_2^T \mathbf{N} - y_2 = -N - y_2 \le 0 \qquad (42)$$

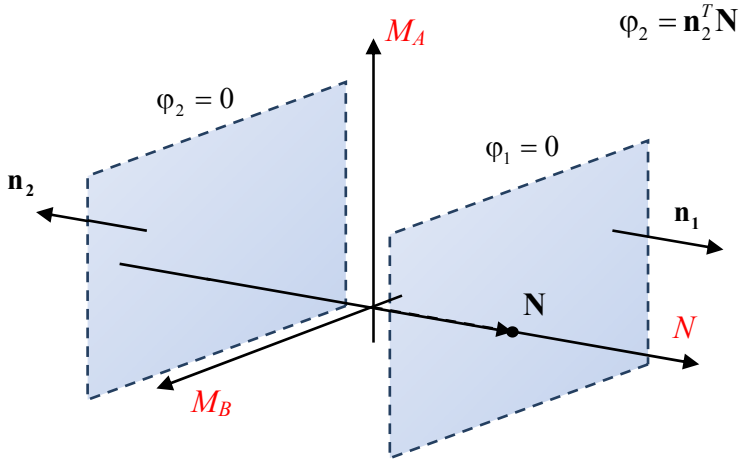

Fig. 16: Representation of the truss beam element's yield domain in the $\mathbf{N}$-dimensional space of the static variables.

Considering, for instance, the activation of the first plane, in light of Eq. (19) the elastic-plastic matrix becomes:

$$\mathbf{n}^T\mathbf{Q} = \begin{bmatrix} 1 & 0 & 0 \end{bmatrix} \begin{bmatrix} 0 & 0 & 0 & 1 & 0 & 0 \\ 0 & 0 & -1 & 0 & 0 & 0 \\ 0 & 0 & 0 & 0 & 0 & 1 \end{bmatrix} = \begin{bmatrix} 0 & 0 & 0 & 1 & 0 & 0 \end{bmatrix} \qquad (43)$$

$$\frac{\mathbf{K}\mathbf{Q}^T\mathbf{n}\,\mathbf{n}^T\mathbf{Q}\mathbf{K}}{\mathbf{n}^T\mathbf{Q}\mathbf{K}\mathbf{Q}^T\mathbf{n}} = \begin{bmatrix} EA/L & 0 & 0 & -EA/L & 0 & 0 \\ 0 & 0 & 0 & 0 & 0 & 0 \\ 0 & 0 & 0 & 0 & 0 & 0 \\ -EA/L & 0 & 0 & EA/L & 0 & 0 \\ 0 & 0 & 0 & 0 & 0 & 0 \\ 0 & 0 & 0 & 0 & 0 & 0 \end{bmatrix} \tag{44}$$

$$\mathbf{K}_{ep} = \mathbf{K} - \frac{\mathbf{K}\mathbf{Q}^T\mathbf{n}\,\mathbf{n}^T\mathbf{Q}\mathbf{K}}{\mathbf{n}^T\mathbf{Q}\mathbf{K}\mathbf{Q}^T\mathbf{n}} = \begin{bmatrix} 0 & 0 & 0 & 0 & 0 & 0 \\ 0 & 12EJ/L^3 & 6EJ/L^2 & 0 & -12EJ/L^3 & 6EJ/L^2 \\ 0 & 6EJ/L^2 & 4EJ/L & 0 & -6EJ/L^2 & 2EJ/L \\ 0 & 0 & 0 & 0 & 0 & 0 \\ 0 & -12EJ/L^3 & -6EJ/L^2 & 0 & 12EJ/L^3 & -6EJ/L^2 \\ 0 & 6EJ/L^2 & 2EJ/L & 0 & -6EJ/L^2 & 4EJ/L \end{bmatrix} \tag{45}$$

The same result can be obtained with the following considerations.

The governing equilibrium system of the element can be written as:

$$\dot{\mathbf{H}} = \mathbf{K}\dot{\mathbf{u}} + \mathbf{D}\dot{\eta}\,, \qquad \dot{\boldsymbol{\eta}} = \begin{bmatrix} \dot{\eta} \\ 0 \\ 0 \end{bmatrix}, \qquad \dot{N} = \dot{H}_B = 0 \tag{46}$$

Above Eq. (46) can be written also, by re-ordering the various quantities, as follows:

$$\underbrace{\begin{bmatrix} 0 \\ \dot{H}_A \\ \dot{V}_A \\ \dot{W}_A \\ \dot{H}_B \\ \dot{V}_B \\ \dot{W}_B \end{bmatrix}}_{\mathbf{R}} = \underbrace{\left[\begin{array}{c|cccccc} \mathbf{D(4,1)} & \multicolumn{6}{c}{\mathbf{K(4,:)}} \\ -EA/L & -EA/L & 0 & 0 & EA/L & 0 & 0 \\ \hline EA/L & EA/L & 0 & 0 & -EA/L & 0 & 0 \\ 0 & 0 & 12EJ/L^3 & 6EJ/L^2 & 0 & -12EJ/L^3 & 6EJ/L^2 \\ 0 & 0 & 6EJ/L^2 & 4EJ/L & 0 & -6EJ/L^2 & 2EJ/L \\ -EA/L & -EA/L & 0 & 0 & EA/L & 0 & 0 \\ 0 & 0 & -12EJ/L^3 & -6EJ/L^2 & 0 & 12EJ/L^3 & -6EJ/L^2 \\ 0 & 0 & 6EJ/L^2 & 2EJ/L & 0 & -6EJ/L^2 & 4EJ/L \end{array}\right]}_{\mathbf{M}} \begin{bmatrix} \dot{\eta} \\ \dot{u}_A \\ \dot{v}_A \\ \dot{\psi}_A \\ \dot{u}_B \\ \dot{v}_B \\ \dot{\psi}_B \end{bmatrix} \tag{47}$$

In order to eliminate the axial plastic strain rate $\dot{\eta}$ from the relation above, if a complete Gaussian elimination is applied to the first column, by considering the element M_{11} as pivot, one obtains:

$$\begin{cases} \hat{\mathbf{M}} = \mathbf{M} - \dfrac{\mathbf{M}(:,1)\mathbf{M}(1,:)}{M_{11}} \\ \hat{\mathbf{R}} = \mathbf{R} - \dfrac{R_1\,\mathbf{M}(:,1)}{M_{11}} \end{cases} \tag{48}$$

$$\hat{\mathbf{M}} = \begin{bmatrix} 0 & 0 & 0 & 0 & 0 & 0 & 0 \\ 0 & 0 & 0 & 0 & 0 & 0 & 0 \\ 0 & 0 & 12EJ/L^3 & 6EJ/L^2 & 0 & -12EJ/L^3 & 6EJ/L^2 \\ 0 & 0 & 6EJ/L^2 & 4EJ/L & 0 & -6EJ/L^2 & 2EJ/L \\ 0 & 0 & 0 & 0 & 0 & 0 & 0 \\ 0 & 0 & -12EJ/L^3 & -6EJ/L^2 & 0 & 12EJ/L^3 & -6EJ/L^2 \\ 0 & 0 & 6EJ/L^2 & 2EJ/L & 0 & -6EJ/L^2 & 4EJ/L \end{bmatrix}, \quad \hat{\mathbf{R}} = \mathbf{R} \tag{49}$$

$\hat{\mathbf{K}}$

where the marked sub-matrix $\hat{\mathbf{K}}$ in Eq. (49) corresponds to the tangent stiffness matrix $\mathbf{K}_{ep}$ determined by Eq. (45). It is worthwhile to observe that matrix $\hat{\mathbf{K}}$ can be directly calculated as follows:

$$\hat{\mathbf{K}} = \mathbf{K} - \frac{\mathbf{D}(:,1)\mathbf{K}(4,:)}{D_{41}} \tag{50}$$

Finally, the governing equilibrium system described by Eq. (46) becomes:

$$\underbrace{\begin{bmatrix} \dot{H}_A \\ \dot{V}_A \\ \dot{W}_A \\ \dot{H}_B \\ \dot{V}_B \\ \dot{W}_B \end{bmatrix}}_{\dot{\mathbf{H}}} = \underbrace{\begin{bmatrix} 0 & 0 & 0 & 0 & 0 & 0 \\ 0 & 12EJ/L^3 & 6EJ/L^2 & 0 & -12EJ/L^3 & 6EJ/L^2 \\ 0 & 6EJ/L^2 & 4EJ/L & 0 & -6EJ/L^2 & 2EJ/L \\ 0 & 0 & 0 & 0 & 0 & 0 \\ 0 & -12EJ/L^3 & -6EJ/L^2 & 0 & 12EJ/L^3 & -6EJ/L^2 \\ 0 & 6EJ/L^2 & 2EJ/L & 0 & -6EJ/L^2 & 4EJ/L \end{bmatrix}}_{\mathbf{K}_{ep}} \underbrace{\begin{bmatrix} \dot{u}_A \\ \dot{v}_A \\ \dot{\psi}_A \\ \dot{u}_B \\ \dot{v}_B \\ \dot{\psi}_B \end{bmatrix}}_{\dot{\mathbf{u}}} \tag{51}$$

where the fourth equation (actually lost by the above Gauss elimination) can be replaced by the original one:

$$\dot{\eta} = \dot{u}_B - \dot{u}_A \tag{52}$$

In the following, the cases in which the relative rotation rate $\dot{\phi}_A$, or $\dot{\phi}_B$, or both of them occur in a critical section are presented.

Plastic hinge at beam extreme A

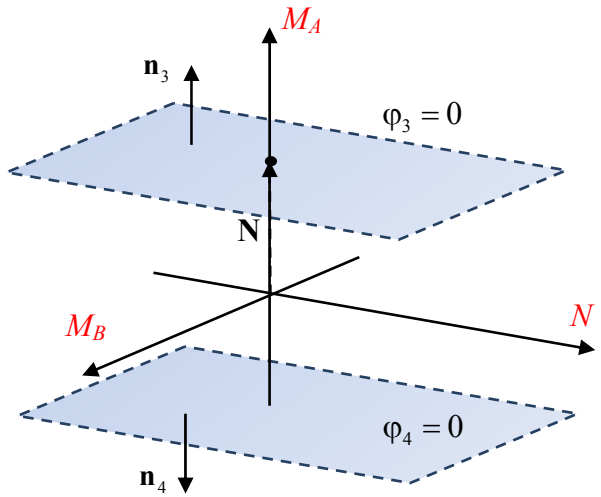

Activation planes:

$$\varphi_3 = \mathbf{n}_3^T\mathbf{N} - y_3 = M_A - y_3 \le 0$$
$$\varphi_4 = \mathbf{n}_4^T\mathbf{N} - y_4 = -M_A - y_4 \le 0 \qquad (53)$$

Fig. 17: Representation of the yield domain in the $\mathbf{N}$-dimensional space of the static variables considering a plastic hinge at node A of the beam finite element.

Considering, for instance, the activation of the upper plane; the elastic-plastic matrix becomes:

$$\mathbf{n}^T\mathbf{Q} = \begin{bmatrix}0 & 1 & 0\end{bmatrix}\begin{bmatrix}0 & 0 & 0 & 1 & 0 & 0\\ 0 & 0 & -1 & 0 & 0 & 0\\ 0 & 0 & 0 & 0 & 0 & 1\end{bmatrix} = \begin{bmatrix}0 & 0 & -1 & 0 & 0 & 0\end{bmatrix} \qquad (54)$$

$$\frac{\mathbf{K}\mathbf{Q}^T\mathbf{n}\,\mathbf{n}^T\mathbf{Q}\mathbf{K}}{\mathbf{n}^T\mathbf{Q}\mathbf{K}\mathbf{Q}^T\mathbf{n}} = \begin{bmatrix}0 & 0 & 0 & 0 & 0 & 0\\ 0 & 9EJ/L^3 & 6EJ/L^2 & 0 & -9EJ/L^3 & 3EJ/L^2\\ 0 & 6EJ/L^2 & 4EJ/L & 0 & -6EJ/L^2 & 2EJ/L\\ 0 & 0 & 0 & 0 & 0 & 0\\ 0 & -9EJ/L^3 & -6EJ/L^2 & 0 & 9EJ/L^3 & -3EJ/L^2\\ 0 & 3EJ/L^2 & 2EJ/L & 0 & -3EJ/L^2 & EJ/L\end{bmatrix} \qquad (55)$$

$$\mathbf{K}^{ep} = \mathbf{K} - \frac{\mathbf{K}\mathbf{Q}^T\mathbf{n}\,\mathbf{n}^T\mathbf{Q}\mathbf{K}}{\mathbf{n}^T\mathbf{Q}\mathbf{K}\mathbf{Q}^T\mathbf{n}} = \begin{bmatrix} EA/L & 0 & 0 & -EA/L & 0 & 0 \\ 0 & 3EJ/L^3 & 0 & 0 & -3EJ/L^3 & 3EJ/L^2 \\ 0 & 0 & 0 & 0 & 0 & 0 \\ -EA/L & 0 & 0 & EA/L & 0 & 0 \\ 0 & -3EJ/L^3 & 0 & 0 & 3EJ/L^3 & -3EJ/L^2 \\ 0 & 3EJ/L^2 & 0 & 0 & -3EJ/L^2 & 3EJ/L \end{bmatrix} \tag{56}$$

The same result can be obtained with the following considerations.

The governing equilibrium system of the element can be written as:

$$\dot{\mathbf{H}} = \mathbf{K}\dot{\mathbf{u}} + \mathbf{D}\dot{\boldsymbol{\eta}}, \qquad \dot{\boldsymbol{\eta}} = \begin{bmatrix} 0 \\ \dot{\phi}_A \\ 0 \end{bmatrix}, \qquad \dot{M}_A = \dot{W}_A = 0 \tag{57}$$

i.e., by re-ordering the various quantities:

$$\underbrace{\begin{bmatrix} 0 \\ \dot{H}_A \\ \dot{V}_A \\ \dot{W}_A \\ \dot{H}_B \\ \dot{V}_B \\ \dot{W}_B \end{bmatrix}}_{\mathbf{R}} = \underbrace{\left[\begin{array}{c|cccccc} 4EJ/L & 0 & 6EJ/L^2 & 4EJ/L & 0 & -6EJ/L^2 & 2EJ/L \\ \hline 0 & EA/L & 0 & 0 & -EA/L & 0 & 0 \\ 6EJ/L^2 & 0 & 12EJ/L^3 & 6EJ/L^2 & 0 & -12EJ/L^3 & 6EJ/L^2 \\ 4EJ/L & 0 & 6EJ/L^2 & 4EJ/L & 0 & -6EJ/L^2 & 2EJ/L \\ 0 & -EA/L & 0 & 0 & EA/L & 0 & 0 \\ -6EJ/L^2 & 0 & -12EJ/L^3 & -6EJ/L^2 & 0 & 12EJ/L^3 & -6EJ/L^2 \\ 2EJ/L & 0 & 6EJ/L^2 & 2EJ/L & 0 & -6EJ/L^2 & 4EJ/L \end{array}\right]}_{\mathbf{M}} \begin{bmatrix} \dot{\phi}_A \\ \dot{u}_A \\ \dot{v}_A \\ \dot{\psi}_A \\ \dot{u}_B \\ \dot{v}_B \\ \dot{\psi}_B \end{bmatrix} \tag{58}$$

In order to eliminate the relative rotation rate $\dot{\phi}_A$ from the relations above, a complete Gaussian elimination is applied to the first column, by considering the element M_{11} as pivot, to obtain:

$$\begin{cases} \hat{\mathbf{M}} = \mathbf{M} - \dfrac{\mathbf{M}(:,1)\mathbf{M}(1,:)}{M_{11}} \;\Rightarrow\; \hat{\mathbf{K}} = \mathbf{K} - \dfrac{\mathbf{D}(:,2)\mathbf{K}(3,:)}{D_{32}} \\ \hat{\mathbf{R}} = \mathbf{R} - \dfrac{R_1\,\mathbf{M}(:,1)}{M_{11}} \end{cases} \tag{59}$$

$$\hat{\mathbf{M}} = \left[\begin{array}{c|cccccc} 0 & 0 & 0 & 0 & 0 & 0 & 0 \\ \hline 0 & EA/L & 0 & 0 & -EA/L & 0 & 0 \\ 0 & 0 & 3EJ/L^3 & 0 & 0 & -3EJ/L^3 & 3EJ/L^2 \\ 0 & 0 & 0 & 0 & 0 & 0 & 0 \\ 0 & -EA/L & 0 & 0 & EA/L & 0 & 0 \\ 0 & 0 & -3EJ/L^3 & 0 & 0 & 3EJ/L^3 & -3EJ/L^2 \\ 0 & 0 & 3EJ/L^2 & 0 & 0 & -3EJ/L^2 & 3EJ/L \end{array}\right], \quad \hat{\mathbf{R}} = \mathbf{R} \tag{60}$$

Then:

$$\begin{bmatrix} \dot{H}_A \\ \dot{V}_A \\ \dot{W}_A \\ \dot{H}_B \\ \dot{V}_B \\ \dot{W}_B \end{bmatrix} = \begin{bmatrix} EA/L & 0 & 0 & -EA/L & 0 & 0 \\ 0 & 3EJ/L^3 & 0 & 0 & -3EJ/L^3 & 3EJ/L^2 \\ 0 & 0 & 0 & 0 & 0 & 0 \\ -EA/L & 0 & 0 & EA/L & 0 & 0 \\ 0 & -3EJ/L^3 & 0 & 0 & 3EJ/L^3 & -3EJ/L^2 \\ 0 & 3EJ/L^2 & 0 & 0 & -3EJ/L^2 & 3EJ/L \end{bmatrix} \begin{bmatrix} \dot{u}_A \\ \dot{v}_A \\ \dot{\psi}_A \\ \dot{u}_B \\ \dot{v}_B \\ \dot{\psi}_B \end{bmatrix} \tag{61}$$

where the third equation (actually lost by this complete elimination) can be replaced by the original one:

$$\dot{\phi}_A = \frac{3}{2}\frac{\dot{v}_B - \dot{v}_A}{L} - \dot{\psi}_A - \frac{1}{2}\dot{\psi}_B \tag{62}$$

Plastic hinge at beam extreme B

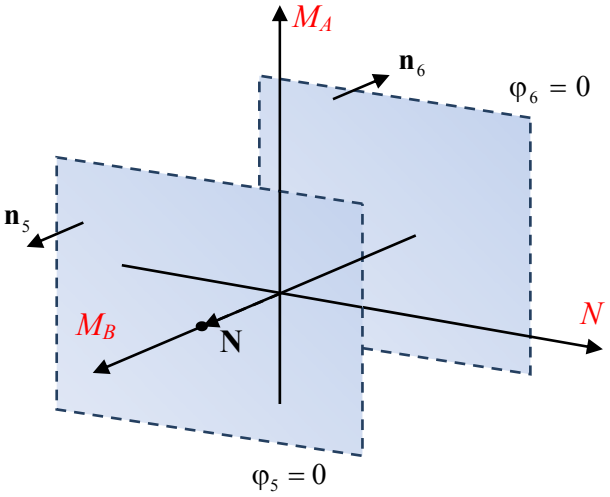

Activation planes:

$$\varphi_5 = \mathbf{n}_5^T\mathbf{N} - y_5 = M_B - y_5 \le 0$$
$$\varphi_6 = \mathbf{n}_6^T\mathbf{N} - y_6 = -M_B - y_6 \le 0 \qquad (63)$$

Fig. 18: Representation of the yield domain in the $\mathbf{N}$-dimensional space of the static variables considering a plastic hinge at node B of the beam finite element.

Considering, for instance, the activation of the front plane, the elastic-plastic matrix becomes:

$$\mathbf{n}^T\mathbf{Q} = \begin{bmatrix}0 & 0 & 1\end{bmatrix}\begin{bmatrix}0 & 0 & 0 & 1 & 0 & 0\\ 0 & 0 & -1 & 0 & 0 & 0\\ 0 & 0 & 0 & 0 & 0 & 1\end{bmatrix} = \begin{bmatrix}0 & 0 & 0 & 0 & 0 & 1\end{bmatrix} \qquad (64)$$

$$\frac{\mathbf{K}\mathbf{Q}^T\mathbf{n}\,\mathbf{n}^T\mathbf{Q}\,\mathbf{K}}{\mathbf{n}^T\mathbf{Q}\,\mathbf{K}\mathbf{Q}^T\mathbf{n}} = \begin{bmatrix}0 & 0 & 0 & 0 & 0 & 0\\ 0 & 9EJ/L^3 & 3EJ/L^2 & 0 & -9EJ/L^3 & 6EJ/L^2\\ 0 & 3EJ/L^2 & EJ/L & 0 & -3EJ/L^2 & 2EJ/L\\ 0 & 0 & 0 & 0 & 0 & 0\\ 0 & -9EJ/L^3 & -3EJ/L^2 & 0 & 9EJ/L^3 & -6EJ/L^2\\ 0 & 6EJ/L^2 & 2EJ/L & 0 & -6EJ/L^2 & 4EJ/L\end{bmatrix} \qquad (65)$$

$$\mathbf{K}^{ep} = \mathbf{K} - \frac{\mathbf{K}\mathbf{Q}^T\mathbf{n}\,\mathbf{n}^T\mathbf{Q}\,\mathbf{K}}{\mathbf{n}^T\mathbf{Q}\,\mathbf{K}\mathbf{Q}^T\mathbf{n}} = \begin{bmatrix} EA/L & 0 & 0 & -EA/L & 0 & 0 \\ 0 & 3EJ/L^3 & 3EJ/L^2 & 0 & -3EJ/L^3 & 0 \\ 0 & 3EJ/L^2 & 3EJ/L & 0 & -3EJ/L^2 & 0 \\ -EA/L & 0 & 0 & EA/L & 0 & 0 \\ 0 & -3EJ/L^3 & -3EJ/L^2 & 0 & 3EJ/L^3 & 0 \\ 0 & 0 & 0 & 0 & 0 & 0 \end{bmatrix} \tag{66}$$

The same result can be obtained by the following considerations.

The governing equilibrium system of the element can be written as:

$$\dot{\mathbf{H}} = \mathbf{K}\dot{\mathbf{u}} + \mathbf{D}\dot{\boldsymbol{\eta}}, \qquad \dot{\boldsymbol{\eta}} = \begin{bmatrix} 0 \\ 0 \\ \dot{\phi}_B \end{bmatrix}, \qquad \dot{M}_B = \dot{W}_B = 0 \tag{67}$$

i.e., by re-ordering the various quantities:

$$\underbrace{\begin{bmatrix} 0 \\ \dot{H}_A \\ \dot{V}_A \\ \dot{W}_A \\ \dot{H}_B \\ \dot{V}_B \\ \dot{W}_B \end{bmatrix}}_{\mathbf{R}} = \underbrace{\left[\begin{array}{c|cccccc} -4EJ/L & 0 & 6EJ/L^2 & 2EJ/L & 0 & -6EJ/L^2 & 4EJ/L \\ \hline 0 & EA/L & 0 & 0 & -EA/L & 0 & 0 \\ -6EJ/L^2 & 0 & 12EJ/L^3 & 6EJ/L^2 & 0 & -12EJ/L^3 & 6EJ/L^2 \\ -2EJ/L & 0 & 6EJ/L^2 & 4EJ/L & 0 & -6EJ/L^2 & 2EJ/L \\ 0 & -EA/L & 0 & 0 & EA/L & 0 & 0 \\ 6EJ/L^2 & 0 & -12EJ/L^3 & -6EJ/L^2 & 0 & 12EJ/L^3 & -6EJ/L^2 \\ -4EJ/L & 0 & 6EJ/L^2 & 2EJ/L & 0 & -6EJ/L^2 & 4EJ/L \end{array}\right]}_{\mathbf{M}} \begin{bmatrix} \dot{\phi}_B \\ \dot{u}_A \\ \dot{v}_A \\ \dot{\psi}_A \\ \dot{u}_B \\ \dot{v}_B \\ \dot{\psi}_B \end{bmatrix} \tag{68}$$

In order to eliminate the relative rotation rate $\dot{\phi}_B$ from the above relation, a complete Gaussian elimination is applied to the first column, by considering the element M_{11} as pivot, to obtain:

$$\begin{cases} \hat{\mathbf{M}} = \mathbf{M} - \dfrac{\mathbf{M}(:,1)\mathbf{M}(1,:)}{M_{11}} \;\Rightarrow\; \hat{\mathbf{K}} = \mathbf{K} - \dfrac{\mathbf{D}(:,3)\mathbf{K}(6,:)}{D_{63}} \\ \hat{\mathbf{R}} = \mathbf{R} - \dfrac{R_1\mathbf{M}(:,1)}{M_{11}} \end{cases} \tag{69}$$

$$\hat{\mathbf{M}} = \left[\begin{array}{c|cccccc} 0 & 0 & 0 & 0 & 0 & 0 & 0 \\ \hline 0 & EA/L & 0 & 0 & -EA/L & 0 & 0 \\ 0 & 0 & 3EJ/L^3 & 3EJ/L^2 & 0 & -3EJ/L^3 & 0 \\ 0 & 0 & 3EJ/L^2 & 3EJ/L & 0 & -3EJ/L^2 & 0 \\ 0 & -EA/L & 0 & 0 & EA/L & 0 & 0 \\ 0 & 0 & -3EJ/L^3 & -3EJ/L^2 & 0 & 3EJ/L^3 & 0 \\ 0 & 0 & 0 & 0 & 0 & 0 & 0 \end{array}\right], \quad \hat{\mathbf{R}} = \mathbf{R} \tag{70}$$

Then:

$$\begin{bmatrix} \dot{H}_A \\ \dot{V}_A \\ \dot{W}_A \\ \dot{H}_B \\ \dot{V}_B \\ \dot{W}_B \end{bmatrix} = \begin{bmatrix} EA/L & 0 & 0 & -EA/L & 0 & 0 \\ 0 & 3EJ/L^3 & 3EJ/L^2 & 0 & -3EJ/L^3 & 0 \\ 0 & 3EJ/L^2 & 3EJ/L & 0 & -3EJ/L^2 & 0 \\ -EA/L & 0 & 0 & EA/L & 0 & 0 \\ 0 & -3EJ/L^3 & -3EJ/L^2 & 0 & 3EJ/L^3 & 0 \\ 0 & 0 & 0 & 0 & 0 & 0 \end{bmatrix} \begin{bmatrix} \dot{u}_A \\ \dot{v}_A \\ \dot{\psi}_A \\ \dot{u}_B \\ \dot{v}_B \\ \dot{\psi}_B \end{bmatrix} \tag{71}$$

where the sixth equation (actually lost by this complete elimination) can be replaced by the original one:

$$\dot{\phi}_B = -\frac{3}{2}\frac{\dot{v}_B - \dot{v}_A}{L} + \frac{1}{2}\dot{\psi}_A + \dot{\psi}_B \tag{72}$$

Plastic hinge at beam extremes A and B

Activation planes:

$$\begin{aligned}
\varphi_3 &= \mathbf{n}_3^T\mathbf{N} - y_3 = M_A - y_3 \le 0 \\
\varphi_4 &= \mathbf{n}_4^T\mathbf{N} - y_4 = -M_A - y_4 \le 0 \\
\varphi_5 &= \mathbf{n}_5^T\mathbf{N} - y_5 = M_B - y_5 \le 0 \\
\varphi_6 &= \mathbf{n}_6^T\mathbf{N} - y_6 = -M_B - y_6 \le 0
\end{aligned} \tag{73}$$

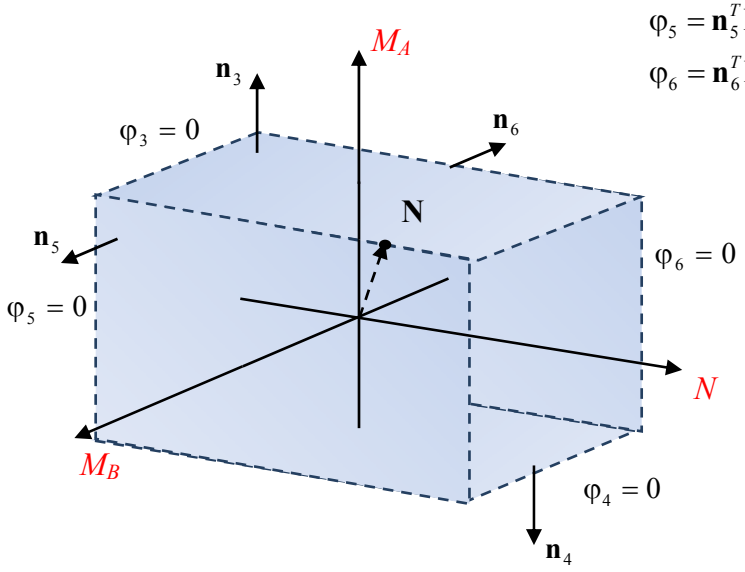

Fig. 19: Representation of the yield domain in the $\mathbf{N}$-dimensional space of the static variables considering a plastic hinges at node A and B of the beam finite element.

Considering, for instance, the activation of the front planes, the elastic-plastic matrix becomes:

$$\begin{bmatrix} \mathbf{n}_3^T \\ \mathbf{n}_5^T \end{bmatrix}\mathbf{Q} = \begin{bmatrix} 0 & 1 & 0 \\ 0 & 0 & 1 \end{bmatrix}\begin{bmatrix} 0 & 0 & 0 & 1 & 0 & 0 \\ 0 & 0 & -1 & 0 & 0 & 0 \\ 0 & 0 & 0 & 0 & 0 & 1 \end{bmatrix} = \begin{bmatrix} 0 & 0 & -1 & 0 & 0 & 0 \\ 0 & 0 & 0 & 0 & 0 & 1 \end{bmatrix} \tag{74}$$

$$\mathbf{K}\mathbf{Q}^T\left[\mathbf{n}_3,\mathbf{n}_5\right]\left(\begin{bmatrix}\mathbf{n}_3^T\\ \mathbf{n}_5^T\end{bmatrix}\mathbf{Q}\,\mathbf{K}\mathbf{Q}^T\left[\mathbf{n}_3,\mathbf{n}_5\right]\right)^{-1}\begin{bmatrix}\mathbf{n}_3^T\\ \mathbf{n}_5^T\end{bmatrix}\mathbf{Q}\,\mathbf{K}=$$

$$=\begin{bmatrix}0 & 0 & 0 & 0 & 0 & 0\\ 0 & 12EJ/L^3 & 6EJ/L^2 & 0 & -12EJ/L^3 & 6EJ/L^2\\ 0 & 6EJ/L^2 & 4EJ/L & 0 & -6EJ/L^2 & 2EJ/L\\ 0 & 0 & 0 & 0 & 0 & 0\\ 0 & -12EJ/L^3 & -6EJ/L^2 & 0 & 12EJ/L^3 & -6EJ/L^2\\ 0 & 6EJ/L^2 & 2EJ/L & 0 & -6EJ/L^2 & 4EJ/L\end{bmatrix} \tag{75}$$

$$\mathbf{K}^{ep}=\mathbf{K}-\mathbf{K}\mathbf{Q}^T\left[\mathbf{n}_3,\mathbf{n}_5\right]\left(\begin{bmatrix}\mathbf{n}_3^T\\ \mathbf{n}_5^T\end{bmatrix}\mathbf{Q}\,\mathbf{K}\mathbf{Q}^T\left[\mathbf{n}_3,\mathbf{n}_5\right]\right)^{-1}\begin{bmatrix}\mathbf{n}_3^T\\ \mathbf{n}_5^T\end{bmatrix}\mathbf{Q}\,\mathbf{K}=\begin{bmatrix}EA/L & 0 & 0 & -EA/L & 0 & 0\\ 0 & 0 & 0 & 0 & 0 & 0\\ 0 & 0 & 0 & 0 & 0 & 0\\ -EA/L & 0 & 0 & EA/L & 0 & 0\\ 0 & 0 & 0 & 0 & 0 & 0\\ 0 & 0 & 0 & 0 & 0 & 0\end{bmatrix} \tag{76}$$

The same result can be obtained with the following considerations.

The governing equilibrium system of the element can be written as:

$$\dot{\mathbf{H}}=\mathbf{K}\dot{\mathbf{u}}+\mathbf{D}\dot{\boldsymbol{\eta}},\qquad \dot{\boldsymbol{\eta}}=\begin{bmatrix}0\\ \dot{\phi}_A\\ \dot{\phi}_B\end{bmatrix},\qquad \begin{cases}\dot{M}_A=\dot{W}_A=0\\ \dot{M}_B=\dot{W}_B=0\end{cases} \tag{77}$$

i.e., by re-ordering the various quantities:

$$\underbrace{\begin{bmatrix}0\\ 0\\ \dot{H}_A\\ \dot{V}_A\\ \dot{W}_A\\ \dot{H}_B\\ \dot{V}_B\\ \dot{W}_B\end{bmatrix}}_{\mathbf{R}}=\underbrace{\left[\begin{array}{cc|c|cccc}4EJ/L & -2EJ/L & 0 & 6EJ/L^2 & 4EJ/L & 0 & -6EJ/L^2 & 2EJ/L\\ 2EJ/L & -4EJ/L & 0 & 6EJ/L^2 & 2EJ/L & 0 & -6EJ/L^2 & 4EJ/L\\ \hline 0 & 0 & EA/L & 0 & 0 & -EA/L & 0 & 0\\ 6EJ/L^2 & -6EJ/L^2 & 0 & 12EJ/L^3 & 6EJ/L^2 & 0 & -12EJ/L^3 & 6EJ/L^2\\ 4EJ/L & -2EJ/L & 0 & 6EJ/L^2 & 4EJ/L & 0 & -6EJ/L^2 & 2EJ/L\\ 0 & 0 & -EA/L & 0 & 0 & EA/L & 0 & 0\\ -6EJ/L^2 & 6EJ/L^2 & 0 & -12EJ/L^3 & -6EJ/L^2 & 0 & 12EJ/L^3 & -6EJ/L^2\\ 2EJ/L & -4EJ/L & 0 & 6EJ/L^2 & 2EJ/L & 0 & -6EJ/L^2 & 4EJ/L\end{array}\right]}_{\mathbf{M}}\begin{bmatrix}\dot{\phi}_A\\ \dot{\phi}_B\\ \dot{u}_A\\ \dot{v}_A\\ \dot{\psi}_A\\ \dot{u}_B\\ \dot{v}_B\\ \dot{\psi}_B\end{bmatrix} \tag{78}$$

In order to eliminate the relative rotation rates $\dot{\phi}_A$ and $\dot{\phi}_B$ from the relations above, a complete Gaussian elimination is applied to the first two columns, by considering the elements M_{11} and $\hat{M}_{22}$ as pivots, in a sequence, to obtain:

$$\begin{cases} \hat{\mathbf{M}} = \mathbf{M} - \dfrac{\mathbf{M}(:,1)\mathbf{M}(1,:)}{M_{11}} \;\Rightarrow\; \hat{\mathbf{K}} = \mathbf{K} - \dfrac{\mathbf{D}(:,2)\mathbf{K}(3,:)}{D_{32}} \\ \hat{\mathbf{R}} = \mathbf{R} - \dfrac{R_1\mathbf{M}(:,1)}{M_{11}}, \quad \hat{\mathbf{D}} = \mathbf{D} - \dfrac{\mathbf{D}(:,2)\mathbf{D}(3,:)}{D_{32}} \end{cases} \tag{79}$$

$$\begin{cases} \hat{\hat{\mathbf{M}}} = \hat{\mathbf{M}} - \dfrac{\hat{\mathbf{M}}(:,2)\hat{\mathbf{M}}(2,:)}{\hat{M}_{22}} \;\Rightarrow\; \hat{\hat{\mathbf{K}}} = \hat{\mathbf{K}} - \dfrac{\hat{\mathbf{D}}(:,3)\hat{\mathbf{K}}(6,:)}{\hat{D}_{63}} \\ \hat{\hat{\mathbf{R}}} = \hat{\mathbf{R}} - \dfrac{\hat{R}_2\hat{\mathbf{M}}(:,2)}{\hat{M}_{22}} \end{cases} \tag{80}$$

$$\hat{\hat{\mathbf{M}}} = \left[\begin{array}{cc:cccccc} 0 & 0 & 0 & 0 & 0 & 0 & 0 & 0 \\ 0 & 0 & 0 & 0 & 0 & 0 & 0 & 0 \\ \hdashline 0 & 0 & EA/L & 0 & 0 & -EA/L & 0 & 0 \\ 0 & 0 & 0 & 0 & 0 & 0 & 0 & 0 \\ 0 & 0 & 0 & 0 & 0 & 0 & 0 & 0 \\ 0 & 0 & -EA/L & 0 & 0 & EA/L & 0 & 0 \\ 0 & 0 & 0 & 0 & 0 & 0 & 0 & 0 \\ 0 & 0 & 0 & 0 & 0 & 0 & 0 & 0 \end{array}\right], \quad \hat{\hat{\mathbf{R}}} = \mathbf{R} \tag{81}$$

Then:

$$\begin{bmatrix} \dot{H}_A \\ \dot{V}_A \\ \dot{W}_A \\ \dot{H}_B \\ \dot{V}_B \\ \dot{W}_B \end{bmatrix} = \begin{bmatrix} EA/L & 0 & 0 & -EA/L & 0 & 0 \\ 0 & 0 & 0 & 0 & 0 & 0 \\ 0 & 0 & 0 & 0 & 0 & 0 \\ -EA/L & 0 & 0 & EA/L & 0 & 0 \\ 0 & 0 & 0 & 0 & 0 & 0 \\ 0 & 0 & 0 & 0 & 0 & 0 \end{bmatrix} \begin{bmatrix} \dot{u}_A \\ \dot{v}_A \\ \dot{\psi}_A \\ \dot{u}_B \\ \dot{v}_B \\ \dot{\psi}_B \end{bmatrix} \tag{82}$$

where the third and sixth equations (actually lost by this complete eliminations) can be replaced by the original ones:

$$\dot{\phi}_A = \frac{\dot{v}_B - \dot{v}_A}{L} - \dot{\psi}_A, \qquad \dot{\phi}_B = \frac{\dot{v}_A - \dot{v}_B}{L} + \dot{\psi}_B \tag{83}$$

It is worth to underline that the order in the sequence of two Gaussian eliminations does not alter the result, as it is expected from the mechanical point of view; namely it can be shown that by defining, as a first sequence:

$$\begin{aligned} \hat{\mathbf{K}} &= \mathbf{K} - \frac{\mathbf{D}(:,2)\mathbf{K}(3,:)}{D_{32}}, \quad \hat{\mathbf{D}} = \mathbf{D} - \frac{\mathbf{D}(:,2)\mathbf{D}(3,:)}{D_{32}} \\ \hat{\hat{\mathbf{K}}} &= \hat{\mathbf{K}} - \frac{\hat{\mathbf{D}}(:,3)\hat{\mathbf{K}}(6,:)}{\hat{D}_{63}}, \quad \hat{\hat{\mathbf{D}}} = \hat{\mathbf{D}} - \frac{\hat{\mathbf{D}}(:,3)\hat{\mathbf{D}}(6,:)}{\hat{D}_{63}} \end{aligned} \tag{84}$$

and as an alternative sequence:

$$\begin{aligned} \hat{\mathbf{K}}' &= \mathbf{K} - \frac{\mathbf{D}(:,3)\mathbf{K}(6,:)}{D_{63}}, \quad \hat{\mathbf{D}}' = \mathbf{D} - \frac{\mathbf{D}(:,3)\mathbf{D}(6,:)}{D_{63}} \\ \hat{\hat{\mathbf{K}}}' &= \hat{\mathbf{K}}' - \frac{\hat{\mathbf{D}}'(:,2)\hat{\mathbf{K}}'(3,:)}{\hat{D}'_{32}}, \quad \hat{\hat{\mathbf{D}}}' = \hat{\mathbf{D}}' - \frac{\hat{\mathbf{D}}'(:,2)\hat{\mathbf{D}}'(3,:)}{\hat{D}'_{32}} \end{aligned} \tag{85}$$

one obtains:

$$\hat{\hat{\mathbf{K}}} = \hat{\hat{\mathbf{K}}}' \tag{86}$$

4.4 Solving structural system for truss frame analysis

Consider the simplest structural conservative problem, with linear elastic materials and fixed loads, within the classical assumptions of linearized kinematics and equilibrium referred to the undeformed configuration.

The kinematic constraints acting on a structure modeled by conventional finite elements are quite often imposed in a "direct" way, i.e. some kinematic variables (*dependent variables*) are defined "a priori", as linear combinations of the remaining kinematic variables (*independent variables*), which become the degrees of freedom (dofs) of the assembled system. The main consequence is the compactness of the formulation, with a reduced number of dofs.

This way of operating requires that the constraint equations must be solved for the dependent variables and therefore the equations must be independent from each other. This requirement appears to be quite loose, but there are some cases in which it can introduce limitations on the formulation; for example, when three-dimensional constraints of rigid-body kind or constraints involving projections of dofs along specific directions non parallel to the reference Cartesian axes need to be considered.

In order to avoid such limitations, in the code *Beam3DStp* an alternative innovative procedure has been implemented, which is discussed below.

As a first step, the structure is discretized, as classically done in the finite element method, and assembled by taking into account only the material continuity among finite elements ("full constraint"). During this phase the relative constraints (like hinges, supports, etc.), the absolute constraints and their reactions, are not considered.

The deformation elastic energy $\mathscr{E}(\mathbf{U})$ of the whole (assembled) system is governed by the following quadratic form:

$$\mathscr{E}(\mathbf{U}) = \frac{1}{2}\mathbf{U}^T\mathbf{K}\,\mathbf{U} \tag{87}$$

in which vector $\mathbf{U}$ collects all nodal dofs and matrix $\mathbf{K}$ is obtained by the classical assembly procedure of the finite element matrices $\mathbf{K}_e$.

To the external work, it can be given the expression (linear in the displacements $\mathbf{U}$):

$$\mathscr{L}(\mathbf{U}) = \mathbf{F}^T\mathbf{U} \tag{88}$$

in which vector $\mathbf{F}$ is created as the assembly of the nodal equivalent force vectors $\mathbf{F}_e$, including only the active loads.

The remaining relative and absolute constraints are represented by linear equations involving the whole set of kinematic variables $\mathbf{U}$:

$$\mathbf{C}\,\mathbf{U} = \mathbf{D} \tag{89}$$

where matrix $\mathbf{C}$ depend only on geometrical quantities and vector $\mathbf{D}$ collects possible given values for the kinematic quantities.

The solution of the problem can be obtained by the Total Potential Energy approach, namely by considering the stationary condition of the following function, to be enforced in the space of the displacements fulfilling the constraint equations Eq. (89):

$$\Pi(\mathbf{U}) = \mathscr{E}(\mathbf{U}) - \mathscr{L}(\mathbf{U}) = \frac{1}{2}\mathbf{U}^T\mathbf{K}\,\mathbf{U} - \mathbf{F}^T\mathbf{U}, \qquad \mathbf{C}\,\mathbf{U} = \mathbf{D} \tag{90}$$

From the analytical point of view, the constraint conditions can be accounted for by enforcing the stationary condition, in the $\mathbf{U}\times\mathbf{R}$ space, of the Lagrangian function:

$$\mathcal{H}\left(\mathbf{U},\mathbf{R}\right)=\frac{1}{2}\mathbf{U}^{T}\mathbf{K}\,\mathbf{U}-\mathbf{F}^{T}\mathbf{U}-\mathbf{R}^{T}\left(\mathbf{C}\,\mathbf{U}-\mathbf{D}\right) \tag{91}$$

in which vector $\mathbf{R}$ collects the so called "*Lagrangian multipliers*", which may be interpreted, from a mechanical point of view, as the reactions given by the constraints. The stationary condition of $\mathcal{H}\left(\mathbf{U},\mathbf{R}\right)$ gives:

$$\begin{cases}\dfrac{\partial\mathcal{H}}{\partial\mathbf{U}}=\mathbf{K}\,\mathbf{U}-\mathbf{F}-\mathbf{C}^{T}\mathbf{R}=\mathbf{0}\\ \dfrac{\partial\mathcal{H}}{\partial\mathbf{R}}=-\mathbf{C}\,\mathbf{U}+\mathbf{D}=\mathbf{0}\end{cases}\quad\Rightarrow\quad\begin{bmatrix}\mathbf{K} & -\mathbf{C}^{T}\\ -\mathbf{C} & \mathbf{0}\end{bmatrix}\begin{bmatrix}\mathbf{U}\\ \mathbf{R}\end{bmatrix}=\begin{bmatrix}\mathbf{F}\\ -\mathbf{D}\end{bmatrix} \tag{92}$$

Now, attention has to be devoted to the system of the constraint equations. In fact, as stated above, some of the constraint equations could be just a repetition of others. Therefore, they have to be eliminated from the system. Further, some equations could be contradicting others, leading to an impossible system (i.e. to a non existing solution).

These aspects may be brought to light by applying a Gaussian elimination to the system of the constraint equations. Specifically, in order to reach the scopes of the present discussion, the Gauss-Jordan elimination[1] is considered. In the code *Beam3DStp* this procedure has been implemented with *partial pivoting*[2], in order to improve numerical stability (Golub and Loan, 1996). Thereafter, the structure of the coefficient matrix and the known term vector can be assumed to be the following

[1] Gauss-Jordan elimination is an algorithm for getting matrices in *reduced row echelon form* using elementary row operations. It is a variation of Gaussian elimination. In fact, meanwhile Gaussian elimination places zeros below each pivot in the matrix, starting with the top row and working downwards (in this case the matrix is said to be in *row echelon form*), the Gauss-Jordan elimination goes a step further by placing zeros above and below each pivot (Golub and Loan, 1996).

[2] Partial Pivoting selects the entry with largest absolute value from the column of the matrix that is currently being considered as the pivot element. Partial pivoting can be represented as multiplication by permutation matrices (Golub and Loan, 1996).

(possibly after some row and/or column exchange, the last governed by a Boolean matrix $\mathbf{A}$):

$$\mathbf{C}'\,\mathbf{U}' = \mathbf{D}', \quad \mathbf{C}' = \begin{bmatrix} \mathbf{I} & \mathbf{S} \\ \mathbf{0} & \mathbf{0} \end{bmatrix}, \quad \mathbf{D}' = \begin{bmatrix} \mathbf{T} \\ \mathbf{W} \end{bmatrix}, \quad \mathbf{U} = \mathbf{A}\,\mathbf{U}' \tag{93}$$

In Eq. (99) a prime indicates that the Gauss-Jordan procedure has been applied, leading to the partition of matrix $\mathbf{C}'$ into sub-matrices $\mathbf{I}$ (identity matrix) and $\mathbf{S}$ (and null parts), and vector $\mathbf{D}'$ in sub-vectors $\mathbf{T}$ and $\mathbf{W}$.

If sub-vector $\mathbf{W}$ is empty, matrix $\mathbf{C}'$ (and the original matrix $\mathbf{C}$) is characterized by a "full-rank" condition: it means that no redundant equations were present in the original system.

Otherwise, if it happens that $\mathbf{W} \neq \mathbf{0}$ (or, due to round-off errors, its norm is higher than a pre-defined tolerance $\|\mathbf{W}\| > w_{tol} = 1e-12$), the original system contains some contradictory equations and the solution does not exist.

Finally, in case that $\mathbf{W} = \mathbf{0}$, the corresponding equations reduce to a repetition of the others and then can be eliminated from the reduced system. In this last case, the displacement vector $\mathbf{U}'$ can therefore be partitioned in dependent variables ($\hat{\mathbf{u}}$) and independent variables ($\mathbf{u}$):

$$\mathbf{U}' = \begin{bmatrix} \hat{\mathbf{u}} \\ \mathbf{u} \end{bmatrix} \;\Rightarrow\; \hat{\mathbf{u}} = \mathbf{T} - \mathbf{S}\,\mathbf{u} \;\Rightarrow\; \mathbf{U} = \mathbf{A}\begin{bmatrix} \mathbf{T} \\ \mathbf{0} \end{bmatrix} + \mathbf{A}\begin{bmatrix} -\mathbf{S} \\ \mathbf{I} \end{bmatrix}\mathbf{u} \tag{94}$$

Consider now the first (equilibrium) equations of the governing system described in Eq. (92); it is worthwhile to consider that:

$$\delta\mathbf{U}^T \frac{\partial \mathcal{H}}{\partial \mathbf{U}} = \delta\mathbf{U}^T\mathbf{K}\,\mathbf{U} - \delta\mathbf{U}^T\mathbf{F} - \delta\mathbf{U}^T\mathbf{C}^T\mathbf{R} = 0 \qquad \forall\delta\mathbf{U} \tag{95}$$

namely, by replacing $\mathbf{U}$ with the independent displacement vector $\mathbf{u}$:

$$\begin{aligned}\delta\mathbf{U} = \mathbf{A}\begin{bmatrix}-\mathbf{S}\\ \mathbf{I}\end{bmatrix}\delta\mathbf{u} \quad \Rightarrow \quad & \delta\mathbf{u}^T\left[-\mathbf{S}^T,\mathbf{I}\right]\mathbf{A}^T\mathbf{K}\,\mathbf{A}\begin{bmatrix}-\mathbf{S}\\ \mathbf{I}\end{bmatrix}\mathbf{u} + \\ & + \delta\mathbf{u}^T\left[-\mathbf{S}^T,\mathbf{I}\right]\mathbf{A}^T\mathbf{K}\mathbf{A}\begin{bmatrix}\mathbf{T}\\ \mathbf{0}\end{bmatrix} + \\ & - \delta\mathbf{u}^T\left[-\mathbf{S}^T,\mathbf{I}\right]\mathbf{A}^T\mathbf{F} + \\ & - \delta\mathbf{u}^T\left[-\mathbf{S}^T,\mathbf{I}\right]\mathbf{A}^T\mathbf{C}^T\mathbf{R} = 0 \qquad \forall\delta\mathbf{u}\end{aligned} \tag{96}$$

From last Eq. (96) it follows that:

$$\underbrace{\left[-\mathbf{S}^T,\mathbf{I}\right]\mathbf{A}^T\mathbf{K}\,\mathbf{A}\begin{bmatrix}-\mathbf{S}\\ \mathbf{I}\end{bmatrix}}_{\mathbf{K}_{uu}}\mathbf{u} + \underbrace{\left[-\mathbf{S}^T,\mathbf{I}\right]\mathbf{A}^T\mathbf{K}\mathbf{A}\begin{bmatrix}\mathbf{T}\\ \mathbf{0}\end{bmatrix}}_{-\mathbf{F}_D} - \underbrace{\left[-\mathbf{S}^T,\mathbf{I}\right]\mathbf{A}^T\mathbf{F}}_{\mathbf{F}_u} - \left[-\mathbf{S}^T,\mathbf{I}\right]\mathbf{A}^T\mathbf{C}^T\mathbf{R} = \mathbf{0} \tag{97}$$

where matrix and vectors

$$\mathbf{K}_{uu} = \left[-\mathbf{S}^T,\mathbf{I}\right]\mathbf{A}^T\mathbf{K}\,\mathbf{A}\begin{bmatrix}-\mathbf{S}\\ \mathbf{I}\end{bmatrix}, \qquad \mathbf{F}_D = -\left[-\mathbf{S}^T,\mathbf{I}\right]\mathbf{A}^T\mathbf{K}\mathbf{A}\begin{bmatrix}\mathbf{T}\\ \mathbf{0}\end{bmatrix}, \qquad \mathbf{F}_u = \left[-\mathbf{S}^T,\mathbf{I}\right]\mathbf{A}^T\mathbf{F} \tag{98}$$

are the reduced stiffness matrix and the reduced known term vectors.

In Eq. (97) the addend that contains the unknown reactions $\mathbf{R}$ given by the constraints can be eliminated from the formulation in light of the following considerations.
From Eq. (89) it can be observed that $\mathbf{U}$ is the general solution to the constraint equation system; this means that:

$$\mathbf{C}\,\mathbf{U} = \mathbf{D} \;\Rightarrow\; \mathbf{C}\mathbf{A}\begin{bmatrix}\mathbf{T}\\ \mathbf{0}\end{bmatrix} + \mathbf{C}\mathbf{A}\begin{bmatrix}-\mathbf{S}\\ \mathbf{I}\end{bmatrix}\mathbf{u} \equiv \mathbf{D} \qquad \forall\mathbf{u} \tag{99}$$

namely:

$$\mathbf{CA}\begin{bmatrix}\mathbf{T}\\ \mathbf{0}\end{bmatrix}=\mathbf{D},\qquad \mathbf{CA}\begin{bmatrix}-\mathbf{S}\\ \mathbf{I}\end{bmatrix}=\mathbf{0} \tag{100}$$

Specifically, from the last identity it follows that the last addend in Eq. (97) becomes zero:

$$\left[-\mathbf{S}^T,\mathbf{I}\right]\mathbf{A}^T\mathbf{C}^T=\left(\mathbf{CA}\begin{bmatrix}-\mathbf{S}\\ \mathbf{I}\end{bmatrix}\right)^T=\mathbf{0} \tag{101}$$

So, the reduced equilibrium system is the following:

$$\mathbf{K}_{uu}\mathbf{u}=\mathbf{F}_D+\mathbf{F}_u \tag{102}$$

If the constraints eliminate the rigid body movements of the structure, matrix $\mathbf{K}_{uu}$ is non singular and the system can be solved for the displacements $\mathbf{u}$:

$$\mathbf{u}=\mathbf{K}_{uu}^{-1}\left(\mathbf{F}_D+\mathbf{F}_u\right),\quad \Rightarrow\quad \mathbf{U}=\mathbf{A}\begin{bmatrix}\mathbf{T}\\ \mathbf{0}\end{bmatrix}+\mathbf{A}\begin{bmatrix}-\mathbf{S}\\ \mathbf{I}\end{bmatrix}\mathbf{u} \tag{103}$$

Finally, the constraints reactions $\mathbf{R}$ can be obtained from the original equilibrium system given by Eq. (92):

$$\mathbf{K}\,\mathbf{U}-\mathbf{F}-\mathbf{Q}^T\mathbf{R}=\mathbf{0} \tag{104}$$

in which the rows in matrix $\mathbf{Q}$ linearly dependent from the other rows, selected by the previous Gaussian elimination, become the columns of matrix $\mathbf{Q}^T$ for which the corresponding reactions cannot be computed in any case, being them interpretable as redundant reactions associated to rigid constraints.

So, in order to proceed, from the operative point of view, the values of redundant reactions can be assumed to be zero and the corresponding row of matrix $\mathbf{Q}$ can be eliminated, by obtaining matrix $\mathbf{Q}^*$ and corresponding (sub-) vector $\mathbf{R}^*$ (whose size is v^*):

$$\mathbf{K}\,\mathbf{U} - \mathbf{F} - \mathbf{Q}^{*T}\mathbf{R}^* = \mathbf{0} \tag{105}$$

Now, in order to solve this system for $\mathbf{R}^*$, it has to be underlined that the number of equations is greater (generally much greater) than the number of reactions $\mathbf{R}^*$.
Then, just a subset of v^* equations has to be considered to compute $\mathbf{R}^*$, but this sub-set has to be chosen in order to have a square and non-singular sub-matrix of $\mathbf{Q}^{*T}$ as a coefficient matrix for $\mathbf{R}^*$.
A simple way to obtain this result is to account only for the equations corresponding to the columns of the identity matrix $\mathbf{I}$ in the Gaussian elimination (extracted by matrix $\mathbf{A}$ in the discussion above), namely:

$$\mathbf{A}^T\left(\mathbf{K}\,\mathbf{U} - \mathbf{F}\right) - \mathbf{B}\,\mathbf{R}^* = \mathbf{0}\ , \qquad \mathbf{B} = \mathbf{A}^T\mathbf{Q}^{*T} \tag{106}$$

from which the v^* reactions follow immediately:

$$\mathbf{R}^* = \mathbf{B}^{-1}\mathbf{A}^T\left(\mathbf{K}\,\mathbf{U} - \mathbf{F}\right) \tag{107}$$

Of course, in the equilibrium system, matrix $\mathbf{Q}^*$ could be replaced by sub-matrix $\left[\mathbf{I}\quad\mathbf{S}\right]$ of $\mathbf{Q}'$, by defining a new set of reactions $\mathbf{R}'$ (still of size v^*):

$$\mathbf{K}\,\mathbf{U} - \mathbf{F} - \begin{bmatrix}\mathbf{I}\\ \mathbf{S}^T\end{bmatrix}\mathbf{R}' = \mathbf{0} \tag{108}$$

Then, the reactions $\mathbf{R}'$ can be immediately obtained by considering the first v^* equations:

$$\mathbf{R}' = \mathbf{K}'\,\mathbf{U} - \mathbf{F}', \qquad \mathbf{K} = \begin{bmatrix} \mathbf{K}' \\ \overline{\mathbf{K}} \end{bmatrix}, \qquad \mathbf{F} = \begin{bmatrix} \mathbf{F}' \\ \overline{\mathbf{F}} \end{bmatrix} \tag{109}$$

However, this last procedure is useless because, contrary to those obtained by Eqs. (106)-(107), it is not possible to give the mechanical interpretation of the reactions $\mathbf{R}'$, being these obtained by a linear combination of the original ones $\mathbf{R}^*$.

4.5 Step-wise holonomic elastoplastic solution

The elastoplastic formulation implemented in the code *Beam3DStp* allows to analyze perfectly-elastoplastic 3D truss frames up to failure.
As stated in previous sections, truss frames subjected to monotonic loading and modelled by conventional finite elements are considered. In these trusses, possible plastic deformations are concentrated in pre-selected "critical sections", whose inelastic behaviour is described by PWL constitutive models (Section 4.1).

In the algorithm, in view of the mathematical peculiarities attached to the adopted PWL constitutive models, the nonlinear problem described in Eqs. (3) and (4) is numerically solved on the bases of the "step-wise holonomic" interpretation of the evolution of a dissipative system (Maier, 1970; De Donato and Maier, 1972; Franchi and Genna, 1991). This means that the dependence on the given loading path does not hold within the step; in other terms, the intrinsic irreversibility of the plastic hinge model is accounted for only by updating the internal variables at the transition from step to step.

This procedure starts from some of the innovative contributions given by Cocchetti and Maier (2003), referred to as "exact time integration" method and step-wise fully holonomic analysis. In this thesis the procedure is further developed, implemented and applied for the first time to the analysis of structure with considerable complexity as the 3D FEM model of the Paderno d'Adda bridge, which involves roughly 5300 beam finite elements and 13300 degrees of freedom.
It has shown to be very much effective and reliable in tracking the limit structural behaviour of the bridge, by reaching convergence with smooth runs up to the true limit load and corresponding collapse displacements.

The procedure rests on the unifying basis provided by the Linear Complementarity Problem (LCP) (see Cottle et al., 1992), a specific account of which is available,

together with its frequent involvement in elastoplasticity theory, e.g. in Maier (1970), Cohn and Maier (1979), Lloyd Smith (1990), Wakefield and Tin-Loi (1990), Giambanco (1999).
In the present formulation such procedure is adopted in conjunction with the peculiarities referred to the determination of the tangent stiffness matrix (Section 4.3) and the treatment of mutual connections by static condensation and Gaussian elimination (Section 4.4).

In the following, a schematic description of the step-by-step elastoplastic analysis implemented in the code *Beam3DStp* is presented.
The main formulation and computational details at the origin of the procedure are provided in Cocchetti and Maier (2003).

Consider a discrete structure and a load configuration applied on it.
Initially, the external actions will be conceived henceforth to be proportionally amplified in time t by a load factor $\alpha > 0$. The time-independent property implied by the assumed elastoplastic constitutive models makes time t just an ordinal, chronological variable (not necessarily a physical time) and allows for identifying t with the load factor α, as long as these increase together.

The resulting incremental procedure applied to the analysis of the elastoplastic behaviour of the Paderno d'Adda bridge is outlined in what follows.

(a) At the beginning of the analysis, the structure is not under the effect of loading or of pre-existing stress states; then, no yield plane is active. Afterwards, the following quantity is set acting on the structure:

$$\mathbf{F}_{Li} = \alpha\, \mathbf{F} \tag{110}$$

where $\mathbf{F}_{Li}$ represents the incremental load and $\mathbf{F}$ represents the assembly of the equivalent nodal force vector coming from the given original load applied to the structure.

(b) Thereafter the formulation determines the incremental solution referred to the above incremental load $\mathbf{F}_{Li}$, in terms of displacement increments. This solution is given by the structural (linear) solving system that has been obtained in Section 4.4. For convenience, the pertinent formulations are reported below, with reference to symbols already introduced in Section 4.4:

$$\mathbf{K}_{uu}\mathbf{u} = \mathbf{F}_D + \mathbf{F}_u \tag{111}$$

$$\mathbf{K}_{uu} = \left[-\mathbf{S}^T, \mathbf{I}\right]\mathbf{A}^T\mathbf{K}\,\mathbf{A}\begin{bmatrix}-\mathbf{S}\\ \mathbf{I}\end{bmatrix}, \qquad \mathbf{F}_D = -\left[-\mathbf{S}^T, \mathbf{I}\right]\mathbf{A}^T\mathbf{K}\mathbf{A}\begin{bmatrix}\mathbf{T}\\ \mathbf{0}\end{bmatrix}, \qquad \mathbf{F}_u = \left[-\mathbf{S}^T, \mathbf{I}\right]\mathbf{A}^T\mathbf{F} \tag{112}$$

During each step, vector $\mathbf{F}$ in Eq. (112)*c* is set equal to $\mathbf{F}_{Li}$. In Eq. (112)*a,b*, matrix $\mathbf{K}$ represents the assembly of the elastic-plastic matrices of each finite element, namely the global tangent stiffness matrix of the structure $\mathbf{K}_{ep}$ determined in Section 4.2. At the beginning of the analysis, the stiffness matrix $\mathbf{K}$ is totally elastic, namely no yield plane is active in the structure's joints.
The incremental solution in term of the displacements is hence given symbolically by the following expression:

$$\Delta\mathbf{u} = \mathbf{K}_{uu}^{-1}\left(\mathbf{F}_U + \mathbf{F}_D\right) \tag{113}$$

(c) From the incremental solution $\Delta\mathbf{u}$, the corresponding increments of the static internal variables can be determined for each beam element, based on the treatment presented in previous Sections 1−3:

$$\Delta\mathbf{N} = \mathbf{Q}\,\Delta\mathbf{H} = \mathbf{Q}\left(\mathbf{K}_{ep}\,\Delta\mathbf{u}\right) \tag{114}$$

The incremental solutions $\Delta\mathbf{u}$ and $\Delta\mathbf{N}$ do not take into account that some modes may be possibly activated during the step; on the other hand it is possible that the extent of the incremental load $\mathbf{F}_{Li}$ is not enough to determine the reaching of at least one internal static variable in a section on the corresponding yield limit.

Through a comparison between each static internal variable at the beginning of the step and the corresponding yield limit, the algorithm calculates for each mode, among all non-activated ones, the specific "scale factor" of the multiplier α leading to possible activations.

(d) Let $\overline{\mathbf{N}}$ be the value of the internal actions at the beginning of the step; the code calculates, for each considered mode, the following relation:

$$\frac{\alpha_i'}{\alpha} = \frac{\left(N_{\lim,i} - \overline{N}_i\right)}{\Delta N_i} \tag{115}$$

In Eq. (115) $N_{\lim,i}$ is the yield limit of the considered mode; α' represents the load multiplier necessary to reach a new activation. The minimum among all such estimated multipliers α' ($\boldsymbol{\alpha}$) determines the "exact" extent of the current step to achieve new activation(s). It is set to determine the above mentioned scale factor of the multiplier α, herein called γ:

$$\gamma = \frac{\min\left\{\alpha_i'\right\}}{\alpha} = \frac{\boldsymbol{\alpha}}{\alpha} \tag{116}$$

(e) Through coefficient γ, the original incremental solution is rescaled proportionally, and the static and kinematic quantities of the structure at the end of the step are updated as follows:

$$\begin{aligned} \overline{\mathbf{U}} &= \overline{\mathbf{U}} + \gamma \Delta \mathbf{U} \\ \overline{\mathbf{N}} &= \overline{\mathbf{N}} + \gamma \Delta \mathbf{N} \end{aligned} \tag{117}$$

At the end of the step some yield planes (at least one) are now activated ($\overline{\varphi}_i = 0$). The stiffness matrix is therefore updated, becoming elastoplastic. The live load $\mathbf{F}_{Li}$ is re-set equal to $\alpha\,\mathbf{F}$ and the procedure *(b)-(c)* is repeated.

At this point the internal kinematic variables, active along the time interval, are selected according to the active yield planes at its beginning. If the computed incremental solution that can be extracted from Eq. (113) would imply negative dissipation for any of the active modes (for instance, if a tensile yielding axial force acts in a beam and, instead, a length shortening would be obtained in the incremental solution), then that active mode is actually deactivated ($\overline{\varphi}_i < 0$), the stiffness matrix is newly updated and the incremental solution is re-computed.
On the other hand, when an active mode has been deactivated at the beginning of the time increment and the incremental solution would render an increment of the static action corresponding to that mode, producing thus a violation of the perfectly-plastic yield condition (for instance, an axial force becoming higher than the yield limit at the end of the time increment), this would mean that such a mode shall be included among the active ones, from the beginning of the time interval; then, the stiffness matrix has to be updated before the new computation of the incremental solution.

Once all conditions of non-negative dissipation and perfectly-plastic yielding described above are fulfilled, the algorithm calculates again, among all non-activated modes, the load multipliers $\boldsymbol{\alpha}$ leading to new possible activations. Steps *(d)-(e)* are therefore repeated and at the end the analysis starts again with a new step.

The collapse of the structure is reached when the minimum eigenvalue of the global (updated) matrix $\mathbf{K}_{uu}$ calculated within step *(b)* vanishes (with numerical tolerances in the order of $1e-15$).

The analysis ends when the collapse is reached or when the cumulative sum of the load multipliers $\boldsymbol{\alpha}$ is equal or higher than 1 ($\boldsymbol{\alpha}_{tot} \geq 1$).

In the next page a flow chart of the procedure implemented in the code *Beam3DStp* is reported.

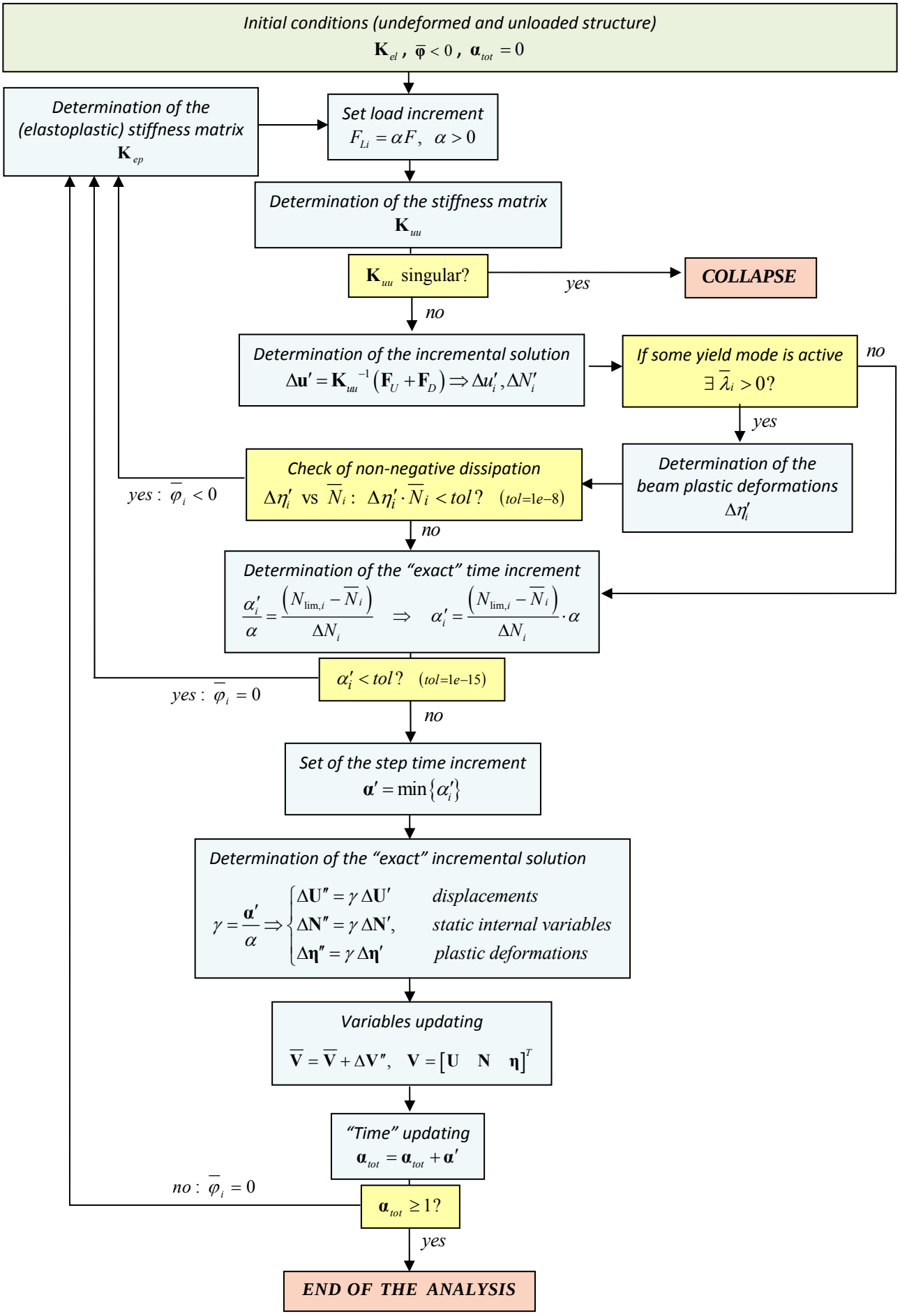

Fig. 20: Flow chart of the elastoplastic algorithm.

Chapter 5

Elastoplastic analysis of the bridge

In this chapter the results obtained by the elastoplastic analyses of the Paderno d'Adda bridge, performed through the code *Beam3DStp,* are presented and discussed. The main characteristics of the non-linear finite element formulation adopted in the analysis have been discussed in Chapter 4.
In this chapter the load multiplier α' treated in Section 4.5 is labelled λ. In the structural solution, boundary conditions are imposed with the "ad-hoc" procedure described in Section 4.4.

As already mentioned, the elastoplastic FEM formulation adopted in the code *Beam3DSep* considers that the deformations of the structure can occur only at pre-selected sections. In particular, plastic deformation is concentrated at the beam element edges, *A*, *B*, where two plastic joints are inserted.

In the elastoplastic analysis of the bridge, the assumed generalized kinematic variables in each plastic joint are: two relative plastic rotations (each around a principal axis of the cross section - labels 1,2); an axial elongation; a relative rotation around the beam axis.

Specifically, axial elongation and axial rotation are (possibly) activated in only one of the two joints (*A* or *B*), in order to avoid unrealistic free rigid body movements; then, only 6 internal kinematic variables are required for each beam element.
Shear effects have not been considered so far.
In particular, a piecewise linear uncoupled behaviour is adopted for such internal static variables, namely a Rankine-type boxed-form yield domain is assumed in the space of the static variables.

The analytical description of the interaction domain for the beam finite element is then stated in terms of the following inequalities:

$$\begin{cases} N^- \le min\left(N^A, N^B\right) \le max\left(N^A, N^B\right) \le N^+ \\ M_t^- \le M_t \le M_t^+ \\ M_1^- \le M_1^A \le M_1^+, \qquad M_2^- \le M_2^A \le M_2^+ \\ M_1^- \le M_1^B \le M_1^+, \qquad M_2^- \le M_2^B \le M_2^+ \end{cases}$$

where N is the axial force, M_t is the torque (uniform along the element), M_1 and M_2 are the bending moments with respect to the two principal axes of inertia of the cross section (indexes *A* and *B* refer again to the beam edges). Yield limits $N^-, N^+, M_t^-, M_t^+, M_{1,2}^-, M_{1,2}^+$ are taken constant and obtained from material yield limits $\left(\sigma_y, \tau_y\right)$ and cross section geometrical characteristics as:

$$\begin{aligned} &N^+ = -N^- = A\,\sigma_y, \\ &M_{1,2}^+ = -M_{1,2}^- = \alpha\, M_{1,2}^e = \alpha\,(2J_{1,2} / h_{1,2})\,\sigma_y, \\ &M_t = \beta\, M_t^e = \beta\,(J_t / b)\,\tau_y \end{aligned}$$

where α and β are bending and torsion section shape factors (taken here as $\alpha = 1.1$ and $\beta = 1.5$ for all the elements) and $J_{1,2}, J_t, h_{1,2}, b$ are flexural inertias, torsional inertia, heights and profile thickness of the cross section.

The data referred to each section of the Paderno d'Adda bridge used to determine the above quantities are gathered in Ferrari and Rizzi (2011a).

As previously presented for the elastic analyses, accidental loading conditions associated to four static try-out tests performed by the SNOS (SNOS, 1889; Nascè et al., 1984) are considered.

Loads have been applied here to the nodes of the FEM model at the railway level.

In Fig. 21 the total load applied to the structure is reported for each test, which is obtained as $Q = n \cdot q \cdot l$, where l is the length of each span of the upper continuous beam (l=33.25 m) and n is the number of loaded spans, according to the load distributions in Fig. 21 (n=2 or 3).

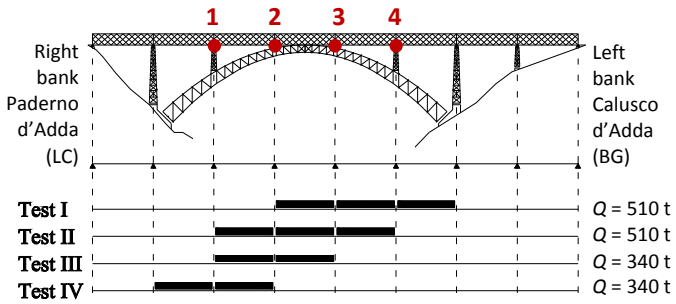

Fig. 21: Scheme of the four considered static try-out configurations (view from down-stream), with value of total load applied to the structure for each test and indication of four control points (red circles).

Self-weight is pre-loaded on the bridge (through specific weight ρ), leading to elastic deformations, before starting the incremental elastoplastic analyses, which develop at increasing accidental load.

Salient results are presented as follows (Figs. 22–25, Table 5).

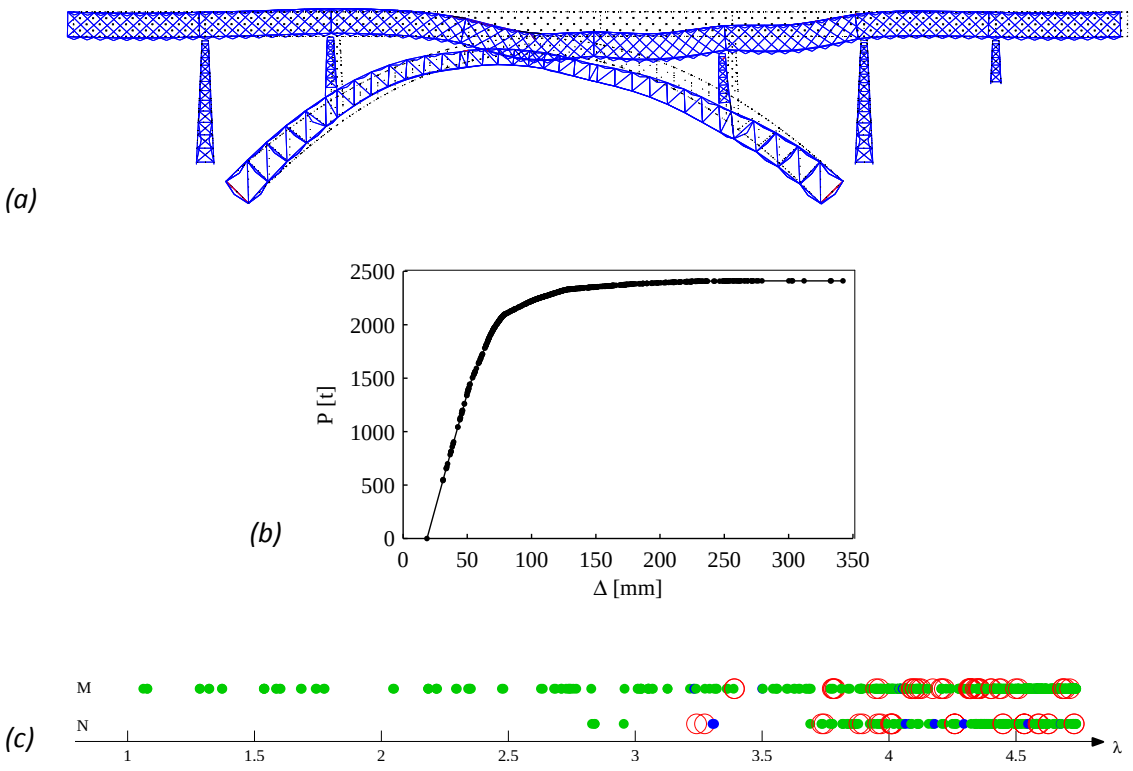

Fig. 22: Elastoplastic analysis of try-out Test I.

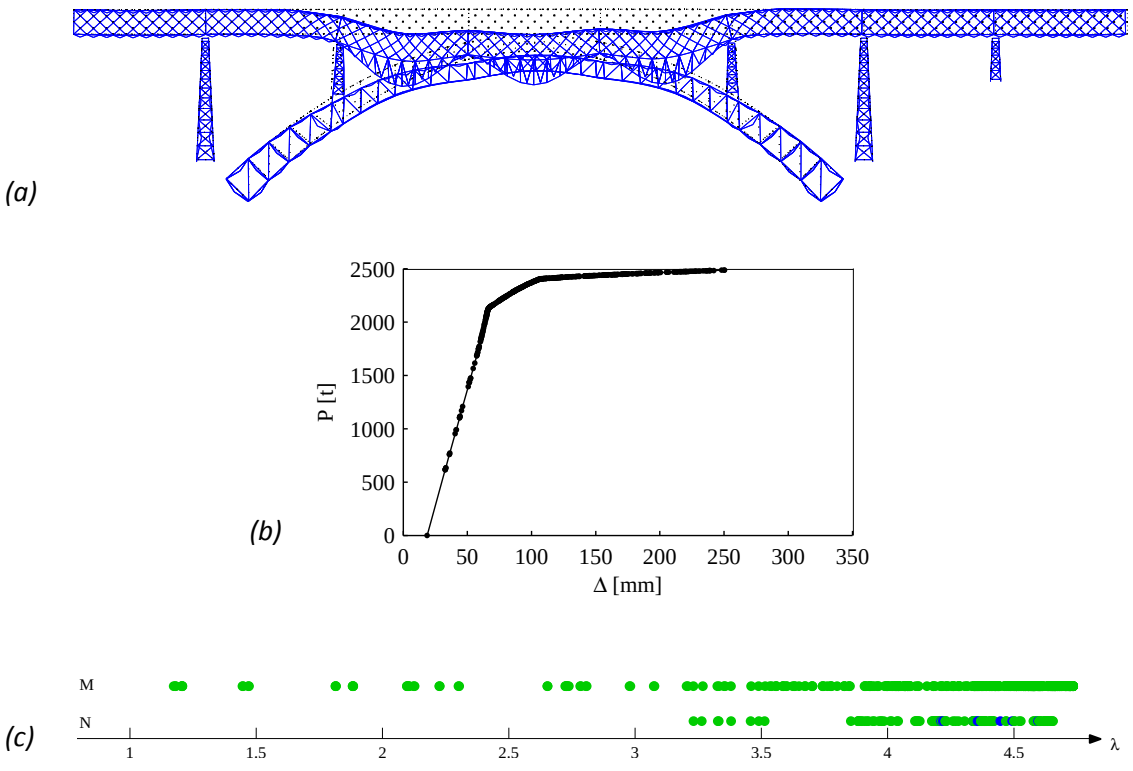

Fig. 23: Elastoplastic analysis of try-out Test II.

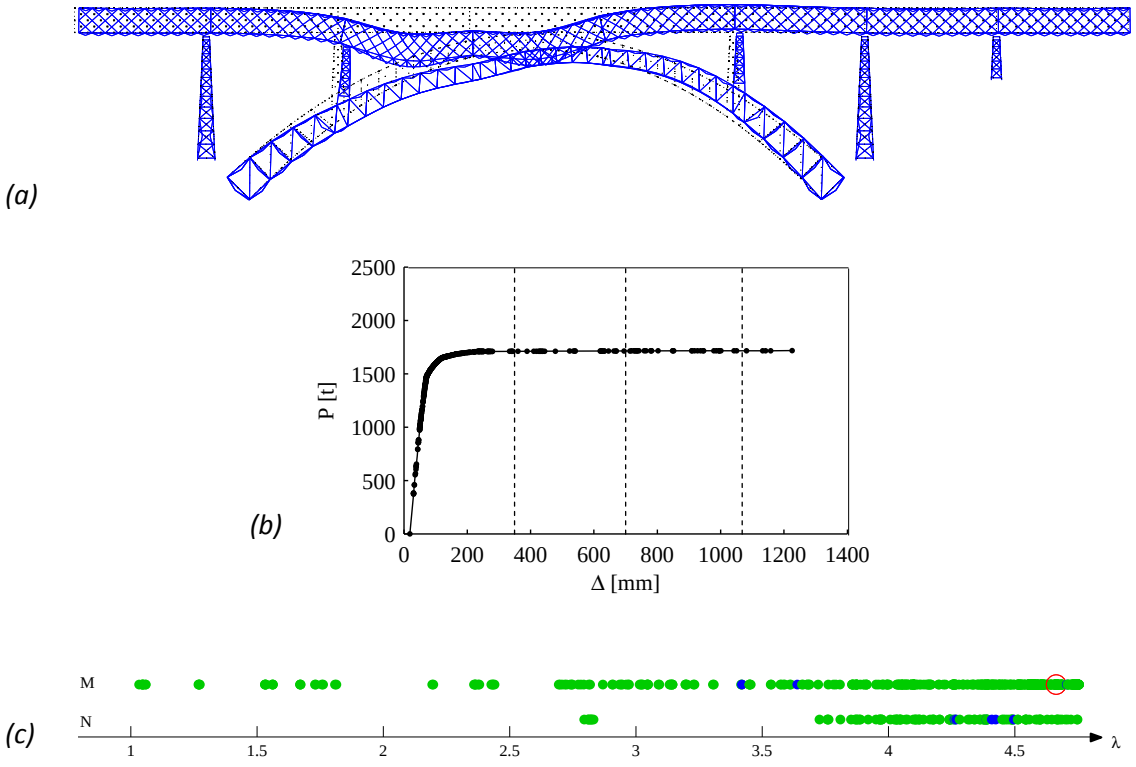

Fig. 24: Elastoplastic analysis of try-out Test III.

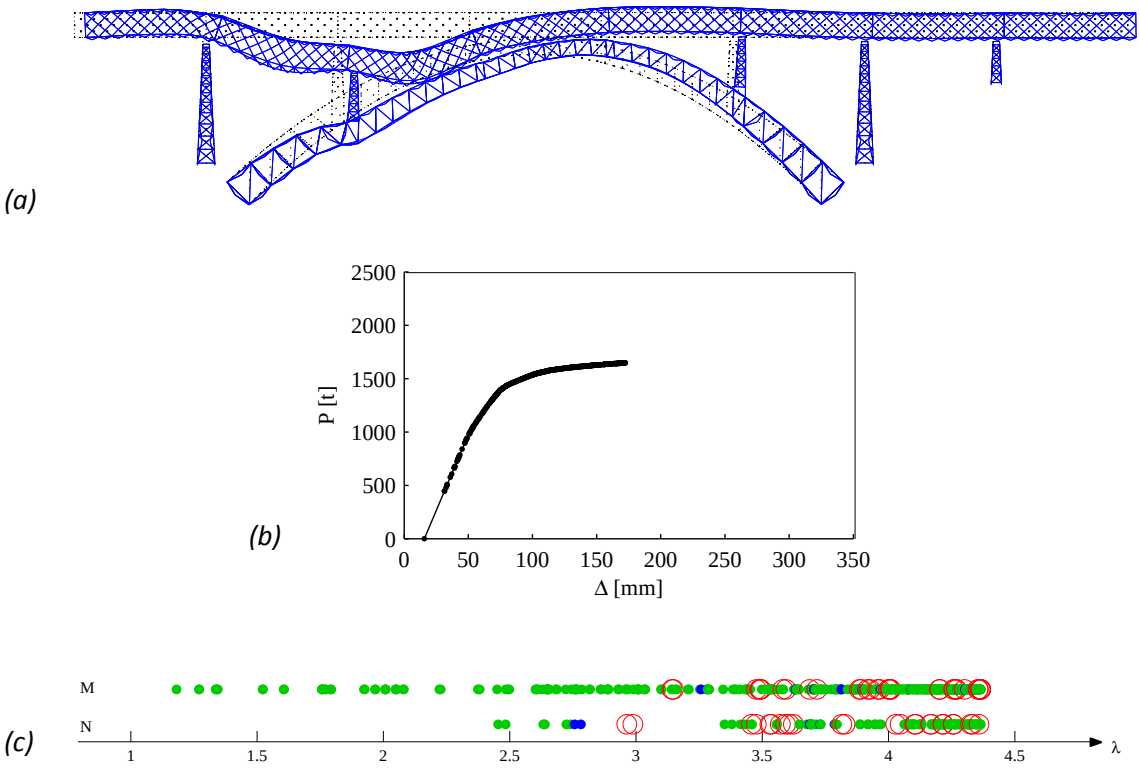

Fig. 25: Elastoplastic analysis of try-out Test IV.

The above representations report, for each of the four try-out loading configurations in Fig. 21:

- the deformed configuration of the bridge at incipient collapse with amplification factor set to 100 (Figs. 22−25*a*)
- the characteristic non-linear load/displacement response curve (Figs. 22−25*b*)
- the localisation of the plasticized members (Figs. 22−25*c*)

These representations have been generated after running the analyses, by appropriate post-processing of the stored data.

The response plots in Figs. 22−25*b* show the computed step-by-step evolutive solutions, with reference to values read at the beginning of each time interval.
In particular, the horizontal axis depicts the vertical displacement (Δ) of the node that, in the end, has shown the maximum displacement at incipient collapse; the vertical axis reports the amplified accidental load $P = \lambda \cdot Q$, where λ is the load multiplier related to the incremental solution of the non-linear elastoplastic analysis (Section 4.5).
Notice that in the plots in Figs. 22−25*b*, the non-zero initial displacement (at $P = 0$) is due to self-weight only, namely to a pre-imposed permanent load not affected by the load multiplier (i.e. load multiplier λ affects just the accidental load linked to the locomotive distributions).
Moreover, for each loading case, the end point of the $P - \Delta$ curve refers to the so-estimated collapse of the structure in terms of vanishing minimum eigenvalue of the tangent stiffness matrix of the structure (Section 4.5).

Figs. 22−25*c* shows a “plasticity map” of plastic activations in the various structural members at increasing load multiplier λ. It scores the plastic modes that are activated at the beginning of each time increment. Each marker represents one activated mode in the structure, as described below.

On the two lines, the activation of axial (N) and bending modes (M) are shown, respectively.

Notice that no torsional modes have been activated during the analyses, which should look reasonable for these vertical loading configurations that are symmetric to the longitudinal plane of the bridge.

The colour of the markers refers to the various parts of the structure in which the activated plastic joint has appeared: to an element of the arch (blue), piers (red), upper continuous beam (green). In particular: the largest hollow circle marks a plastic mode activated in an element of the piers resting on the arch; the diagonal cross symbol marks a plastic mode activated in an element of the big biers; the hollow triangle marks a plastic mode activated in an element of the intermediate pier.

So, in inspecting the maps reported in Figs. 22*c*−25*c*, it is possible to appreciate the sequence of activation of plastic joints and the overall plastic response of the bridge, at increasing applied accidental load $P = \lambda \cdot Q$.

The load multipliers λ_c at incipient structural collapse of the bridge for the four loading configurations are reported in Table 5, with type and number of activated modes. Table 5 lists as well the maximum vertical node displacement of the bridge at incipient collapse (all maximum values actually refer to nodes of the upper continuous beam, at the railway level).

Table 5: Collapse load multiplier, active modes and maximum vertical displacement of the bridge.

Load conf.	***Q* [t]**	**Load mult. λ_c**	***P* = λ*Q* [t]**	**Nr. of active axial modes**				**Nr. of active flexural modes**				**Total nr. of active modes**	**Max vertical displ. [mm]**
				Arch	**Piers**	**Beam**	**Total**	**Arch**	**Piers**	**Beam**	**Total**		
Test I	510	**4.74**	**2417**	8	16	112	**136**	14	12	91	**117**	**253**	343
Test II	510	**4.73**	**2412**	8	0	59	**67**	0	0	455	**455**	**522**	250
Test III	340	**4.75**	**1615**	6	0	96	**102**	3	2	525	**530**	**632**	1231
Test IV	340	**4.37**	**1486**	6	21	113	**140**	21	24	364	**409**	**549**	172

The obtained results show that, among the four tests (Fig. 21), the collapse load multipliers are almost the same, except for case IV (with two loaded spans), where the lower value λ_c =4.37 is obtained.

This may be due to the fact that Test IV is the more eccentric one with respect to the crown of the arch. In particular, the load is concentrated on the pier on the arch on the side of the Paderno d'Adda bank. As it can be appreciated in Table 5 and in Fig. 25*c* this test presents the higher number of active modes in the piers (21 axial modes and 24 flexural modes). These modes are activated when the load multiplier reaches a value close to λ =2.4 and seem then to rule collapse.

Moreover, the maximum vertical displacement obtained at incipient collapse is, by far, the lowest. It may be said that, in Test IV, plastic collapse is reached without showing significant plastic resources in terms of global ductility.

If the same total load is considered (in terms of resultant Q, Tests I-II and III-IV), but almost symmetrically distributed with respect to the crown of the arch, the collapse load multiplier obtained by the analysis increases (in particular, it becomes the highest in Test III).

Fig. 24*c* for Test III shows that almost all yield modes activated at increasing load refer to the elements of the upper continuous beam; only few plastic modes are activated in the elements of arch and piers.

The results obtained by the analysis referred to Test III show significant plastic resources in terms of global structural ductility.

In fact, as it can be appreciated in Fig. 24*b*, at incipient collapse, this loading configuration leads to a prolonged plateau and to the higher maximum vertical displacement (Table 5), up to about four times the maximum displacement in the other tests, which is referred to a node of the lower frame connecting the two main vertical longitudinal truss girders of the upper continuous beam, right underneath the rails, where the distributed load has been applied.

In Tests I and II three spans of the upper continuous beam are interested by the accidental load distribution. Despite this, in these tests the collapse load multiplier is not much different from those in Tests III and IV.

In Test I the total number of active modes is actually minimal and, near collapse, as in Test IV, many internal static variables in the elements of the piers do reach yield planes referred to both bending moments and axial force (Figs. 22*c* and 25*c*).
In Test II many yield modes still refer to the elements of the upper continuous beam; no yield modes appear in the piers. The maximum vertical displacement obtained for Test II is quite limited (Fig. 23*b*, Table 5).
Also in this case, collapse is reached without significant plastic displacements.

Fig. 26 shows, for each loading test (Fig. 21), the characteristic non-linear load/displacement response ($P-\Delta$) curves at the four control points (*CP* 1–4) represented in Fig. 21. These are localised at the pier/beam and arch/beam interfaces, on the railway frame level and refer to the four bearings on the arch.

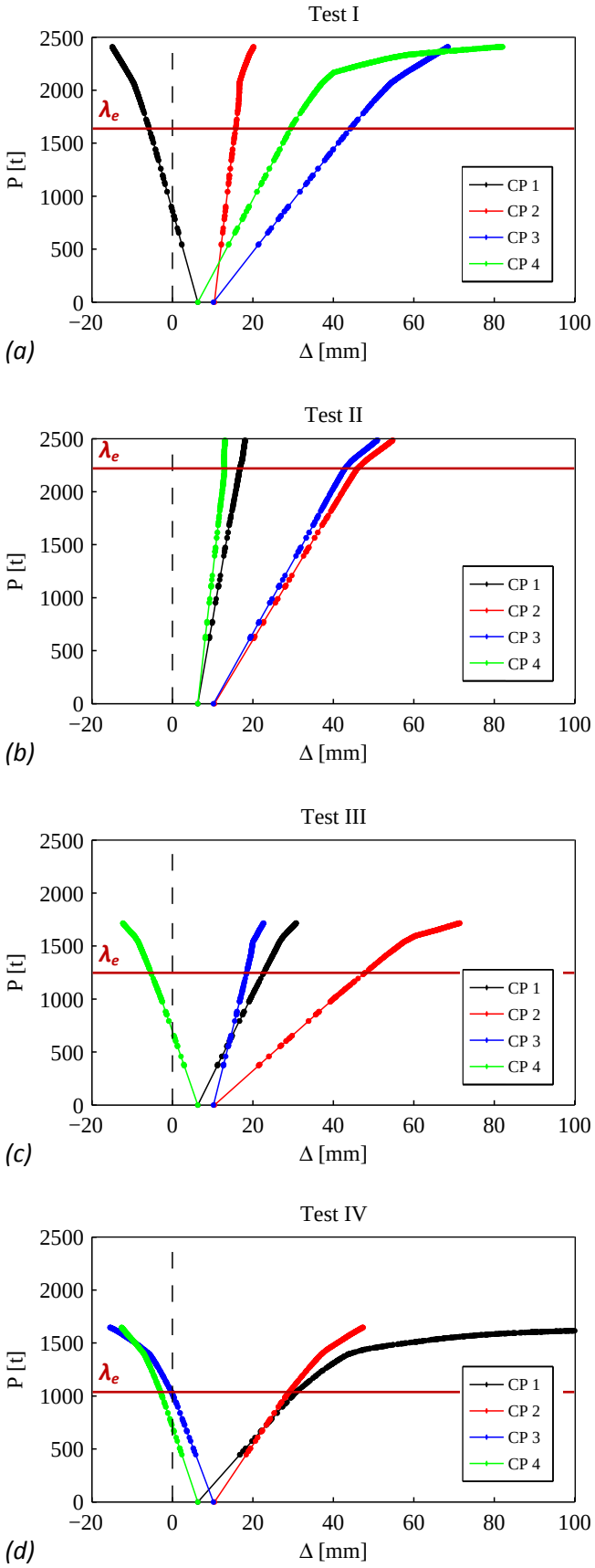

Fig. 26: Characteristic P-Δ curves at Control Points 1–4 (Fig. 21).

In Figs. 26*a*–*d* it is possible to note that, at selected CP_s, the collapse of the bridge is generally reached without significant plastic deformation at this level. Only in Tests I and IV (where the loads are much un-symmetrically located to the crown of the arch), Figs. 26*a*,*d*, plastic displacements are visible at CP_s 4 and 1, respectively.

In Tests II and III the characteristic $P-\Delta$ curves stop quite early: global structural collapse of the bridge is achieved without appreciable vertical displacement at the CP_s.

The $P-\Delta$ curves abandon the linear elastic trend at total load $P_e = \lambda_e \cdot Q$ (marked in Figs. 26*a*–*d* by a red horizontal line).

This load level marks a threshold beyond which further loading generates permanent deformation in each of the tests (λ_e in the order of 3.1–3.2 for Test I and II, and the order of 3.7–3.2 for Test III and IV).

The $P-\Delta$ trends are almost linear, so that all response curves at *CP* 1–4 display almost a bi-linear trend, with visible kink at the level of the threshold line.

The further post-kink load gain is quite limited, with respect to the threshold load.

This seems to show that, for the considered loading configurations, the arch looks quite far from collapse, while structural collapse is reached for the bridge with reference to failure in the upper continuous beam and, in some cases, in some elements of the piers.

Instead, in all considered tests, the elements of the upper continuous beam appear to be the most critical within the structure.

For each span of the beam, Fig. 27 below shows the location of the elements with activated plastic modes.

Specifically, with counting of the number of activated modes, three couples of bars are displayed, on three levels, for each span of the beam:

- the top couple in the elements of the upper frame of the beam (thus at road level)
- the middle couple in the elements of the vertical frame of the longitudinal truss beams
- the bottom couple in the lower frame (at the railway level)

Blue bars refer to axial modes and red bars to flexural modes. The width of the bars is related to the total number of active modes in the pertinent elements.

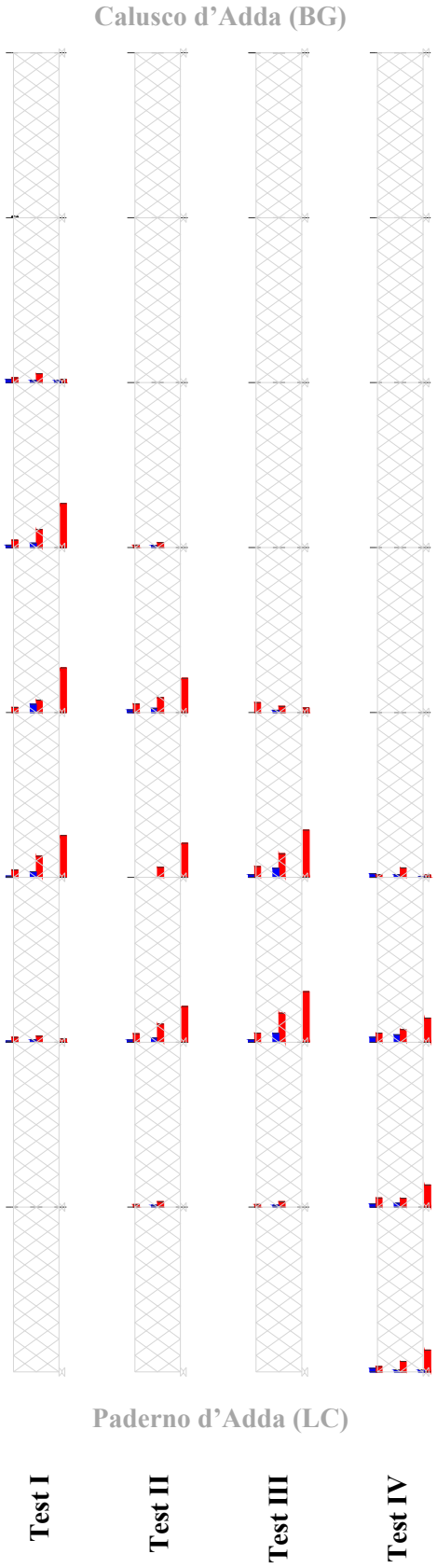

Fig. 27: Distribution of activated plastic modes in the upper continuous beam.

Obviously, most active modes in the beam arise in the zones where the loads are applied, namely in the elements of the lower frame of the loaded spans.
In Fig. 27 it is possible to appreciate that, for each loading configuration, these active modes are approximately one third of all the potential modes related to the lower frame. This ratio increases even more if (non activated) torsional modes are not taken into account and considering that very few elements do reach yield planes for the axial force.
The number of active modes in the vertical and upper frames, of the same spans, does not appear negligible, with respect to that of the modes in the lower frame. Some active modes arise also in non-directly loaded contiguous spans.
It may be said that loads applied at the railway level are able to involve the neighbouring elements in the plastic response of the continuous beam.

Notwithstanding that the plastic response of the structure in all tests appears to be governed mainly by the activation of the yield modes in the elements of the upper continuous beam, in Tests I and IV the modes referred to the elements of the piers directly lying on the arch are involved in the final collapse. No elements of the other piers yield.
The analyses show that, in both Tests I and IV, the active modes in the piers on the arch refer to elements at the piers/arch connections and elements of the upper rectangular closing frame on top of the piers, hosting as well the bearing devices of the beam.
No active modes arise in the elements of the four faces of the box profile of the piers.

The obtained results, which refer to geometrical characteristics at design stage, show a good global elastoplastic performance of the bridge.

Specifically, for the analysed loading conditions (with vertical loads acting symmetrically to the longitudinal plane of the bridge), the arch is basically never

involved in the collapse. Actually, in all try-out tests only few elements of the arch yield. In this sense, it appears that the doubly-built-in parabolic arch, a marvellous characteristic feature of the bridge, represents a well-set structural element, in terms of the global structural response of the viaduct.

For all the analysed loading conditions, the elements of the upper continuous beam appear to be the most critical. It is worth-mentioning that, despite interventions on the roadway deck in the seventies and the more recent stiffening of the metallic box girder, the railway deck should not have undergone substantial modifications.
Thus, further checks on the structural performance of the beam should be specifically pursued.

The analyses have also shown that only tests with loading configurations much un-symmetrically located to the crown of the arch have involved plasticity in the elements of the piers, but right underneath the loaded spans, in particular at the arch/pier and pier/beam stiffened interfaces, where the FEM model is actually not that detailed so far (and could be refined), to deal appropriately with the stress concentrations that may produce at these locations.
The other elements of the piers appear far from collapse.

The structural members of the arch also appear rather in safe position, since they are hardly involved in the plastic sequence leading to collapse.

The considerable level of load amplification at collapse (absolute λ_c in the order of 4.4–4.7, elastic λ_e in the order of 3.1–4.2 and multiplier ratio λ_c / λ_e in the order of 1.1–1.5) is certainly warranted by the assumed unlimited perfectly-plastic behaviour of all the structural members of the bridge, as linked to the stiff “hyperstatic” nature of the structure, as conceived at original design, which appears to allow for considerable stress transfer and redistribution at increasing load and resulting plastic deformation in the structure.

Additional simulation loading settings, directly acting at the beam/piers or pier/arch interfaces may provide further information on the specific plastic resources of bearing structural subparts constituted by piers and arch.

Conclusions

In this doctoral thesis a comprehensive structural analysis of the Paderno d'Adda bridge has been performed.

First, through a scrupulous screening of the original technical drawings of the bridge, it was possible to create a database of the geometrical features of the structure (Ferrari and Rizzi, 2011). Through this work it has been possible to put in place a FEM model of the bridge.
The FEM model of the bridge is comprised of 5337 beam elements and 2216 tied nodes. To the author's knowledge, it represents the most comprehensive existing FEM model of the bridge. It is presented in Chapter 1, together with a brief description of the main technical features of the viaduct.
Some analyses attempted in the linear elastic range have been performed through the model. The outcomes of these analyses appeared to be consistent with available data reported in SNOS, 1889. This comparison showed that the model is able to provide a coherent account of the structural properties of the bridge at design stage.
The outcomes of the analyses are reported in Chapter 2.

In light of this, further studies have been carried-out by means of the FEM. First of all, the modal dynamic characteristics of the bridge have been inquired. In Chapter 3, the salient results obtained from the modal analysis of the bridge are reported.
Among them, it is worthwhile to restate that the first vibration modes of the structure are characterized, in terms of effective masses, by predominantly transverse and longitudinal components, meanwhile the dominant vertical components of the mode

shapes of the bridge are observed only for higher natural frequencies: this appears to be consistent with the originally-conceived high stiffness of the railway viaduct in its vertical plane.
Furthermore, a quite reasonable agreement has been found with respect to recent identified data from current experimental campaigns on the bridge response (Gentile et al., 2010; Gentile and Saisi, 2010).

After these preliminary studies about static and dynamic responses of the bridge, the research was extended to the modelling of the global nonlinear elastoplastic behaviour of the structure.

To this end, a dedicated computer program has been implemented, in which 3D beam finite elements, perfectly plastic joints (as an extension of classical plastic hinges), piece-wise linear yield domains and “exact” time integration have been considered as main characteristic ingredients of the elastoplastic FEM formulation.

The algorithm, which has been developed by applying the “exact” and stepwise holonomic step-by-step analysis method described in Cocchetti and Maier (2003), has shown very much able to track the limit structural behaviour of the bridge, by reaching convergence with smooth runs up to the true limit load and corresponding collapse displacements.
This held true despite the considerable complexity of the complete bridge structure, involving roughly 5300 beam finite elements and 13300 degrees of freedom.

In the algorithm, some original features have been also implemented: treatment of mutual connections by static condensation and Gaussian elimination; determination of the tangent stiffness formulation through Gaussian elimination. These contributions have been presented in Section 4.3 and Section 4.4 of the thesis.

The implemented code (*Beam3DStp*) has been used to comply with the first goal of performing an elastoplastic analysis of the Paderno d'Adda bridge.
Its development has involved a large part of the doctoral programme. The code has been arranged to import the morphological and geometrical features of the structure from ABAQUS and it can therefore be applied to elastoplastic analysis of generic 3D truss frame structures. For these reasons, the code *Beam3DStp* shall be considered as a research product on its own.

Through the code *Beam3DStp* an elastoplastic analysis of the Paderno d'Adda bridge has been performed at design stage.
The obtained results have been presented and discussed in detail in Chapter 5.
Some the major considerations that have been delineated therein are reported in the following.
Among the different design loadings acting on the bridge, the collapse load multipliers are almost the same despite the variation of the total load. The collapse mechanism seems to be related to the position of the loads applied on the structure more than to their consistency.
For the considered loading configurations, the arch looks quite far from collapse, while structural collapse is reached for the bridge with reference to failure in the upper continuous beam and, only in some cases, in some elements of the piers. In particular, only in the tests with loading configurations much un-symmetrically located to the crown of the arch, the modes referred to the elements of the piers directly lying on the arch are involved in the final collapse of the viaduct.
For all the analysed loading conditions, the elements of the upper continuous beam appear to be the most critical.

While the present design-stage analyses seem to be rather encouraging about the bearing capacity of the bridge (under the assumption of unlimited ductility of its structural members), mainly regarding its vertical supporting structure made by arch and piers, degradation and aging may imply reduced structural performance.

This should be checked in view of possible restoration actions, which appear worthwhile to be pursued, given the present results and the considerable importance and value that this historic infrastructure still keeps today in the local transportation network and in the architectural and industrial heritage of the territory.

The bridge is undoubtedly a beautiful, living industrial monument of the scientific and technological developments of the time of its construction. For this reason, in the opinion of the author, the bridge should aspire to be added to the UNESCO World Heritage List.

The present preliminary results on the elastoplastic structural performance of the bridge have referred just to design stage conditions.
Further analyses should consider additional refinements of the present FEM model of the bridge so that to implement the existing morphology of the bridge structure, possibly in connection also to non-linear and damage analyses, as related to the present state of conservation of its structural elements.

With regards to the considerations mentioned above, the code *Beam3DStp* could also be improved, for example in connection to damage analyses.
Also, it could be extended to dynamic purposes. First steps have already been done in this direction.

Bibliography

[1] Alvin, K.F., Robertson, A.N., Reich, G.W., Park, K.C. (2003). Structural system identification: from reality to models. Computers and Structures, 81(12), 1149–1176.

[2] Bažant, Z.P., Cedolin, L. (1991). Stability of Structures. Oxford University Press, New York.

[3] Belluzzi, O. (1942). Scienza delle Costruzioni. Bologna: Zanichelli.

[4] Belytschko, T., Liu, W.K., Moran, B. (2000). Nonlinear Finite Element Analysis for Continua and Structures. Wiley, Chichester.

[5] Benvenuto, E. (1981). La Scienza delle Costruzioni e il suo Sviluppo Storico. Firenze: Sansoni.

[6] Brencich, A., Gambarotta, L. (2008). Assessment procedure and rehabilitation of riveted railway girders: The Campasso Bridge. Engineering Structure, 31, 224–239.

[7] Brincker, R.; Zhang, L.M.; Andersen, P. (2001). Modal identification of output-only systems using frequency domain decomposition. Smart Materials and Structures, 10(3), 441-445.

[8] Capurso, M. (1971). Limit analysis of continuous media with piecewise linear yield condition. Meccanica, 6, 53–58.

[9] Chiang, D-Y, Lin, C-S (2010). Identification of modal parameters from ambient vibration data using eigensystem realization algorithm with correlation technique. Journal of Mechanical Science and Technology, 24(12), 2377-2382.

[10] Cocchetti, G., Maier, G., Shen, X.P. (2002). Piecewise linear models for interfaces and mixed mode cohesive cracks. Computer Modeling in Engineering and Sciences, 3(3), 279–298.

[11] Cocchetti, G., Maier, G. (2003). Elastic-plastic and limit-state analyses of frames with softening plastic-hinge models by mathematical programming. International Journal of Solids and Structures, 40(25), 7219–7244.

[12] Cohn, M., Maier, G. (Eds.) (1979). Engineering Plasticity by Mathematical Programming. Pergamon Press.

[13] Cottle, R.W., Pang, J.S., Stone, R.E. (1992). The Linear Complementarity Problem. Academic Press, San Diego.

[14] Cunha, A., Caetano, E. (2006). Experimental modal analysis of civil engineering structures. Journal of Sound and Vibrations, 6(40), 12–20.

[15] Culmann, K. (1880). Traitè de Statique Graphique. Paris: Dunod.

[16] De Callafon, R.A., Moaveni, B., Conte, J.P., He, X., Udd, E. (2008). General realization algorithm for modal Identification of linear dynamic systems. Journal of Engineering Mechanics, 134(9), 712-722.

[17] De Donato, O., Maier, G. (1972). Mathematical programming methods for the inelastic analysis of reinforced concrete frames allowing for limited rotation capacity. International Journal for Numerical Methods in Engineering, 4(3), 307–329.

[18] Facheris, M. (2009). Analisi morfologica e modellazione per elementi finiti della pila sull'arco del ponte di Paderno d'Adda. Laurea Thesis in Building Engineering, Advisor E. Rizzi, Co-Advisor R. Ferrari, Università di Bergamo, Facoltà di Ingegneria, 125 pages, September 2009.

[19] Ferrari, R. (2006). Sulla concezione strutturale ottocentesca del ponte in ferro di Paderno d'Adda secondo la teoria dell'ellisse d'elasticità. Laurea Thesis in Building Engineering. Advisor E. Rizzi, Università di Bergamo, Facoltà di Ingegneria, 228 pages.

[20] Ferrari, R., Rizzi, E. (2008). On the theory of the ellipse of elasticity as a natural discretisation method in the design of Paderno d'Adda Bridge (Italy). In Proc. of VI Int. Conf. on Structural Analysis of Historic Construction (SAHC08), Bath, UK, 2–4 July 2008, Vol. 1, 583–591.

[21] Ferrari, R. (2009). Analisi strutturale degli elementi portanti del ponte di Paderno d'Adda. Master Thesis in Building Engineering, Advisor E. Rizzi, Università di Bergamo, Facoltà di Ingegneria, 108 pages, September 2009.

[22] Ferrari, R., Facheris, M., Rizzi, E. (2010a). Structural modelling of the piers of the Paderno d'Adda bridge (1889, Italy), in Proc. of 34th IABSE International Symposium on Bridge and Structural Engineering, Venice, Italy, 22–24 September 2010, Book of Abstracts, Vol. 97, 778–779, CD-ROM Proc., 8 pages.

[23] Ferrari, R., Facheris, M., Rizzi, E. (2010b). Structural analysis of the Paderno d'Adda Bridge (Italy, 1889). In Proc. of 7th Int. Conference on Structural Analysis of Historical Constructions (SAHC10), Shanghai, China, 6–8 October 2010, Advanced Materials Research, Vols. 133–134 (2010), 459–465.

[24] Ferrari, R., Rizzi, E. (2011a°). Analisi strutturale del ponte in ferro di Paderno d'Adda (1889). Technical Report SdC2011/03. Università degli Studi di Bergamo, Facoltà di Ingegneria (Dalmine), Dipartimento di Progettazione e Tecnologie, I-24044 Dalmine (BG), Italy, June 2011, 97 pages.

[25] Ferrari, R., Rizzi, E. (2011b). FEM modelling of the Paderno d'Adda bridge (Italy, 1889). In Proc. of Structural Engineers World Congress (SEWC 2011), Como, Italy, 4-6 April 2011, Book of Abstracts p. 159; CD-ROM Proceedings, Paper 210, 9 pages.

[26] Ferrari, R., Cocchetti, G., Rizzi, E. (2012). Elastoplastic Structural Analysis of the Paderno d'Adda bridge (Italy, 1889) based on Limit Analysis. 8th Int. Conf. on Structural Analysis of Historical Constructions (SAHC2012), Ed. Jerzy Jasie, Wroclaw, Poland, October 15–17, 2012, Vol. 3, pp. 2171–2180.

[27] Franchi, A., Genna, F. (1991). A stable/neutral equilibrium path for the numerical solution of elastic–plastic softening problems. Computer Methods in Applied Mechanics and Engineering, 90(1–3), 921–942.

[28] Gentile, C., Saisi, A. (2010a). Dynamic assessment of the iron bridge at Paderno d'Adda (1889). In Proc. of 7th Int. Conference on Structural Analysis of Historical Constructions (SAHC10), Shanghai, China, 6−8 October 2010, Advanced Materials Research, Vols. 133–134 (2010), 709–714.

[29] Gentile, C., Saisi, A. (2010b). Dynamic monitoring of the Paderno iron arch bridge (1889). In Proc. of 6th Int. Conference on Arch Bridges (ARCH'10), Baochun Chen, Jiangang Wei (Eds.), Fuzhou, China, 11–13 October 2010, 22–37.

[30] Gentile, C., Saisi, A., Valsecchi, A. (2010). Caratterizzazione dinamica e monitoraggio del ponte sull'Adda a Paderno (1889). Strade & Autostrade, 2-2010, 2–7.

[31] Gentile, C., Saisi, A., Busatta, F. (2011). Dynamic testing and permanent monitoring of an historic iron arch bridge, in Proc. of 8th Int. Conf. on Structural Dynamics (EURODYN 2011). Eds. G. De Roeck, G. Degrande, G. Lombaert, G. Müller, Leuven, Belgium, 4–6 July 2011, Book of Abstracts p. 46; CD-ROM Proceedings, Paper MS07-243, 8 pages.

[32] Giambanco, F. (1999). Elastic–plastic analysis by asymptotic pivoting method. Computers and Structures, 71(2), 215–238.

[33] Golub, G.H., Loan, C.F. (1996). Matrix Computations, 3rd edition, Johns Hopkins.

[34] Hodge Jr., P.G. (1977). Automatic piecewise linearization in ideal plasticity. Computer Methods in Applied Mechanics and Engineering, 10(3), 249–272.

[35] Jiràsek, M., Bažant, Z.P. (2002). Inelastic Analysis of Structures. Wiley, Chichester, UK.

[36] Lloyd Smith, D. (1990). Mathematical Programming Methods in Structural Plasticity. Springer Verlag, New York.

[37] Magalhães, F., Cunha, À, Caetano, E., Brincker, R (2010). Damping estimation using free decays and ambient vibration tests. Mechanical Systems and Signal Processing, 24(5), 1274–1290.

[38] Maier, G. (1968). A quadratic programming approach for certain classes of non linear structural problems. Meccanica, 3(2), 121–130.

[39] Maier, G. (1970). A matrix structural theory of piecewise-linear plasticity with interacting yield planes. Meccanica 5(1), 54–66.

[40] Maier, G. (1976). Piecewise linearization of yield criteria in structural plasticity. Solid Mechanics Archives, 1(2/3), 239–281.

[41] Maier, G., Giacomini, S., Paterlini, F. (1979). Combined elastoplastic and limit analysis via restricted basis linear programming. Computer Methods in Applied Mechanics and Engineering, 19(1), 21–48.

[42] Nascè, V., Zorgno, A.M., Bertolini, C., Carbone, V.I., Pistone, G., Roccati, R. (1984). Il ponte di Paderno: storia e struttura – Conservazione dell'architettura in ferro. Restauro, Anno XIII, n. 73-74, 215 pages.

[43] Nascè, V. (1993). Restoration of a 100 year old iron bridge, Paderno. Structural Engineering International, IABSE, 3(1), 37–38.

[44] Olsen, P.C. (1998). The influence of the linearization of the yield surface on the load-bearing capacity of reinforced concrete slabs. Computer Methods in Applied Mechanics and Engineering, 162, 351–358.

[45] Società Nazionale delle Officine di Savigliano (1889). Viadotto di Paderno sull'Adda (Ferrovia Ponte S. Pietro-Seregno). Torino: Tip. e Lit. Camilla e Bertolero.

[46] Timoshenko, S.P. (1953). History of Strength of Materials. New York: McGraw-Hill.

[47] Tin-Loi, F. (1990). A yield surface linearization procedure in limit analysis. Mechanical Structures and Machines, 18(1), 135–149.

[48] Wakefield, R.R., Tin-Loi, F. (1990). Large scale nonholonomic elastoplastic analysis using a linear complementarity formulation. Computer Methods in Applied Mechanics and Engineering, 84(3), 229–242.

[49] Zienkiewicz, O.C., Taylor, R.L. (2000). The Finite Element Method, 5th ed. Butterworth-Heinemann. Oxford.

Appendices

Appendix A: Core routine of the code *Beam3DStp*

Appendix B: Illustrations of the Paderno d'Adda bridge

Appendix C: Original design drawings of the Paderno d'Adda bridge

Appendix A

```
%%%%%%%%%%%%%%%%%%%%%%%%%%%%%%%%%%%%%%%%%%%%%%%%%%%%%%%%%%%%%%%%%%%%%%%%%%%
%                              Beam3DStp.m                               %
%%%%%%%%%%%%%%%%%%%%%%%%%%%%%%%%%%%%%%%%%%%%%%%%%%%%%%%%%%%%%%%%%%%%%%%%%%%
%                                                                        %
%           Elastoplastic analysis of truss frame structures             %
%                                                                        %
%                     Authors: Rosalba FERRARI                           %
%                              prof. Giuseppe COCCHETTI                  %
%                                                                        %
%                          Version: dec07.2012                           %
%                                                                        %
%%%%%%%%%%%%%%%%%%%%%%%%%%%%%%%%%%%%%%%%%%%%%%%%%%%%%%%%%%%%%%%%%%%%%%%%%%%
%        THIS SOFTWARE IS TO BE USED FOR LEARNING PURPOSES ONLY          %
%%%%%%%%%%%%%%%%%%%%%%%%%%%%%%%%%%%%%%%%%%%%%%%%%%%%%%%%%%%%%%%%%%%%%%%%%%%
% This code is made of a core routine transferring data to the following  %
% functions:                                                             %
% - geotop: defines geometry and topology data                           %
% - mecpar: defines mechanical parameters                                %
% - locons: defines boundary conditions (loads and constraints)          %
% - stiffm12: generates the stiffness matrix of the beam element         %
% - assilc: assigns boundary conditions (nodal loads and constraints)    %
% - xKepNM_tvar: generates the elastic-plastic stiffness matrix          %
% - syssolpKep: solves the equation system                               %
% - axialfKep_tvar: ev. st. int. var. and plastic strain in the elements  %
%%%%%%%%%%%%%%%%%%%%%%%%%%%%%%%%%%%%%%%%%%%%%%%%%%%%%%%%%%%%%%%%%%%%%%%%%%%

%%%%%%%%%%%%%%%%%%%
% Initializations %
%%%%%%%%%%%%%%%%%%%

clear all
close all
fclose('all')
clc
format short e
disp('Static elastoplastic analysis of (3D) truss frame structures')

diary off
diary on

%%%%%%%%%%%%%%%%%%%%%%%%%%%%%%%%%%%%%%%%%%%%%
% INPUT: Acquisition of the structural data %
%%%%%%%%%%%%%%%%%%%%%%%%%%%%%%%%%%%%%%%%%%%%%

byesread=1;

if (byesread==1)

  fid=fopen('fileDATabaqus.txt','rt');

  % Geometry and topology data
  [nAsserv,nMasserv,nInc,nEtichElem,nBeams,dXYZ,nEtichNodi,nNode,nProp]=geotop(fid);

  % Mechanical parameters
  [dPar,dParEtich,dParSNOS]=mecpar(nProp,nBeams,nEtichElem,fid);

  bAbaqus=true;
```

```
  % Loads and constrains
  [nCons,dC,nForce,dF]=locons(nEtichNodi,nNode,fid);

  fclose(fid);

  if bAbaqus

  % Collapse loads amplification
  dF(:,3)=dF(:,3)*100;

  end
  save('ABdataMetri')
else
  load('ABdataMetri')
end

%%%%%%%%%%%%%%%%%%%%%%%%%%%%%%%%%%
% Setting up the solving system %
%%%%%%%%%%%%%%%%%%%%%%%%%%%%%%%%%%

% Total number of dofs (before imposing boundary conditions)
nDofTot=max(max(nInc(:,3:14)));

% Global stiffness matrix
dK=spalloc(nDofTot,nDofTot,60*nDofTot);
dTq=spalloc(nDofTot,1,nDofTot);

% Set up and assembly of the stiffness matrix of each truss element
 for ne=1:nBeams

   n12=nInc(ne,1:2);

   dXYZ12=dXYZ(n12,:);

   dVAJEne=dPar(ne,:);

   % Stiffness matrix dKne for the n-th beam element
   [dKne,dPQne]=stiffm12(dXYZ12,dVAJEne);

   % Assembly of the overall stiffness matrix
   nVne=nInc(ne,3:14); % Recovers the Dofs of the n-th element

   for na=1:12
     dTq(nVne(na),1)=dTq(nVne(na),1)+dPQne(na,1); % Global force vector dTq (non-
                                                    amplified loads)
     for nb=1:12
       dK(nVne(na),nVne(nb))=dK(nVne(na),nVne(nb))+dKne(na,nb); % dK: global stiffness
                                                                  matrix; dKne: el.
                                                                  stiffness matrix
     end
   end
 end

save dK
clear dK


% Boundary conditions: nodal constraints and loads
[nEff,dQ,dS,dUs2,nUs,dUs,nUu,dT]=assilc(nAsserv,nMasserv,dXYZ,nForce,dF,nCons,dC,nDofTot
,nInc,nBeams);

save('geo');

load('geo');
```

```
%%%%%%%%%%%%%%%%%%%%%%%%%%%
% Elastoplastic analysis %
%%%%%%%%%%%%%%%%%%%%%%%%%%%

  %Initialization of variables
  dUinc=spalloc(nDofTot,1,nDofTot);
  dUn=spalloc(nDofTot,1,nDofTot);
  dEp=spalloc(6*nBeams,1,6*nBeams);
  dEpn=spalloc(6*nBeams,1,6*nBeams);
  nEpbus=spalloc(6*nBeams,1,6*nBeams);
  nEpbusn=spalloc(6*nBeams,1,6*nBeams);
  dNMn_nn=spalloc(7*nBeams,1,7*nBeams);
  dNMn=spalloc(7*nBeams,1,7*nBeams);
  dRn=spalloc(max(size(nUs)),1,max(size(nUs)));
  dtn=0;

  dtime=0;
  dtimetotal=1;
  dtimeinc0=.1;
  nn=1;
  nr=0;
  nnrMax=30;


  bFile=true;
  bRestart=false;

  if ~bFile
    dEpinc=spalloc(6*nBeams,1,6*nBeams);
    dNMinc=spalloc(7*nBeams,1,7*nBeams);
    dRinc=spalloc(max(size(nUs)),1,max(size(nUs)));
    dtinc=[0,0];

    save('dUinc','dUinc');
    clear dUinc;
    save('dUn','dUn');
    clear dUn;
    save('dNMinc','dNMinc');
    clear dNMinc;
    save('dNMn','dNMn');
    clear dNMn;
    save('dRinc','dRinc');
    clear dRinc;
    save('dRn','dRn');
    clear dRn;
    save('dEpinc','dEpinc');
    clear dEpinc;
    save('dEpn','dEpn');
    clear dEpn;
    save('nEpbusn','nEpbusn');
    clear nEpbusn;
    save('dtinc','dtinc');
    clear dtinc;
    save('dtn','dtn');
    clear dtn;
  elseif ~bRestart
    fid=fopen('dUinc','w');
    fprintf(fid,'\n');
    fprintf(fid,'%g ',zeros([1,nDofTot]));
    fclose(fid);

    fid=fopen('dUn','w');
    fprintf(fid,'%g ',zeros([1,nDofTot]));
    fprintf(fid,'\n');
```

```
  fclose(fid);

  fid=fopen('dNMinc','w');
  fprintf(fid,'%g ',zeros([1,7*nBeams]));
  fprintf(fid,'\n');
  fclose(fid);

  fid=fopen('dNMn','w');
  fprintf(fid,'%g ',zeros([1,7*nBeams]));
  fprintf(fid,'\n');
  fclose(fid);

  fid=fopen('dRinc','w');
  fprintf(fid,'%g ',zeros([1,max(size(nUs))]));
  fprintf(fid,'\n');
  fclose(fid);

  fid=fopen('dRn','w');
  fprintf(fid,'%g ',zeros([1,max(size(nUs))]));
  fprintf(fid,'\n');
  fclose(fid);

  fid=fopen('dEpinc','w');
  fprintf(fid,'%g ',zeros([1,6*nBeams]));
  fprintf(fid,'\n');
  fclose(fid);

  fid=fopen('dEpn','w');
  fprintf(fid,'%g ',zeros([1,6*nBeams]));
  fprintf(fid,'\n');
  fclose(fid);

  fid=fopen('nEpbusn','w');
  fprintf(fid,'%d ',zeros([1,6*nBeams]));
  fprintf(fid,'\n');
  fclose(fid);

  fid=fopen('dtinc','w');
  fprintf(fid,'%g ',[0,0]);
  fprintf(fid,'\n');
  fclose(fid);

  fid=fopen('dtn','w');
  fprintf(fid,'%g ',0);
  fprintf(fid,'\n');
  fclose(fid);
end


disp(sprintf('\nBeginning Q-step nr.%d at time %g, with %d active modes (%d N, %d Mt,
%d Mf)',[nn,dtime,0,0,0,0]))
while true
  dtimeinc=dtimeinc0;

  %Build the force vector equivalent to plastic strains
  [dKep]=xKepNM_tvar(nBeams,nInc,dXYZ,dPar,nEpbus);

  %Vector of known terms in solving (linear) system
  dTinc=(dTq/dtimetotal)*dtimeinc;

  %Vector of given displacements in solving (linear) system
  dUs2inc=(dUs2/dtimetotal)*dtimeinc;

  %Solution of linear system (estimation of incremental quantities)
```

```
[nSingKuu,du,dR]=syssolpKep(dKep,dTinc,nDofTot,nUu,nUs,nEff,dQ,dS,dUs2inc);
if (nSingKuu==0)
  %Computation of increments of internal actions (axial forces)
  [nRipeti_passo,nEpbus_new,dNM_inc,dEp,dt_n]=azintKep_tvar(nBeams,nInc,dXYZ,dPar,du
  ,dNMn_nn,nEpbus,dtimeinc,1);
else
  disp(sprintf('\nStructural collapse!'))
  disp(sprintf('\nEnd of analysis, time %g',[dtime]))
  break
end

if (~nRipeti_passo)
  if (dtime+dt_n>dtimetotal)
    dt_n=dtimetotal-dtime;
  else
    nEpbus=nEpbus_new;
  end

  %Updating variables
  dEp=dEp/dtimeinc*dt_n;
  du=du/dtimeinc*dt_n;
  dNM_inc=dNM_inc/dtimeinc*dt_n;
  dNMn_nn=dNMn_nn+dNM_inc;
  dR=dR/dtimeinc*dt_n;

  if ~bFile
    load('dEpinc');
    dEpinc=[dEpinc,dEp];
    save('dEpinc','dEpinc');
    clear dEpinc;

    load('dEpn');
    dEpn=[dEpn,dEpn(:,nn)+dEp];
    save('dEpn','dEpn');
    clear dEpn;

    load('nEpbusn');
    nEpbusn=[nEpbusn,nEpbus];
    save('nEpbusn','nEpbusn');
    clear nEpbusn;

    load('dUinc');
    dUinc=[dUinc,du];
    save('dUinc','dUinc');
    clear dUinc;

    load('dUn');
    dUn=[dUn,dUn(:,nn)+du];
    save('dUn','dUn');
    clear dUn;

    load('dNMinc');
    dNMinc=[dNMinc,dNM_inc];
    save('dNMinc','dNMinc');
    clear dNMinc;

    load('dNMn');
    dNMn=[dNMn,dNMn_nn];
    save('dNMn','dNMn');
    clear dNMn;

    load('dRinc');
    dRinc=[dRinc,dR];
    save('dRinc','dRinc');
```

```
    clear dRinc;

    load('dRn');
    dRn=[dRn,dRn(:,nn)+dR];
    save('dRn','dRn');
    clear dRn;

    load('dtinc');
    dtinc=[dtinc; [nr, dt_n]];
    save('dtinc','dtinc');
    clear dtinc;

    load('dtn');
    dtn=[dtn,dtn(nn)+dt_n];
    save('dtn','dtn');
    clear dtn;
  else
    fid=fopen('dEpinc','a');
    fprintf(fid,'%g ',full(dEp));
    fprintf(fid,'\n');
    fclose(fid);

    dEpn=dEpn+dEp;

    fid=fopen('dEpn','a');
    fprintf(fid,'%g ',full(dEpn));
    fprintf(fid,'\n');
    fclose(fid);

    fid=fopen('nEpbusn','a');
    fprintf(fid,'%d ',full(nEpbus));
    fprintf(fid,'\n');
    fclose(fid);

    fid=fopen('dUinc','a');
    fprintf(fid,'%g ',full(du));
    fprintf(fid,'\n');
    fclose(fid);

    dUn=dUn+du;

    fid=fopen('dUn','a');
    fprintf(fid,'%g ',full(dUn));
    fprintf(fid,'\n');
    fclose(fid);

    fid=fopen('dNMinc','a');
    fprintf(fid,'%g ',full(dNM_inc));
    fprintf(fid,'\n');
    fclose(fid);

    fid=fopen('dNMn','a');
    fprintf(fid,'%g ',full(dNMn_nn));
    fprintf(fid,'\n');
    fclose(fid);

    fid=fopen('dRinc','a');
    fprintf(fid,'%g ',full(dR));
    fprintf(fid,'\n');
    fclose(fid);

    dRn=dRn+dR;

    fid=fopen('dRn','a');
```

```
      fprintf(fid,'%g ',full(dRn));
      fprintf(fid,'\n');
      fclose(fid);

      fid=fopen('dtinc','a');
      fprintf(fid,'%g ',[nr, dt_n]);
      fprintf(fid,'\n');
      fclose(fid);

      dtn=dtn+dt_n;

      fid=fopen('dtn','a');
      fprintf(fid,'%g ',dtn);
      fprintf(fid,'\n');
      fclose(fid);
    end
    dEp=spalloc(6*nBeams,1,6*nBeams);
    dNM_inc=spalloc(7*nBeams,1,7*nBeams);

    dtime=dtime+dt_n;
    nr=0;
    nn=nn+1;

    if (dtime < dtimetotal)
      disp(sprintf('\nBeginning Q-step nr.%d at time %g, with %d active modes (%d N,
      %d Mt, %d Mf)',[nn,dtime,length(find(nEpbus_new>0)),...

      length(find(nEpbus_new(1:6:end,1)>0)),length(find(nEpbus_new(2:6:end,1)>0)),...
         length(find(nEpbus_new>0))-length(find(nEpbus_new(1:6:end,1)>0))-
      length(find(nEpbus_new(2:6:end,1)>0))]))
    else
      disp(sprintf('\nEnd of Q-analysis, time %g',[dtime]))
      break
    end
  else
    if (nr>nnrMax)
      %Convergence is lost
      disp('Excess of iterations')
      disp(sprintf('Loss of convergence at time %g',dtime))
      break
    else
      %Time step repeated
      nEpbus=nEpbus_new;
      nr=nr+1;
      disp(sprintf(' iteration nr. %d, with %d active modes (%d N, %d Mt, %d
      Mf)',[nr,length(find(nEpbus_new>0)),...

      length(find(nEpbus_new(1:6:end,1)>0)),length(find(nEpbus_new(2:6:end,1)>0)),...
         length(find(nEpbus_new>0))-length(find(nEpbus_new(1:6:end,1)>0))-
      length(find(nEpbus_new(2:6:end,1)>0))]))
    end
  end
end


dtn=0;
dtime=0;
dtimetotal=1;
dtimeinc0=.1;
nr=0;

disp(sprintf('\nBeginning step nr.%d at time %g, with %d active modes (%d N, %d Mt, %d
Mf)',[nn,dtime,0,0,0,0]))
while true
```

```
dtimeinc=dtimeinc0;

%Build the force vector equivalent to plastic strains
[dKep]=xKepNM_tvar(nBeams,nInc,dXYZ,dPar,nEpbus);

%Vector of known terms in solving (linear) system
dTinc=(dT/dtimetotal)*dtimeinc;

%Vector of given displacements in solving (linear) system
dUs2inc=(dUs2/dtimetotal)*dtimeinc;

%Solution of linear system (estimation of incremental quantities)
[nSingKuu,du,dR]=syssolpKep(dKep,dTinc,nDofTot,nUu,nUs,nEff,dQ,dS,dUs2inc);
if (nSingKuu==0)
  %Computation of increments of internal actions (axial forces)
  [nRipeti_passo,nEpbus_new,dNM_inc,dEp,dt_n]=azintKep_tvar(nBeams,nInc,dXYZ,dPar,du
  ,dNMn_nn,nEpbus,dtimeinc,0);
else
  disp(sprintf('\nStructural collapse!'))
  disp(sprintf('\nEnd of analysis, time %g',[dtime]))
  break
end

if (~nRipeti_passo)
  if (dtime+dt_n>dtimetotal)
    dt_n=dtimetotal-dtime;
  else
    nEpbus=nEpbus_new;
  end

  %Updating variables
  dEp=dEp/dtimeinc*dt_n;
  du=du/dtimeinc*dt_n;
  dNM_inc=dNM_inc/dtimeinc*dt_n;
  dNMn_nn=dNMn_nn+dNM_inc;
  dR=dR/dtimeinc*dt_n;

  if ~bFile
    load('dEpinc');
    dEpinc=[dEpinc,dEp];
    save('dEpinc','dEpinc');
    clear dEpinc;

    load('dEpn');
    dEpn=[dEpn,dEpn(:,nn)+dEp];
    save('dEpn','dEpn');
    clear dEpn;

    load('nEpbusn');
    nEpbusn=[nEpbusn,nEpbus];
    save('nEpbusn','nEpbusn');
    clear nEpbusn;

    load('dUinc');
    dUinc=[dUinc,du];
    save('dUinc','dUinc');
    clear dUinc;

    load('dUn');
    dUn=[dUn,dUn(:,nn)+du];
    save('dUn','dUn');
    clear dUn;

    load('dNMinc');
```

```
    dNMinc=[dNMinc,dNM_inc];
    save('dNMinc','dNMinc');
    clear dNMinc;

    load('dNMn');
    dNMn=[dNMn,dNMn_nn];
    save('dNMn','dNMn');
    clear dNMn;

    load('dRinc');
    dRinc=[dRinc,dR];
    save('dRinc','dRinc');
    clear dRinc;

    load('dRn');
    dRn=[dRn,dRn(:,nn)+dR];
    save('dRn','dRn');
    clear dRn;

    load('dtinc');
    dtinc=[dtinc; [nr, dt_n]];
    save('dtinc','dtinc');
    clear dtinc;

    load('dtn');
    dtn=[dtn,dtn(nn)+dt_n];
    save('dtn','dtn');
    clear dtn;
  else
    fid=fopen('dEpinc','a');
    fprintf(fid,'%g ',full(dEp));
    fprintf(fid,'\n');
    fclose(fid);

    dEpn=dEpn+dEp;

    fid=fopen('dEpn','a');
    fprintf(fid,'%g ',full(dEpn));
    fprintf(fid,'\n');
    fclose(fid);

    fid=fopen('nEpbusn','a');
    fprintf(fid,'%d ',full(nEpbus));
    fprintf(fid,'\n');
    fclose(fid);

    fid=fopen('dUinc','a');
    fprintf(fid,'%g ',full(du));
    fprintf(fid,'\n');
    fclose(fid);

    dUn=dUn+du;

    fid=fopen('dUn','a');
    fprintf(fid,'%g ',full(dUn));
    fprintf(fid,'\n');
    fclose(fid);

    fid=fopen('dNMinc','a');
    fprintf(fid,'%g ',full(dNM_inc));
    fprintf(fid,'\n');
    fclose(fid);

    fid=fopen('dNMn','a');
```

```
      fprintf(fid,'%g ',full(dNMn_nn));
      fprintf(fid,'\n');
      fclose(fid);

      fid=fopen('dRinc','a');
      fprintf(fid,'%g ',full(dR));
      fprintf(fid,'\n');
      fclose(fid);

      dRn=dRn+dR;

      fid=fopen('dRn','a');
      fprintf(fid,'%g ',full(dRn));
      fprintf(fid,'\n');
      fclose(fid);

      fid=fopen('dtinc','a');
      fprintf(fid,'%g ',[nr, dt_n]);
      fprintf(fid,'\n');
      fclose(fid);

      dtn=dtn+dt_n;

      fid=fopen('dtn','a');
      fprintf(fid,'%g ',dtn);
      fprintf(fid,'\n');
      fclose(fid);
    end
    dEp=spalloc(6*nBeams,1,6*nBeams);
    dNM_inc=spalloc(7*nBeams,1,7*nBeams);

    dtime=dtime+dt_n;
    nr=0;
    nn=nn+1;

    if (dtime < dtimetotal)
      disp(sprintf('\nBeginning step nr.%d at time %g, with %d active modes (%d N, %d
      Mt, %d Mf)',[nn,dtime,length(find(nEpbus_new>0)),...

      length(find(nEpbus_new(1:6:end,1)>0)),length(find(nEpbus_new(2:6:end,1)>0)),...
         length(find(nEpbus_new>0))-length(find(nEpbus_new(1:6:end,1)>0))-
      length(find(nEpbus_new(2:6:end,1)>0))]))
    else
      disp(sprintf('\nEnd of analysis, time %g',[dtime]))
      break
    end
  else
    if (nr>nnrMax)
      %Convergence is lost
      disp('Excess of iterations')
      disp(sprintf('Loss of convergence at time %g',dtime))
      break
    else
      %Time step repeated
      nEpbus=nEpbus_new;
      nr=nr+1;
      disp(sprintf(' iteration nr. %d, with %d active modes (%d N, %d Mt, %d
      Mf)',[nr,length(find(nEpbus_new>0)),...

      length(find(nEpbus_new(1:6:end,1)>0)),length(find(nEpbus_new(2:6:end,1)>0)),...
         length(find(nEpbus_new>0))-length(find(nEpbus_new(1:6:end,1)>0))-
      length(find(nEpbus_new(2:6:end,1)>0))]))
    end
  end
```

```
  end


save('vars');

load('vars');

%%%%%%%%%%%%%%%%%%%%%%%%%%%%%%%%%%%%
% OUTPUT 1: Computational results %
%%%%%%%%%%%%%%%%%%%%%%%%%%%%%%%%%%%%

if ~bFile
  load('dUn');
  du=dUn(:,nn);
  clear dUn;

  load('dRn');
  dR=dRn(:,nn);
  clear dRn;

  load('dNMn');
  dNM=dNMn(:,nn);
  clear dNMn;

  load('dEpn');
  dEp=dEpn(:,nn);
  clear dEpn;
else
  fid=fopen('dUn','r');
  for nq=1:nn
    du=fscanf(fid,'%g ',size(dUn));
  end
  fclose(fid);

  fid=fopen('dEpn','r');
  for nq=1:nn
    dEp=fscanf(fid,'%g ',size(dEp));
  end
  fclose(fid);

  fid=fopen('nEpbusn','r');
  for nq=1:nn
    nEpbus=fscanf(fid,'%d ',size(nEpbus));
  end
  fclose(fid);

  fid=fopen('dNMn','r');
  for nq=1:nn
    dNM=fscanf(fid,'%g ',size(dNM_inc));
  end
  fclose(fid);

end

%%%%%%%%%%%%%%%
%%% The end %%%
%%%%%%%%%%%%%%%
```

Appendix B

Fig. B1: View of the Paderno d'Adda bridge from the Paderno bank.

Fig. B2: Bottom view of the arch/pier/upper beam connection.

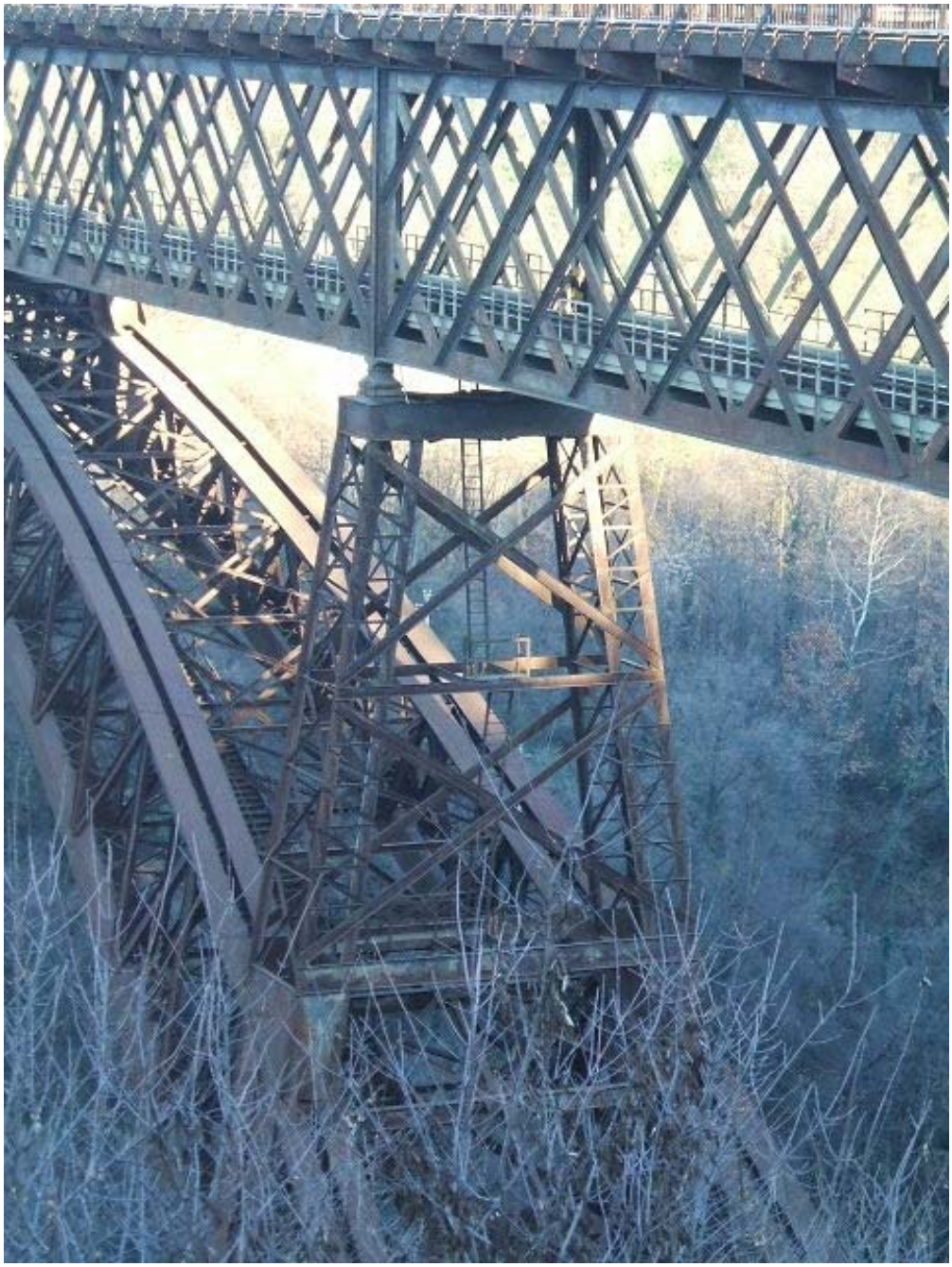

Fig. B3: Top view of the arch/pier/upper beam connection.

Fig. B4: View of the shoulder of the arch and the pier on the Calusco bank.

Fig. B5: Particular of the shoulder of the arch and the big pier on the Paderno bank.

Fig. B6: Prospective view from the inner of the arch near the Paderno bank.

Fig. B7: Prospective view of the arch of the bridge; particular on: the two couples of secondary inclined arches, the transverse brace systems and the boardwalk located into the arch's body.

Appendix C

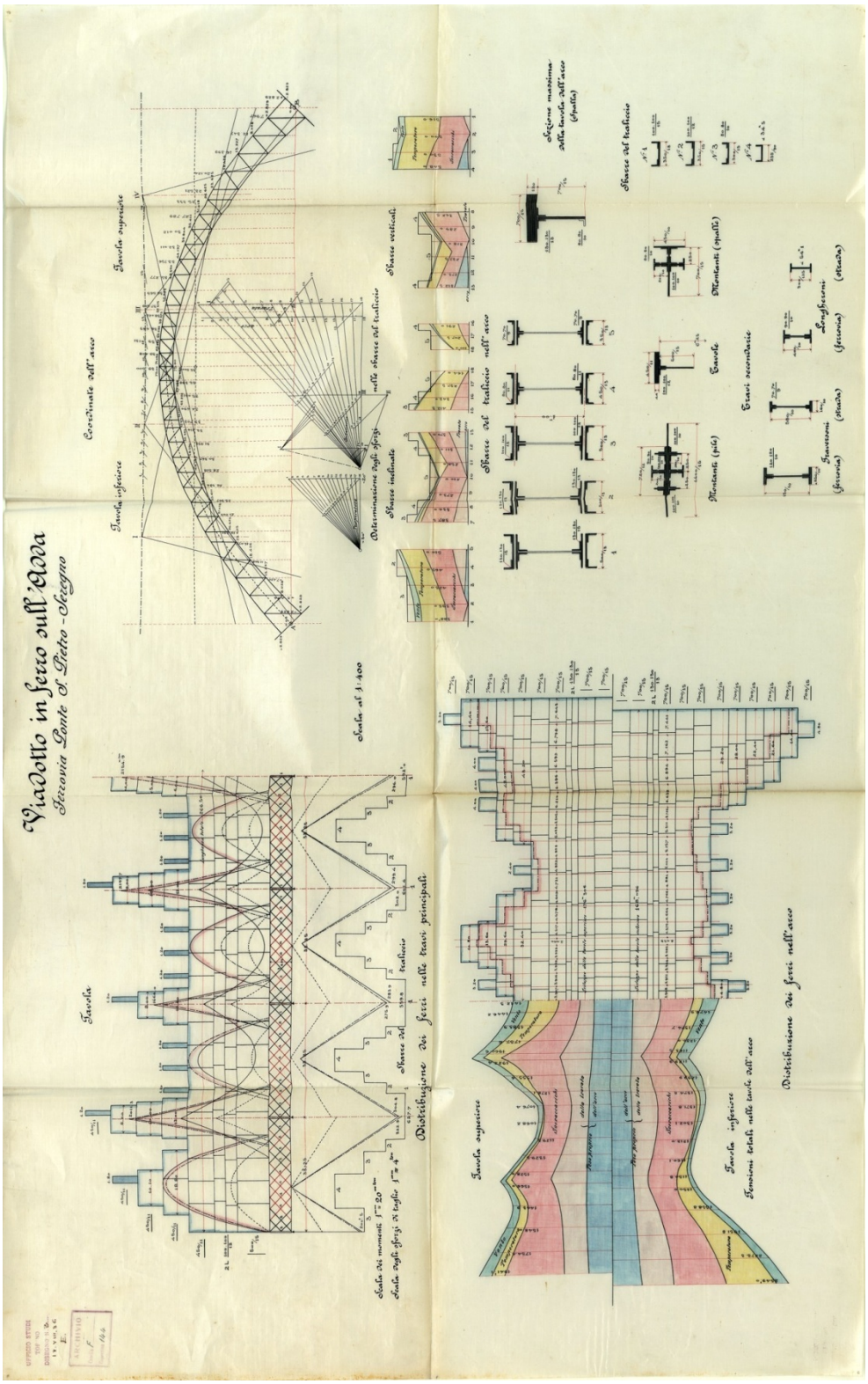
Viadotto in ferro sull'Adda
Ferrovia Lecco a Chiasso - Disegno
Scala al 1:400
Corrente dell'arco
Tavola superiore
Tavola inferiore
Sforzi verticali
Sforzi inclinati
Sforzi nel traliccio nell'arco
Sforzi nel traliccio
Sezione massima della tavola dell'arco (piatta)
Montanti (piatti)
Montanti (quadri)
Tavole
Travi secondarie
Longherini (ferrovia)
Distribuzione dei ferri nell'arco
Tavola superiore
Tavola inferiore

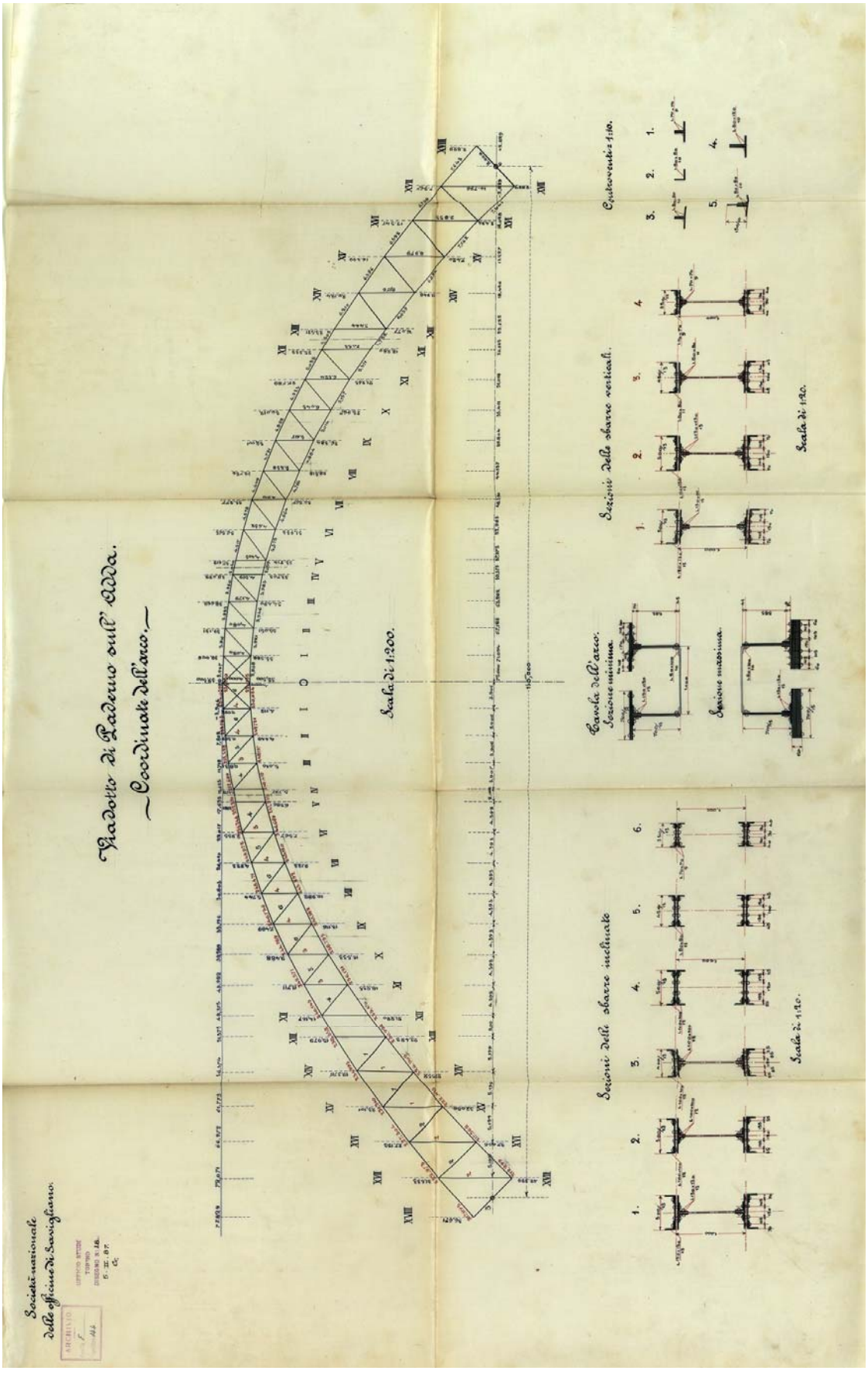
Società nazionale
delle officine di Savigliano.
Ponte di Paderno sull' Adda.
Coordinate dell'arco.
Scala di 1:200.
Sezioni delle sbarre inclinate
Scala di 1:20.
Sezioni delle sbarre verticali.
Scala di 1:20.
Equivalenti 1:10.
Corda dell'arco.
Sezione minima.
Sezione massima.

Società nazionale
delle officine di Savigliano.

Viadotto di Paderno sull'Adda.

— Sezioni trasversali —

N° 0.

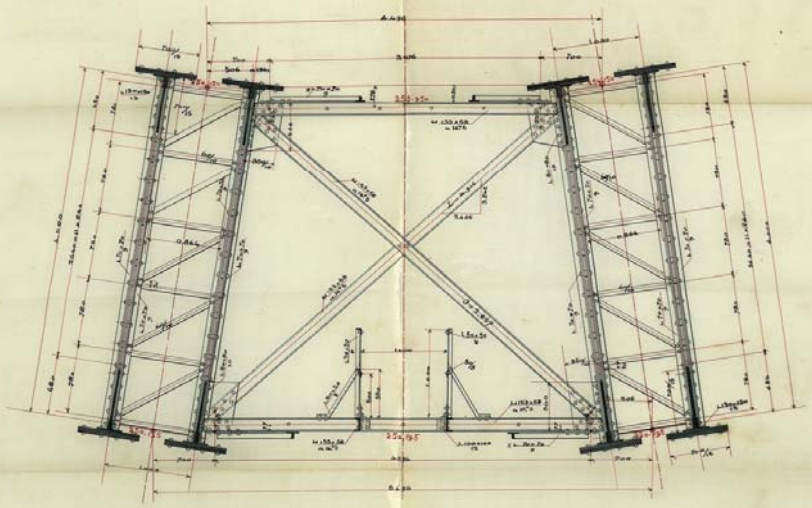

N° I

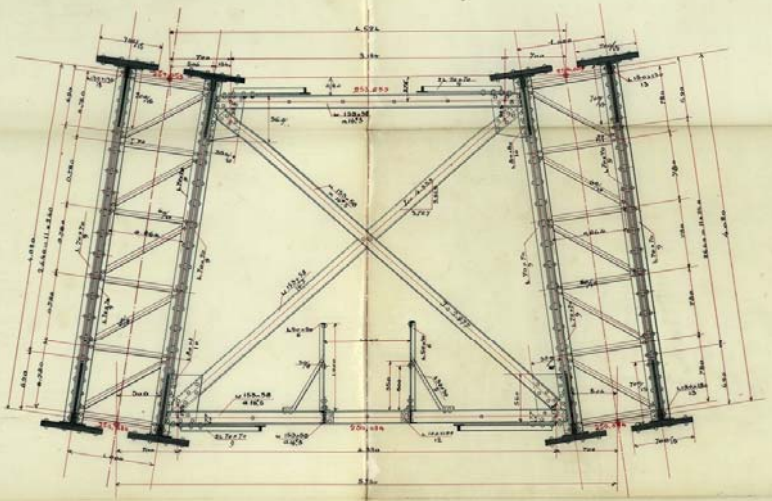

Scala al 1:20.

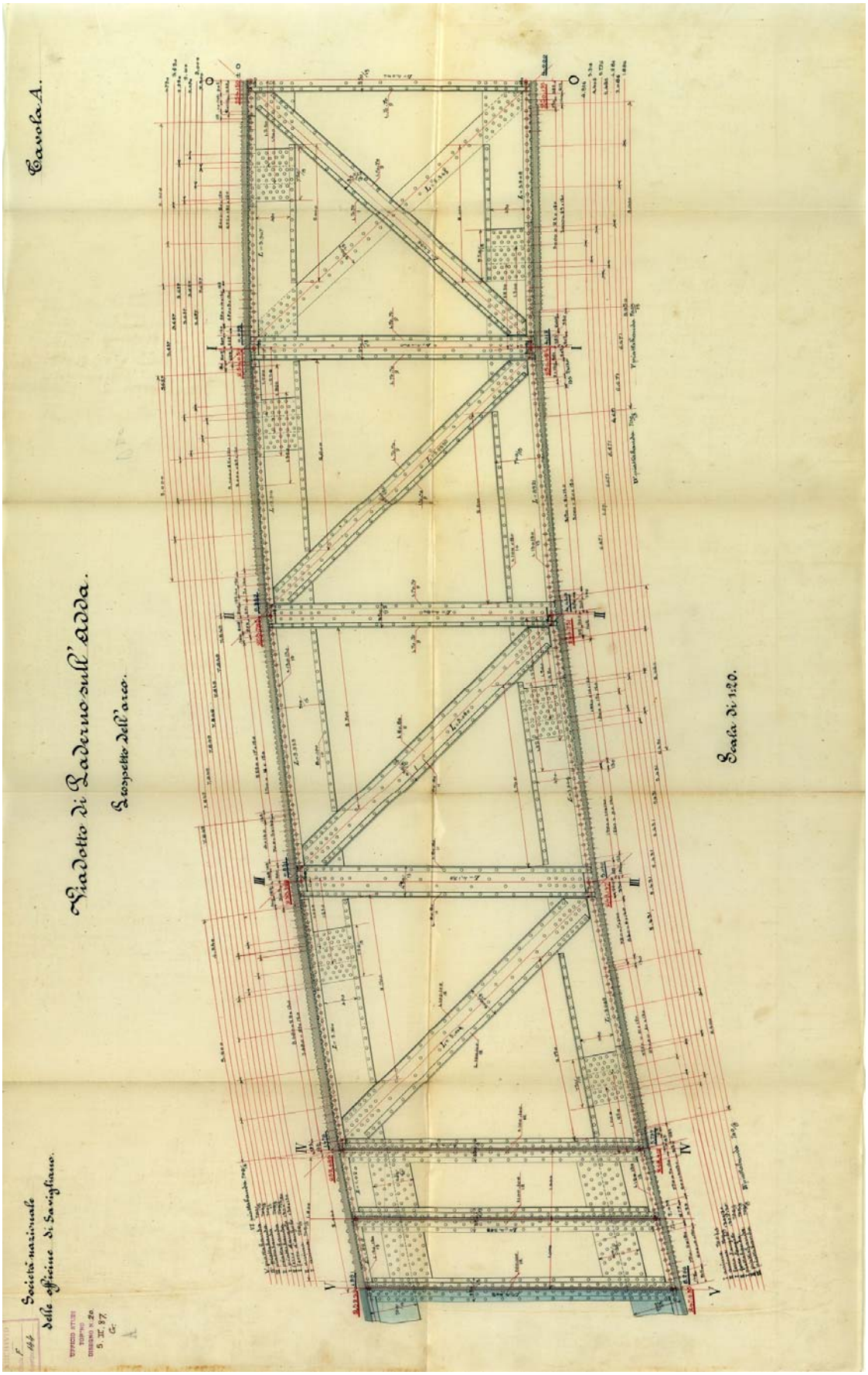
Tavola A.
Viadotto di Paderno sull'Adda.
Prospetto dell'arco.
Società nazionale
delle officine di Savigliano.
Scala di 1:250.

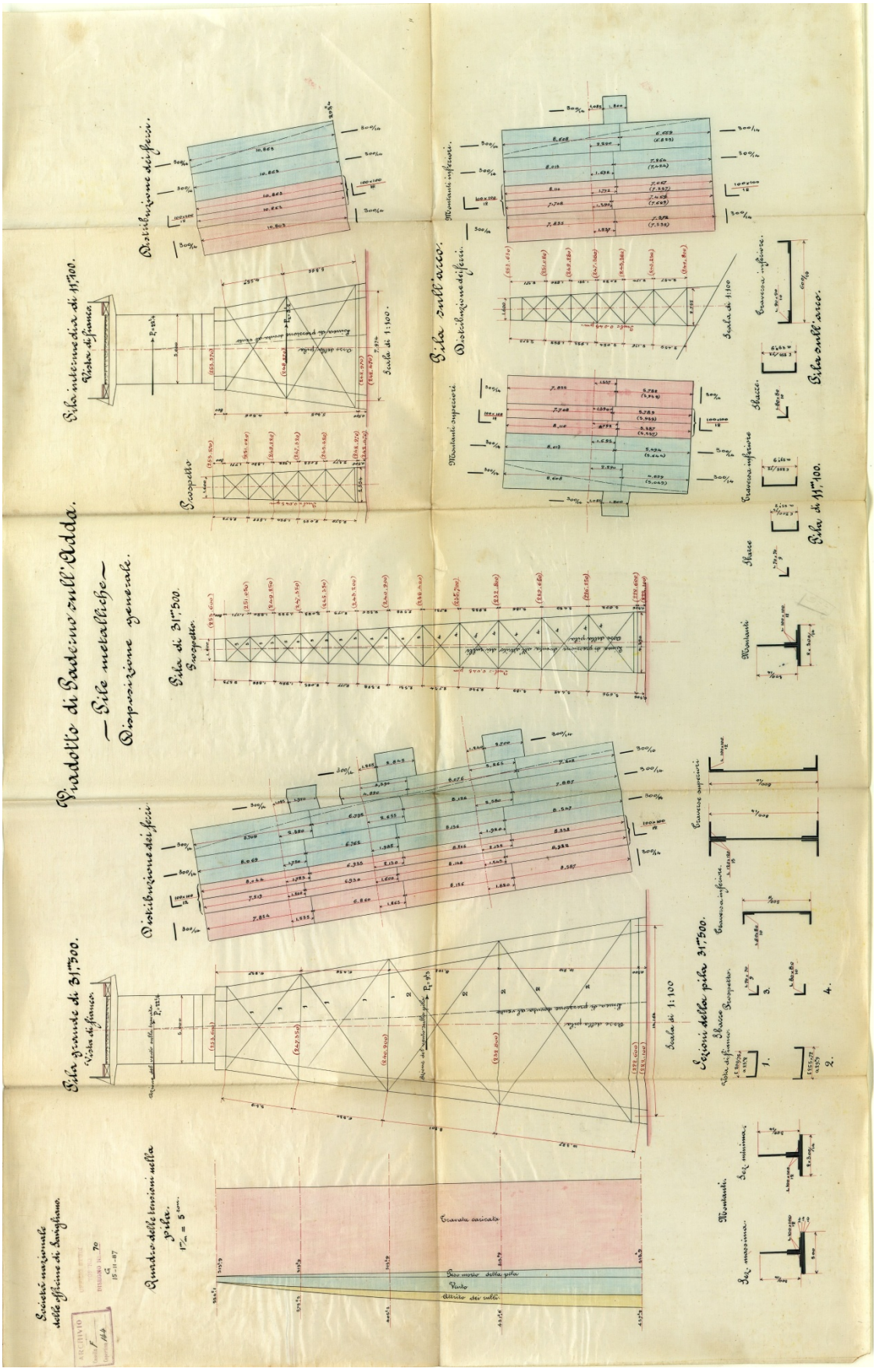
Ponte di Paderno sull'Adda.
— Sito metalliche —
Disposizione generale.
Sezioni normali
delle officine di Sampierdarena.
Sezioni della pila 31,500.
Scala di 1:100

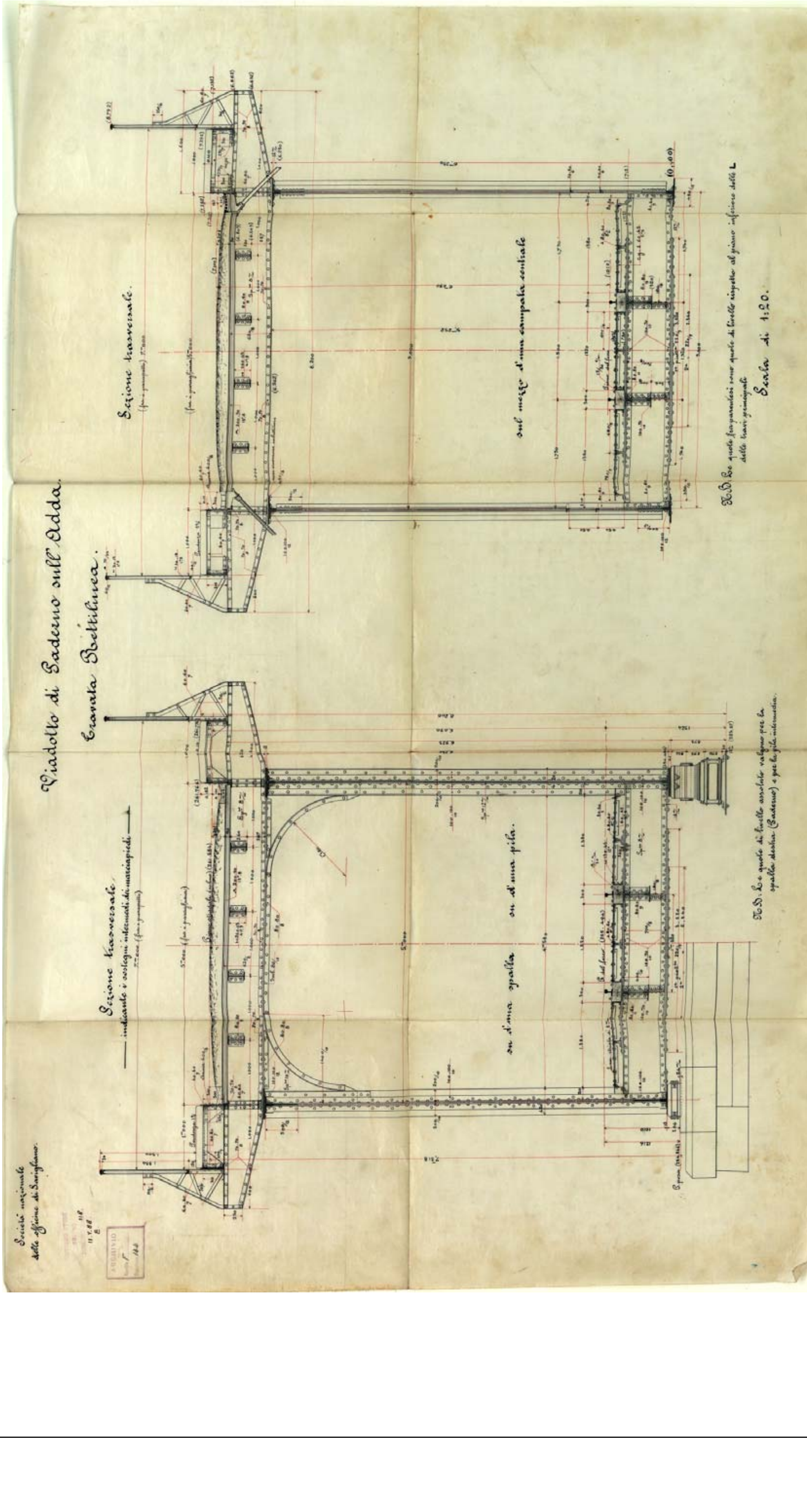
Viadotto di Paderno sull' Adda
Travata Rettilinea
Sezione trasversale
Scala di 1:20